SNAP-21 PROGRAM, PHASE II

DEEP SEA RADIOISOTOPE-FUELED THERMOELECTRIC GENERATOR POWER SUPPLY SYSTEM

QUARTERLY REPORT NO. 3

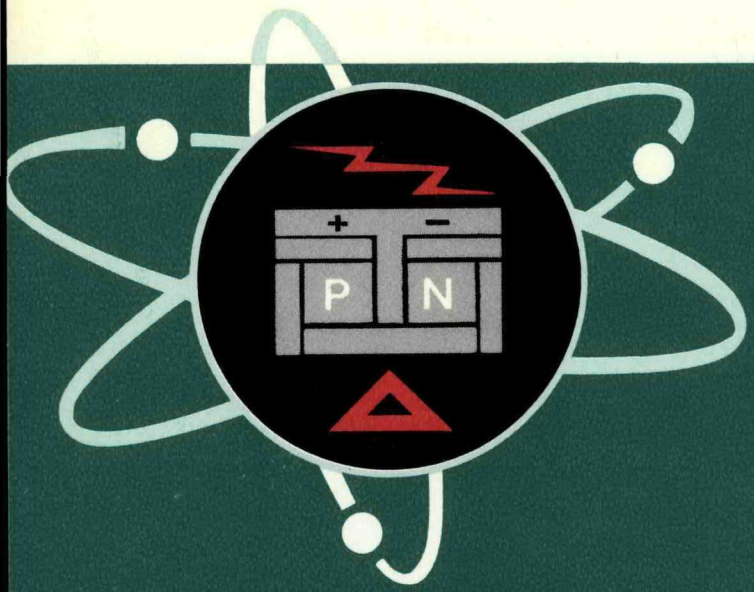

3M Isotope Power Products
MINNESOTA MINING & MANUFACTURING CO.
2501 HUDSON ROAD, ST. PAUL, MINN. 55119 PH. 631-2500

DISCLAIMER

Report No. MMM 3691-17

AEC RESEARCH AND DEVELOPMENT REPORT

This report has been prepared under contract AT(30-1)3691
with the U. S. Atomic Energy Commission

SNAP-21 PROGRAM, PHASE II

DEEP SEA RADIOISOTOPE-FUELED THERMOELECTRIC GENERATOR POWER SUPPLY SYSTEM

QUARTERLY REPORT NO. 3

MAY 1967

Period Covered

January 1, 1967 - March 31, 1967

Prepared by
J. F. X. Weinig

Approved by
V. Yanisch
Manager
SNAP-21 Program

Issued by:
ISOTOPE POWER PRODUCTS
MINNESOTA MINING AND MANUFACTURING COMPANY
ST. PAUL, MINNESOTA 55119

LEGAL NOTICE

This report was prepared as an account of Government sponsored work. Neither the United States, nor the Commission, nor any person acting on behalf of the Commission:

A. Makes any warranty or representation, expressed or implied, with respect to the accuracy, completeness, or usefulness of the information contained in this report, or that the use of any information, apparatus, method, or process disclosed in this report may not infringe privately owned rights; or

B. Assumes any liabilities with respect to the use of, or for damages resulting from the use of any information, apparatus, method, or process disclosed in this report.

As used in the above, "person acting on behalf of the Commission" includes any employee or contractor of the commission, or employee of such contractor, to the extent that such employee or contractor of the Commission, or employee of such contractor prepares, disseminates, or provides access to, any information pursuant to his employment or contract with the Commission, or his employment with such contractor.

THIS DOCUMENT FOR OFFICIAL USE ONLY PENDING PATENT CLEARANCE

DISTRIBUTION

Distribution of this document is in accordance with M 3679 (44th Edition) category C-92a.

page blank

TABLE OF CONTENTS

TABLE OF CONTENTS (Continued)

LIST OF FIGURES

LIST OF FIGURES (Continued)

LIST OF FIGURES (Continued)

page blank

LIST OF TABLES

page blank

1.0 SUMMARY

The SNAP-21 Program Plan was resubmitted to the Commission on February 2 and approved as a planning document on March 1.

The Dynamic Load Criteria Sub-task topical report was submitted to the Commission on March 9. This resulted in a request for a specification change of from 3g to 6g shock requirements. The Commission approved the January 5th preliminary results with the dynamic specification changes on March 7. No other specifications were changed.

Other significant accomplishments during this report period are summarized below:

- A system design and trade-off study to investigate possible means of improving system performance was initiated.
- Fuel capsule weld development work was initiated.
- Ultrasonic weld testing was started at Battelle Northwest Laboratories.
- The biological shield plug design was completed.
- Wrapping of the SNAP-21 residual Phase I insulation system was completed.
- Three tension tie rods and a neck tube were selected as the biological shield support system.

- Insulation system offgassing tests continued.
- Insulation system vacuum sealoff and getter retention tests continued.
- The segmented retaining ring design was analyzed and a design change was prepared.
- Seven candidate pressure vessel materials were examined and a candidate material (Ti 621. 8) was selected.
- The design for the second three development generators (in-line concept) was initiated.
- Generator test equipment design parameters were established and long lead time items were placed on order.
- The Quality Program Plan was revised and released.
- Test plans for Naval Radiological Development Laboratory testing of fuel capsules and SNAP-21 materials were completed.
- Cold end heat transfer tests 4 through 15 were completed.
- Thermoelectric leg inspection testing was initiated.
- Arrangements for radiation testing of the SNAP-21 biological shield in the insulation system were completed.

2.0 TASK I– 10-WATT SYSTEM

The dynamic load criteria subtask was completed during this report period. The results indicated that the shock requirements for the system should be increased from 3g to 6g with the vibration levels remaining at 3g peak.

A systems design and trade-off study was initiated to evaluate possible means of increasing performance.

The following sections contain the results of design and analytical studies conducted for each component during the report period.

2.1 SYSTEMS ENGINEERING

2.1.1 DYNAMIC LOAD CRITERIA SUBTASK

The Dynamic Load Criteria Study, initiated in October 1966, was completed during this report period and the final report, "Dynamic Load Criteria Study", MMM 3691-13, was submitted on March 3, 1967.

The most significant finding of this study was that the existing system design specification for shock capability was inadequate. Consequently, it was recommended that the specification for shock capability be increased from the original limit of 3g in 6 ms to 6g in 6 ms. The Commission accepted this recommendation.

2.1.2 SYSTEM DESIGN AND PERFORMANCE TRADE-OFF STUDY

This study consisted of an analysis of each component in the SNAP-21 System, thereby obtaining sufficient information to make logical trade-offs in terms of system efficiency, performance, size, weight, and potential increases in reliability. Based on this study, recommendations for changes to the present component design were made which would benefit the overall SNAP-21 Program. Details of the work done are given in Section 2.2, Component Design and Development.

Although some improvements have been made in components, a system integration analysis has not yet been performed to determine what effect they will have on overall system efficiency. In the SNAP-21 system, overall system efficiency is directly related to the heat leak through the biological shield support system. Consequently, a reduction in shield weight will permit a reduction in the structual capability of the support system and thus reduce the heat leak and increase system efficiency. Since the shield size, and thus weight, is directly related to the size of the heat source, several methods of reducing the heat source size were investigated. The more promising methods are described below.

The system integration analysis will be performed when component designs are made final. The following paragraphs summarize the results of this study:

a) Fuel Form

Strontium oxide was investigated as a possible replacement for the strontium titanate now being used. Because it has a greater power density than the strontium titanate, strontium oxide would permit using a smaller capsule and therefore a smaller, lighter weight shield.

Strontium oxide is more soluble in sea water than strontium titanate and thus could be somewhat more hazardous if the fuel capsule were to broach. However, since complete containment is a requirement, the solubility is not considered a major problem.

b) Fuel Capsule

Changing the geometry of the fuel capsule from a cylindrical to spherical shape was also considered as a means of lightening the system. However, because of the long development program required for a spherical capsule and the difficulty of wrapping insulation material around the shield surface, the spherical capsule will not be used for the 10-watt system.

c) Biological Shield

In an attempt to reduce the weight of the biological shield, a spherical shield was investigated in conjunction with the spherical fuel capsule. The fabrication of such a shield is feasible and a weight saving of approximately 30 pounds could be realized.

Further weight reduction could be made by allowing a higher radiation level at the surface of the system. If the allowable radiation level were increased from 200 mr/hr at the surface and 10 mr/hr at one meter from the surface to 500 mr/hr at the surface and 25 mr/hr at one meter from the surface, the resulting weight saving with respect to the present design would be approximately 45 pounds.

Tungsten was considered as a shield material and calculations were made using the strontium oxide fuel form and 200 mr/hr radiation level. The results indicated about 60 pounds increase in weight over the present design.

Because the biological shield is an integral part of the insulation system, a spherical shield would considerably increase the difficulty of wrapping insulation around it. Because of this and the difficulty of supporting and assembling the shield and insulation system, the spherical shield concept was discarded for the 10-watt system. The higher radiation level concept was also discarded since the technical specification requires the unit to be designed to 200 mr/hr. 3M feels that negotiations required to change the specification would not be completed in sufficient time to incorporate the concept into the system.

d) Insulation System

In an effort to reduce the heat loss from the system, ceramic compression supports were investigated for use with a neck tube bellows as an alternate biological shield support system. Although the calculated total heat loss through this insulation system would be 24.9 watts, technology using ceramic material is not sufficiently advanced to ensure success in this application.

Gas filled MIN-K 1301 was also considered. The total system heat loss is 40 watts greater than the heat loss through the present insulation system. This was calculated using a 1-inch thickness of MIN-K with a 4-inch long neck tube. With a MIN-K system of the present size, the heat loss would be 100 watts greater than the heat loss through the present insulation system design. The cost of the MIN-K insulation system is much less than the current foil and spacer system and the time saved in assembly of an insulation system using MIN-K would be approximately one month compared with a foil and spacer type. However, in order to meet the technical specification requirements the decision was made to use the Linde insulation system.

e) Segmented Retaining Ring

A detailed analysis was made of the segmented retaining ring assembly. The analysis was made to determine the redesign required to make the ring capable of withstanding the specified dynamic environment, and to improve the heat rejection path from the generator cold frame to the pressure vessel wall. The hold-down ring is required to compensate for deflection of the pressure vessel wall under 10,000 psi external pressure without transmitting the loads to the generator or the insulation system.

The results of the analysis are as follows:

1. The total vertical spring force must be increased by 70 percent to ensure that vertical movement does not occur between the insulation system and the pressure vessel.

2. A lubricant will be used between contact surfaces to ensure movement under external pressure and to increase the heat transfer between contact surfaces. The pressure angle between the segments and the insulation system will be changed to provide a balance between the vertical and horizontal forces. This balance of forces is required to ensure that the segmented ring maintains uniform contact on the pressure vessel wall.

f) Pressure Vessel

An analysis of the pressure vessel was conducted to evaluate the following materials:

Titanium Alloy 621.8

Beryllium Copper Alloy

Corrosion Resistant Steel Alloys

High Strength Steel Alloys

Aluminum Alloys

The materials were compared primarily on the basis of strength, weight, corrosion resistance and thermal conductivity. Titanium alloy 621.8 is the only material which met the size and weight specifications. It provides the greatest structural strength for its weight and also has the best known corrosion resistance for deep sea applications.

g) Thermoelectric Generator

The following areas were analytically evaluated in an attempt to improve the thermoelectric generator:

1) Methods of lowering cold end temperature.

2) Use of either MIN-K 1301 or micro-quartz for insulation within the generator.

3) Use of argon or xenon backfill gas.

4) Use of 347 stainless steel or Hastelloy-C for the outer case.

5) Decrease electrical resistance at cold end of the thermoelectric leg.

6) Use of aluminum or copper for the cold frame material.

The following variable parameters are being evaluated experimentally to determine the optimum generator design:

1) Follower hole depth of 2.213 inches versus that of 0.500 inches.

2) Argon versus xenon backfill gas.

3) MIN-K 1301 versus micro-quartz insulation.

4) Hastelloy-C versus 347 stainless steel outer case.

5) Aluminum versus copper cold frame.

6) Ball and socket versus in-line follower concept.

The above variables have not yet been sufficiently analyzed to make a decision on the final design of the SNAP-21 generator.

h) Power Conditioner

A study of the power conditioner component performance was made. Component vendors were contacted to determine whether components with higher efficiency could be produced. Response from vendors indicates that standard components are not available and that efficiencies higher than in the present power conditioner cannot be attained. This problem will be investigated further, but until some indication of improvement in the present design is apparent, no redesign of this component will be made. The demonstrated efficiency of the present power conditioner is 89 percent.

2.2 COMPONENT DESIGN AND DEVELOPMENT

2.2.1 FUEL CAPSULE

2.2.1.1 Heat Source Trade-Off Study

The major influence of the heat source on the system is the effect it has on the size and weight of the biological shield. Several approaches may be used to minimize shield weight; the more promising are described here.

a. Fuel Form

A fuel form with a higher power density than the strontium titanate ($SrTiO_3$) now being used would reduce the size and weight of the capsule and shield. Strontium oxide (SrO) was investigated as a possible replacement. It has a power density of 1.5 watts/cm^3 as compared to 0.85 watt/cm^3 for strontium titanate. Although calculations show that strontium oxide would permit an appreciably lighter capsule and shield, it is more soluble in sea water than strontium titanate and could thus present a greater safety hazard if the fuel capsule were to broach. This characteristic must be more fully evaluated before a decision is made.

Current fuel fabrication techniques at Oak Ridge National Laboratory use a hot press method wherein a platinum jacket encases the fuel pellet during pressing. This platinum jacket eliminates the need for the stainless steel inner liner. The interaction of strontium oxide with the platinum clading should not be significantly different from that of strontium titanate.

b. Fuel Capsule

The capsule design is another area where weight reduction could be achieved. Calculations were made to determine what possible advantage there might be in a spherical fuel capsule; the results are shown in Figure 2-1. Note that the calculations were made considering strontium oxide as the fuel. (The calculations are given in Appendix A.)

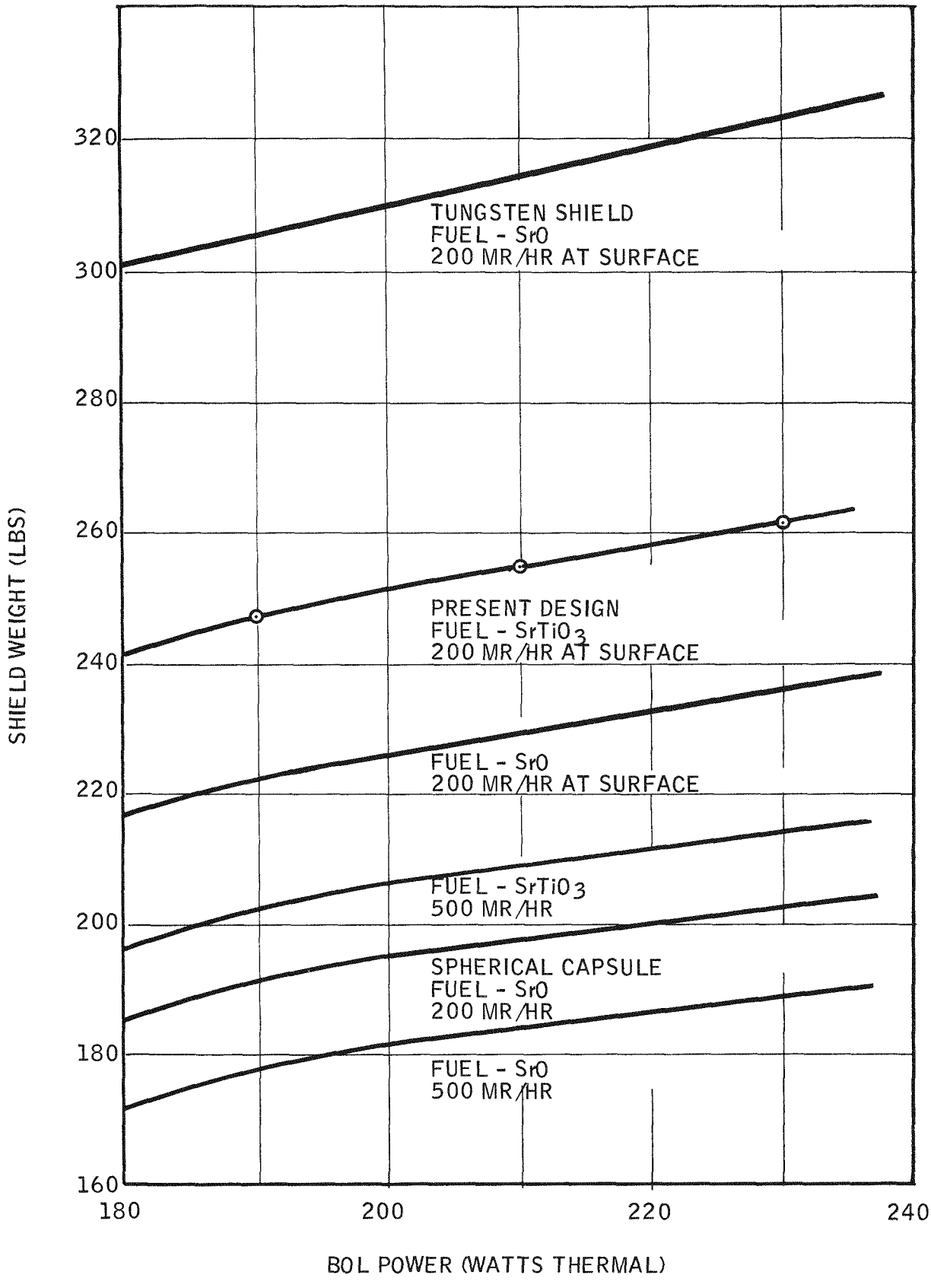

Figure 2-1. Effect of Fuel Form, Radiation Level, Capsule Geometry and Shield Material on Shield Weight

c. Biological Shield

Two methods were evaluated for directly effecting a shield weight reduction. Consideration was given to relaxing allowable radiation levels to 500 mr/hr at the system surface and 25 mr/hr at one meter from the surface (Figure 2-1). The use of tungsten was considered as an alternate to depleted uranium – 8% molybdenum alloy shield material. Although it has a high density, the much lower absorption cross section of the tungsten results in an appreciable increase in shield weight.

A spherical shield would be required with the spherical fuel capsule. Such a design is feasible – both Oak Ridge and Battelle Northwest Laboratories can fabricate the capsule – and the weight saving would be about 30 pounds over the present design. At relaxed radiation levels, the weight saved would be about 45 pounds.

Because of the long development program required for a spherical fuel capsule, the complexity of wrapping insulation material around a spherical surface, and because of the difficulty in supporting and assembling a spherical shield, the concept of a spherical shield and capsule has been discarded for the 10-watt system.

2.2.1.2 Weld Development

The fuel capsule weld design approach has been mutually agreed to by Oak Ridge National Laboratory (ORNL) and 3M. The design features a shoulder support for the end plate and a 0.100 inch minimum weld penetration with a single tungsten-inert gas (TIG) weld pass. ORNL now has capability to perform "in cell" electron beam welding and this method is also being considered.

Four fuel capsule weld development samples were prepared and preliminary weld closures were made at ORNL. Subsequently eight additional samples were fabricated from Hastelloy-C tubing. Two closure welds per capsule were made; five of them by the TIG process and three by electron beam. An additional set of four is being fabricated for electron beam closure, since the

weld conditions are not as well established. Alsimag 614, encased in a stainless steel envelope, serves as a fuel simulant for weld development capsules. Figure 2-2 illustrates the weld profile sought. These capsules are currently being ultrasonically tested at Pacific Northwest Laboratory.

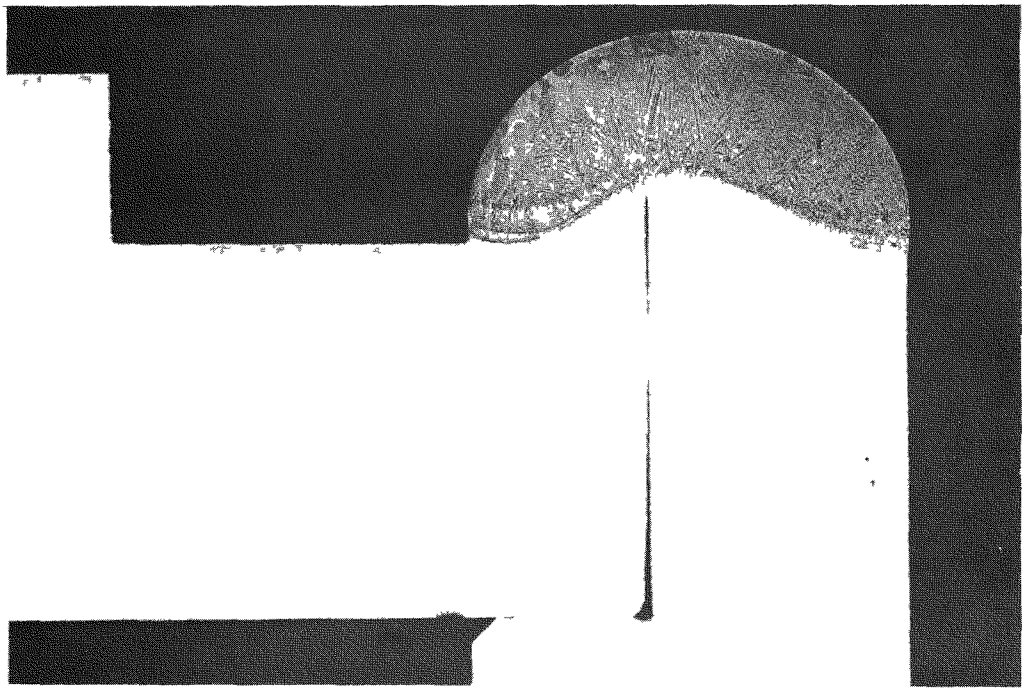

Figure 2-2. Welded at 170 amps, 60 sec/rev Travel Speed with Electrode Centered on Joint. Penetration - 0.090 inch. Magnification 10X.

Some modification of the design to accommodate ultrasonic testing may be required since the shoulder is not as desirable as a reference point as the top outside edge. The outside edge is currently melted over. This is undesirable not only because of the loss of an ultrasonic reference point, but because additional clearance must be provided for capsule insertion.

If the fuel form were changed to strontium oxide, the capsule size would be reduced somewhat; however, it is expected that welding conditions will change only slightly. The first two sets of capsules are of the size required for the strontium titanate ($SrTiO_3$) fuel form. Fuel form will be selected in time for modification of subsequent sets of development capsules.

The Commission expressed concern that the use of bar stock for the fuel capsule could result in stringers which would create paths for accelerated corrosion in sea water. The manufacturer of Hastelloy-C indicated that the probability of stringers in bar and plate would be very low. Since they start with a 20-22 inch diameter ingot, which is reduced by forging, they state that little improvement would be gained from further forging. Additional investigation of this potential problem area will be conducted.

The manufacturer recommended the modified Hastelloy-C-276 which, by virtue of its low carbon and silicon content not only reduces the possibility of stringers but has slightly better welding properties.

Cost comparisons were made for three methods of fabrication being considered. The methods are illustrated in Figure 2-3. Welding and non-destructive testing costs must be added to the manufacturing costs shown in Table 1 to obtain true cost comparisons. The use of tubing for the capsule body entails two welds and requires additional non-destructive testing. Also, fabrication by forging incurs substantial tool costs. The accompanying reduction in machining costs are further offset by this expense. Lead times given are for the 276 alloy. A supply of standard Hastelloy-C is on hand and will be used for weld development. Additional stock can be procured with a short lead time.

FORGING

1.

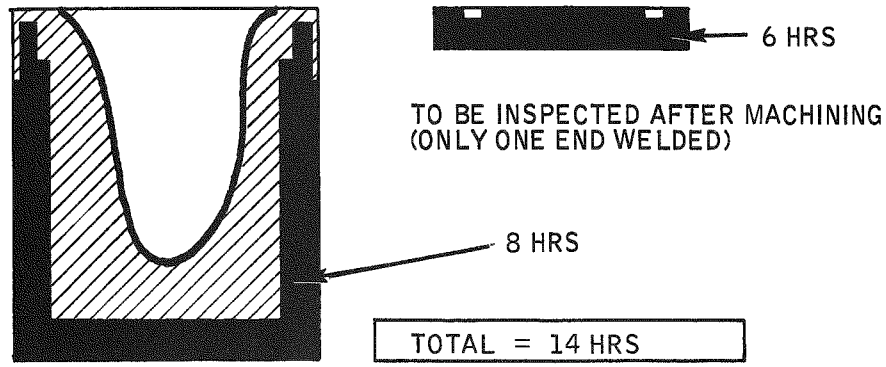

TUBING

2.

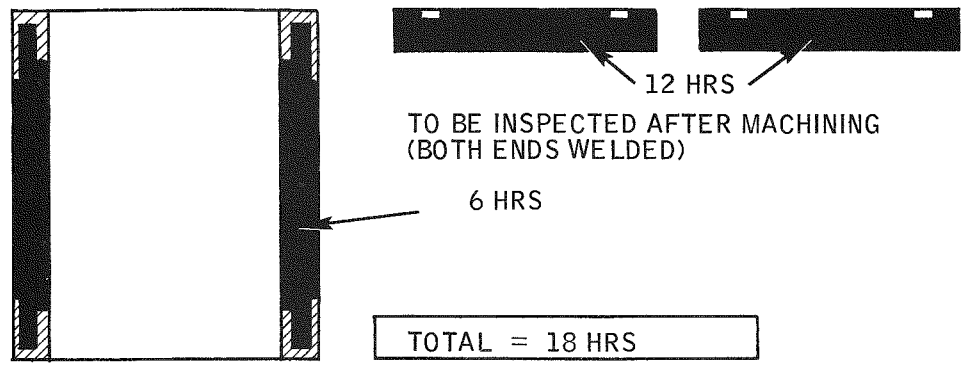

BAR STOCK

3.

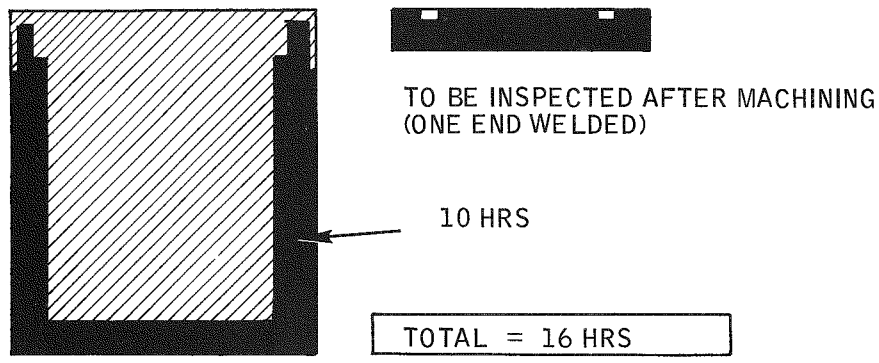

Figure 2-3. Fuel Capsule Fabrication Methods

Table 1. Fuel Capsule Fabrication Cost Comparison

	Tube	Bar Stock	Forging
Material Cost	$75.00/ft.	$4.00/lb.	$4.00/lb.
Capsule Dia. (inches)	3.198	3.198	3.198
Capsule Length (inches)	3.332	3.332	3.332
Length Req. for Fabrication (inches)	3.5	3.5	3.5
Vol. Bar/Capsule (in^3)	-----	28.21	-----
Capsules/Foot of Tube	3.4	-----	-----
Density of Mat'l. ($\#/in^3$)	0.32	0.32	0.32
Wt. of Bar/Capsule (lb)	-----	9.027	9.027
Mat'l. Cost/Capsule	$22.10	$36.10	$36.10
Machine Time/Capsule	18 hrs.	16 hrs.	14 hrs.
Machine Cost/Capsule	$144	$128	$112
Cost Forging/Capsule	-----	-----	$35-$50
Tot. Cost/Capsule	$167	$165	$183-$198
Tot. Cost/10 Capsules	$1,670	$1,650	$1,980
Tot. Cost/50 Capsules	$8,350	$8,250	$9,900
Forging Tooling Cost (if not available)	-----	-----	$1,000-$1,500
Lead Time (weeks)	57	28	30

2.2.2 BIOLOGICAL SHIELD

The design of the biological shield plug has been completed. Hastelloy-C or -X, separated by a compatibility barrier, will be used to encase the uranium-8 molybdenum alloy. The compatibility barrier material will be the same as that used for the biological shield inner liner as determined during compatibility testing. Details of the plug are shown in Figure 2-4.

Since creep and tensile strength data are lacking for depleted uranium-8 molybdenum alloy at the operating temperature of the shield, special test specimens will be prepared to simulate actual load conditions of the shield mounting bolts to verify the design parameters used.

2.2.3 INSULATION SYSTEM

2.2.3.1 Linde Subcontract

Linde has continued work under letter subcontract AT(30-1)-3691-5511. Work has progressed on the assembly of the SNAP-21B Prototype, analysis of the structural support of the biological shield, development testing, and development test procedures.

a) SNAP-21B Prototype

The completed cylindrical wrap of the insulation is shown in Figure 2-5. The outer protective nickel foil is seen in the center of the unit. The quartz paper extends past the edges of nickel foil.

To minimize the insulation buildup, it was necessary to cut the end of the cylindrical insulation into sections and fold the sections back as shown in Figure 2-6. Each tab was wrapped tightly around the radiation shield and welded to the nickel disk. The buildup was checked at ten-layer intervals as shown in Figure 2-7. Each successive insulation composite was installed in the above manner, thus completing the lower head (Figure 2-8).

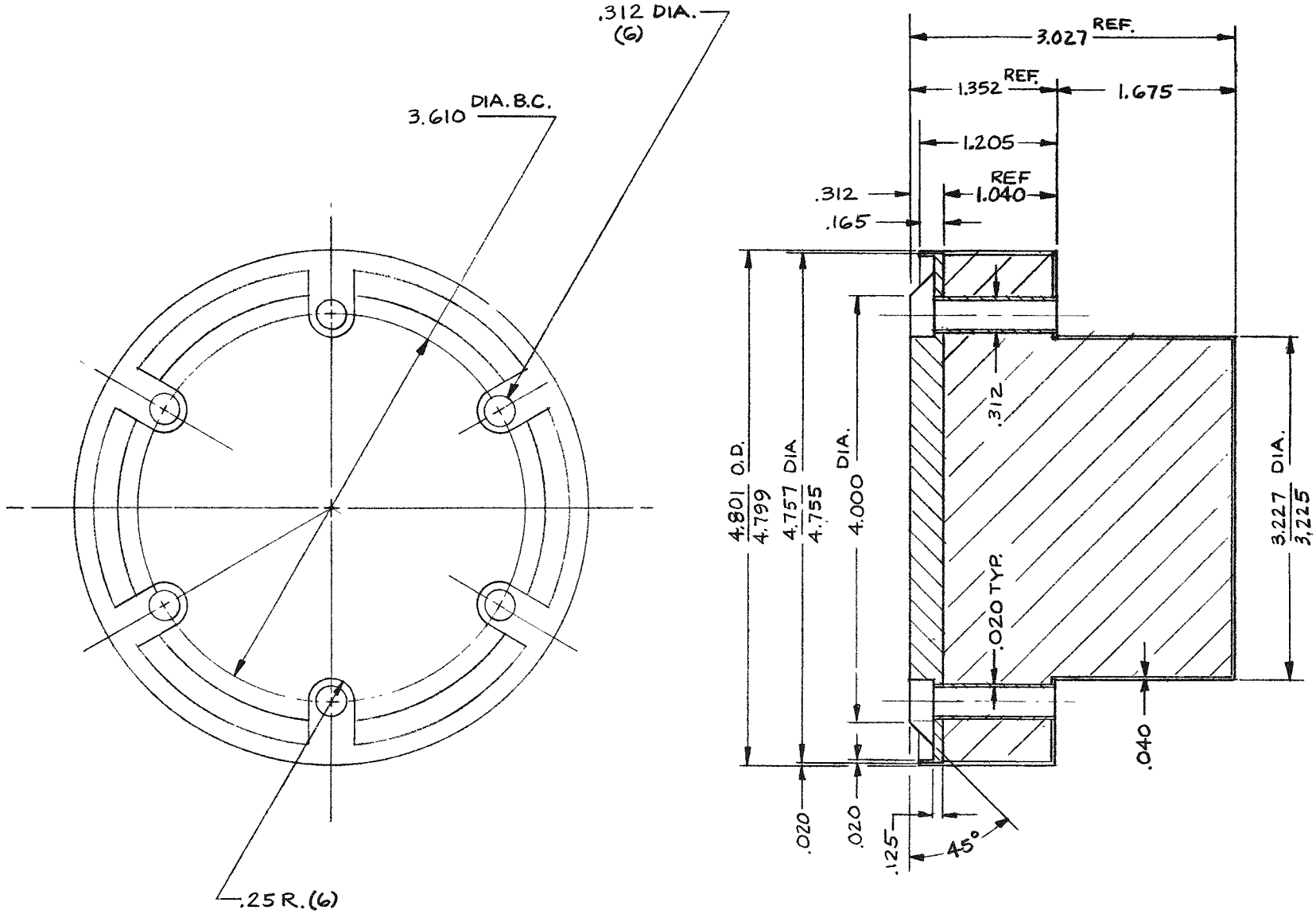

Figure 2-4. Biological Shield Plug Details

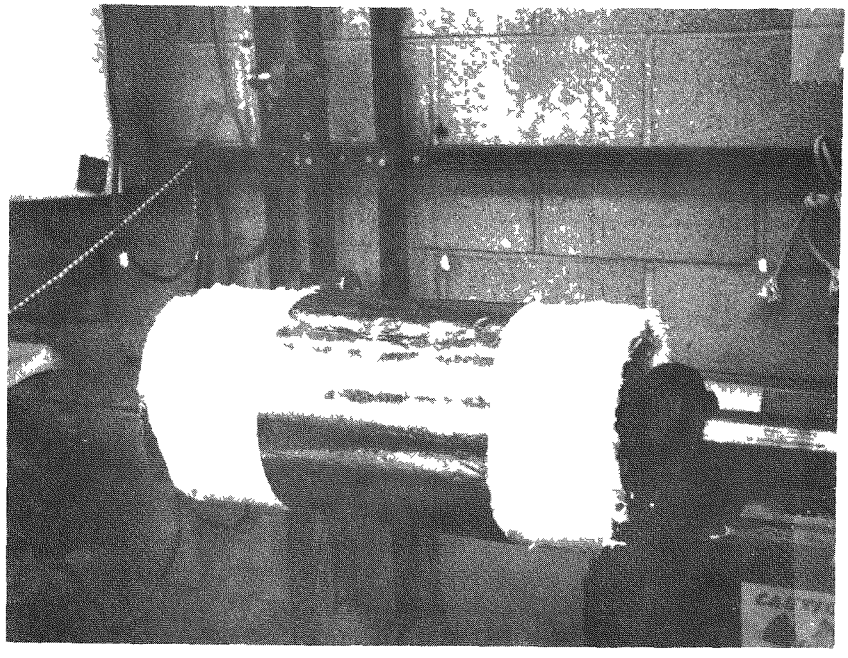

Figure 2-5. SNAP-21B Prototype - Cylindrical Insulation Installed

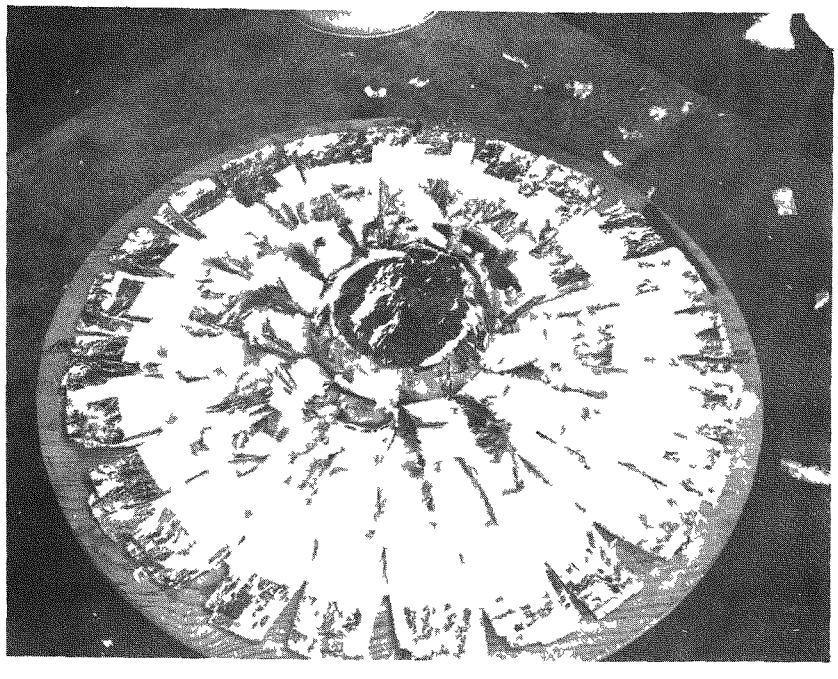

Figure 2-6. SNAP-21B Prototype - Lower Head Insulation Cut Back

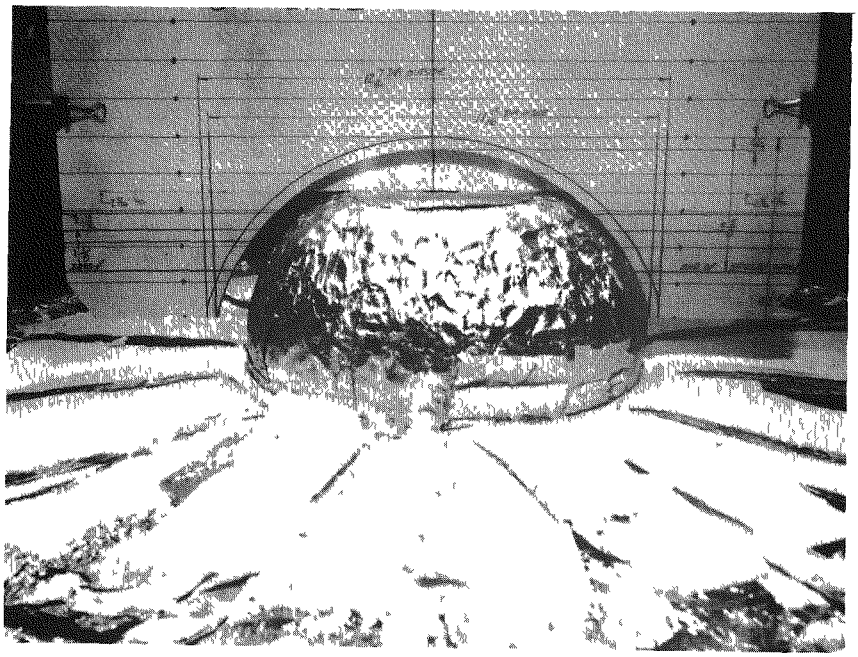

Figure 2-7. SNAP-21B Prototype - Measuring Insulation Buildup

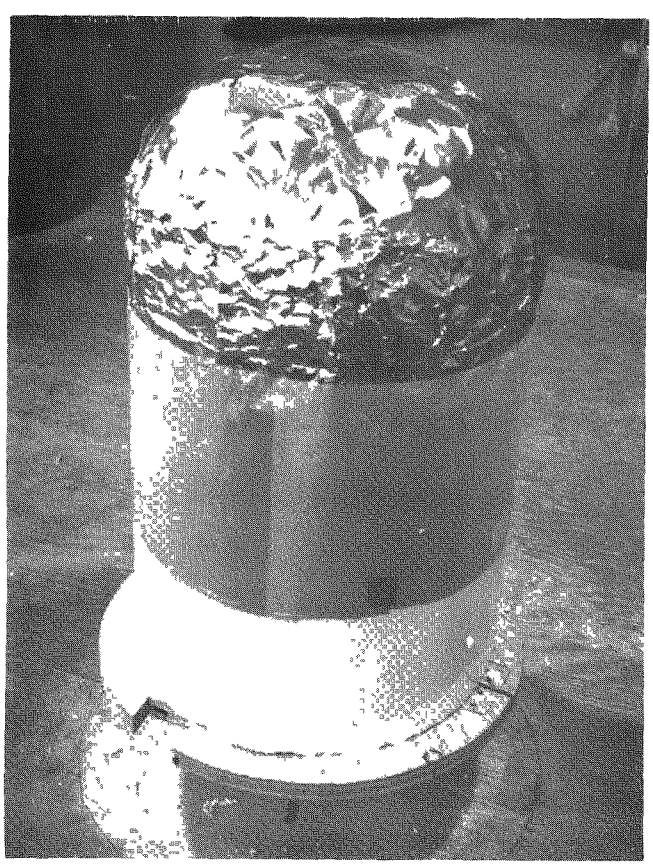

Figure 2-8. SNAP-21B Prototype - Completed Lower Head Insulation

With the lower head completed, the radiation shield was inverted in the test stand and supported by the test stand shaft. The top cylindrical insulation wrap was cut into segment tabs and folded back as shown in Figure 2-9. Three layers of quartz cloth insulation were installed on the neck tube. This was protected by a plastic sheet which was raised as the insulation tabs were folded into a washer-type disk. The weld was then performed. Figure 2-10 shows the insulation of the top head in progress with the nickel foil-quartz paper composite being applied.

Drawings of the upper and lower head of the vacuum enclosure and the top works, which includes the getter package and the seal-off valve, were prepared. These components were fabricated and assembled onto the unit, after which the girth weld was made and a leak check was performed. The unit was instrumented with thermocouples, the heaters were placed in the unit and the conditioning process was begun. The temperature of the shield rose steadily to 1430°F with a constant 100-watt input of one heater. The temperature would not rise above this point even though the calculated heat loss was only 70 watts. After approximately 48 hours of 100-watt input, with the shield temperature remaining at 1430°, the heater burned out. The spare heater was energized and it also burned out within a few hours. The internal pressure in the insulation system at this point was 60 microns. The unit then had to be cooled to remove the heaters and block from the unit. The heater block will be machined for larger diameter heaters and two heaters, connected in parallel, will be inserted into the heater block. This will reduce the heater power density and should allow the shield temperature to reach the desired 1550°F for further processing.

b) Structural Support of the Biological Shield

The biological shield support system has been re-evaluated with the objective of reducing the insulation system heat loss. A parametric study was performed to show the estimated heat loss. Some of the parameters investigated were:

1) Neck tube length.
2) Increasing neck tube length and insulation thickness.
3) Increasing neck tube length with reduced shield weight.
4) Ceramic compression rods with bellows type neck tube.

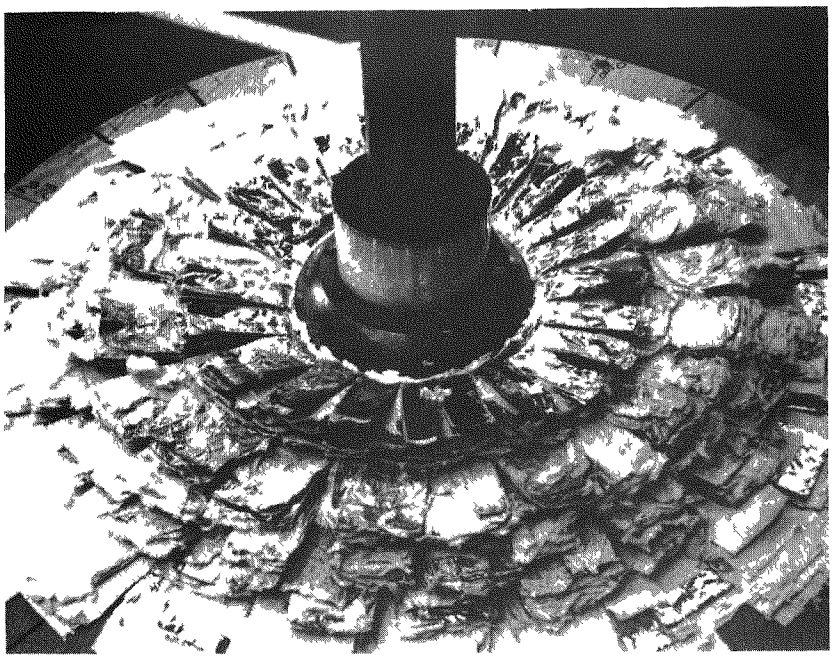

Figure 2-9. SNAP-21B Prototype - Upper Head Insulation Cut Back

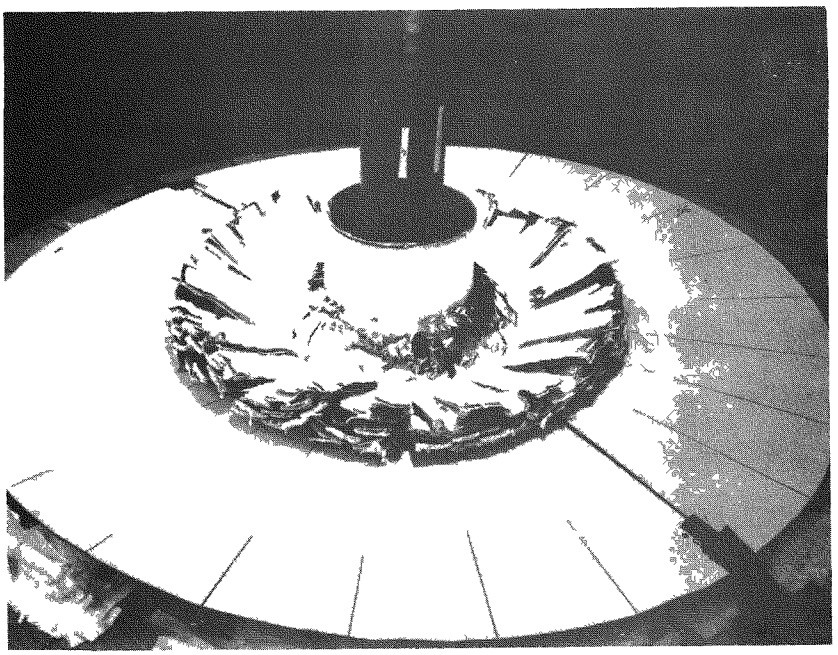

Figure 2-10. SNAP-21B Prototype - Installing Upper Head Insulation

Results of this investigation are shown below:

Variable Length Neck Tube				
Neck Tube Length (in.)	Q Neck Tube	Q Rods	Q Insulation	Q Total
2.5	20.4	21.5	9	50.9
3.25	15.7	22.7	9	47.4
4.00	12.8	23.9	9	45.7

Variable Length Neck Tube With One Inch Larger Outer Enclosure Diameter				
Neck Tube Length (in.)	Q Neck Tube	Q Rods	Q Insulation	Q Total
2.5	20.4	21.5	7	48.9
3.25	15.7	22.7	7	45.4
4.0	12.8	23.9	7	43.7

Four-Inch-Long Neck Tube with Reduced Shield Weight				
Shield Weight Reduction (lb)	Q Neck Tube	Q Rods	Q Insulation	Q Total
30	11.5	18.2	7	36.7
60	11.5	16.3	7	34.8
90	11.5	14.4	7	32.9

If six ceramic (ZrO_2) compression supports with a 0.008 inch thick Hastelloy-X bellows neck tube were used, the following heat loss could be achieved using the present geometry:

Neck Tube Length (in.)	Q Bellows	Q Rods	Q Insulation	Q Total
2.5	6.9	9	9	24.9

The compression rod supports with bellows should be considered if the heat loss goal is to remain at 30 watts. It does not appear that the tension rod support systems will achieve a heat loss of 30-watts or less.

Although the total calculated heat loss through the insulation system would be only 24.9 watts using the ceramic compression rods, the technology using ceramic material is not sufficiently advanced to ensure success in this type of application. The decision was therefore made to discard the ceramic compression rod concept.

A detailed analysis of the biological shield support system has been started. Using a molybdenum spider arm approximately 2-1/2 inches long and tension rods approximately 3-1/2 inches long, the angle of the tension rod is 11° -39', as shown on Figure 2-11. Figure 2-11 is a preliminary concept of the tension tie rod support system.

It will be necessary to adjust the tie rod positions to eliminate stress buildup in the rods due to heat-up.

2.2.4 SEGMENTED RETAINING RING

The segmented retaining ring must prevent movement of the insulation system under dynamic load conditions, and yet allow relative motion between the pressure vessel and the insulation system during pressurization. To meet these requirements, the pressure areas between the ring segments and the insulation system must be controlled to produce forces in the proper directions and at proper values. Also, friction forces should be kept as low as possible to permit movement of the individual segments to compensate for manufacturing tolerances, and adaptation to shock and vibration induced motions.

A more certain location of contact between the parts involved should be achieved by changing the ring segment contour, as shown in Figure 2-12. Figures 2-13 and 2-14 indicate the approximate location and magnitudes of the vertical load "P" forces involved. The reacting force at the cylinder wall must pass through the intersection of the vertical load line (produced by the spring) point. If the contact point is allowed to move down far enough, the reacting force can move down below the bottom edge of the segment. In this condition, contact between the segment

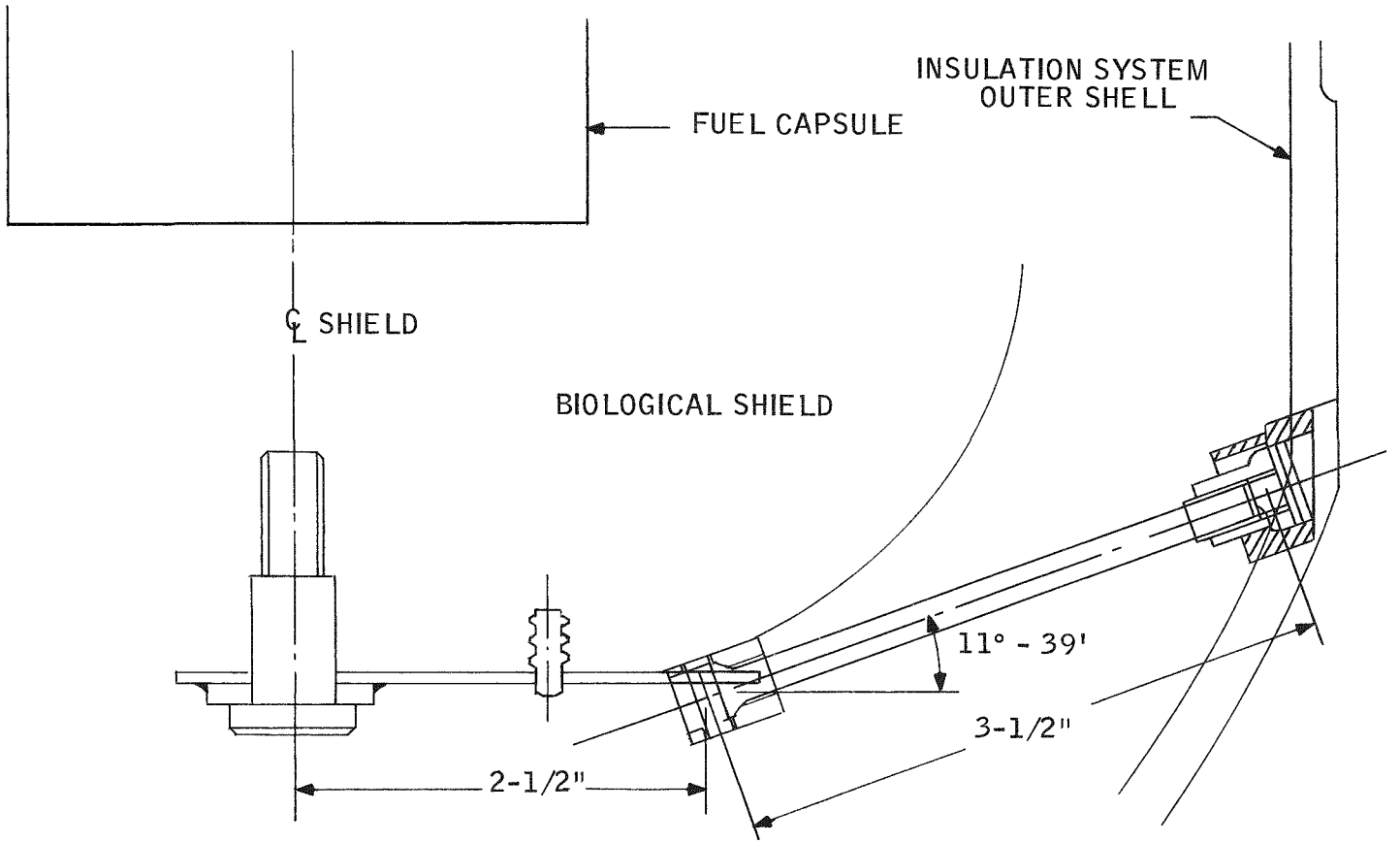

Figure 2-11. Tension Rod Support Concept

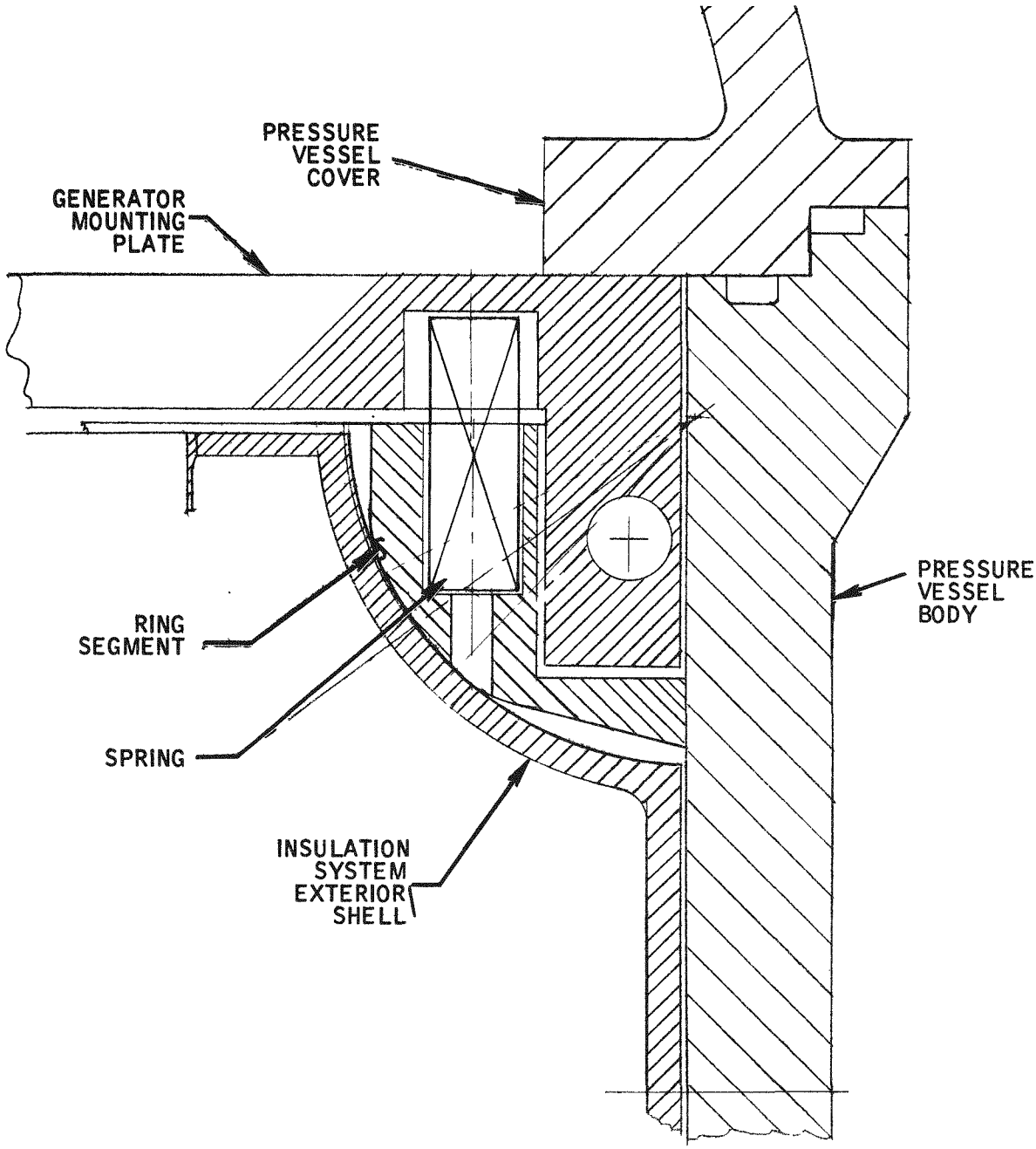

Figure 2-12. Segmented Retaining Ring Configuration Showing Revised Segment Contour

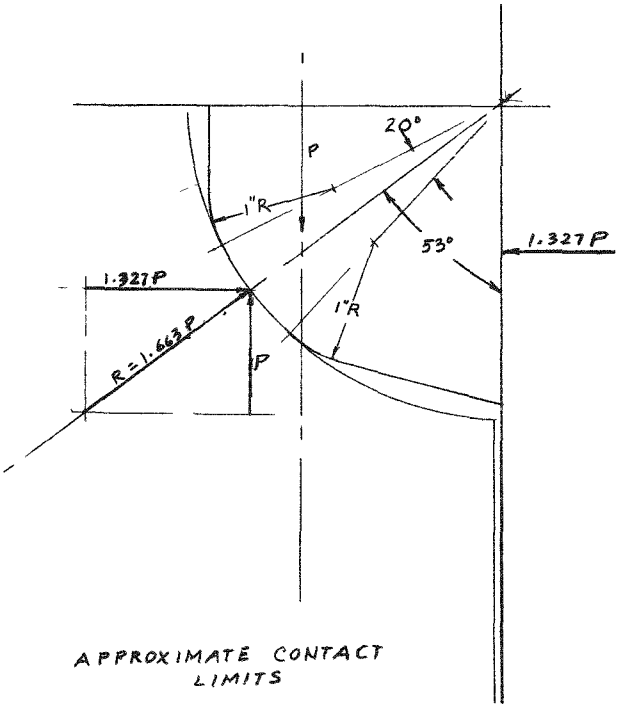

Figure 2-13. Segmented Retaining Ring, Approximate Contact Limits

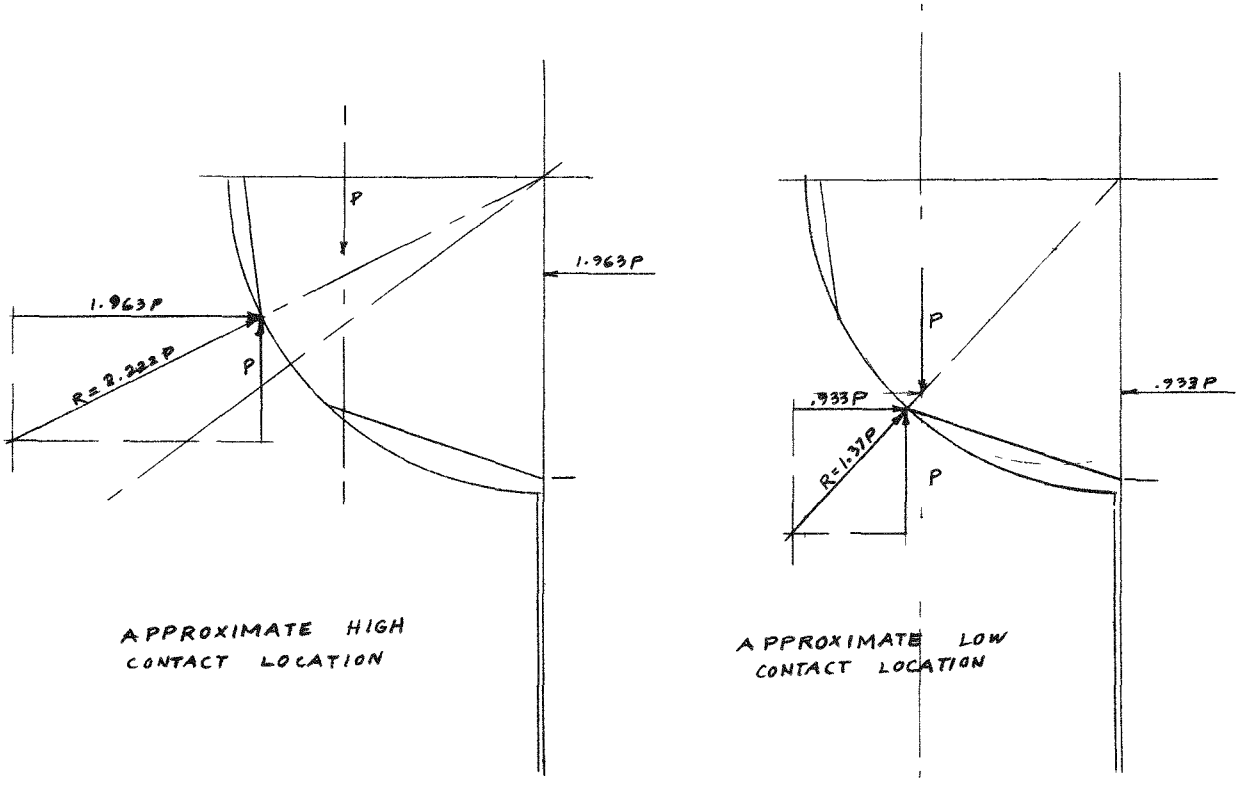

Figure 2-14. Segmented Retaining Ring, Approximate High and Low Contact Locations

and the pressure vessel wall would be uncertain. In addition, the horizontal forces involved would become very small and would not adequately position the insulation-generator system.

An analysis of possible tolerance buildup between the segmented retaining ring, pressure vessel and insulation system envelope has been conducted. The analysis indicates that under certain conditions tolerance build-up can cause the contact between the segment and insulation envelope to occur at unfavorable locations. The segment design is therefore being revised to limit the possible contact area to the area calculated to produce desirable results.

The following contact surfaces will be coated with either an aliphatic grease or one of the dry lubricants to reduce friction forces and assure that the segments will adapt readily to the existing geometry:

1) Between segment and insulation envelope.

2) Between segment slot wall and vertical protrusion on generator mounting ring.

3) Between segment face and pressure vessel wall.

The lubricant will serve a dual purpose. Besides reducing friction forces, it will improve heat conductance between the various contacting surfaces.

The friction forces cause considerable shock and vibration damping. However, the possibility of motion occurring may be reduced by increasing the vertical spring force to a point where the insulation and generator system will not move.

2.2.5 PRESSURE VESSEL

The past quarter was devoted to determining the pressure vessel parameters required for various materials. Pressure vessel weights were then approximated using the resulting dimensions.

Individual materials examined were:

1. Glass
2. Titanium alloy 721 (Ti-7Al-2Cb-1Ta)

3. Titanium alloy 621.8 (Ti-6Al-2Cb-1Ta-0.8 Mo)
4. Berylco alloy 165 (Cu+1.6 to 1.8 Be-0.2 to 0.3 Co)
5. Aluminum alloy 6061-T6
6. Corrosion resistant steel alloy 17-4PH
7. High strength steel alloys

For each material calculations were performed to determine minimum wall thickness for the cylindrical portion and for the two hemispheres. In each case wall thickness was based on two criteria. First was the restriction that, when considered as a thick-walled shell, the direct elastic compression stresses should not exceed the allowable compression yield stress of the particular material for an applied hydrostatic pressure loading of 15,000 psi. For the cylindrical portion, the desired relationship is given by:

$$f_{cyl} = \sqrt{\frac{3}{2}} \left(\frac{R_o^2 p}{tR} \right)$$

where:

f_{cyl} = max stress in cylinder wall (psi)

R_o = radius to outer surface (in.)

R = radius to median surface (in.)

t = wall thickness (in.)

p = applied external pressure (psi)

For the hemispheres, the equivalent expression is

$$f_{hem} = \frac{3p}{4t} = \left[\frac{(2R + t)^3}{12R^2 + t^2} \right]$$

where the symbols have the same definitions as previously.

With a 3 to 4 percent decrease in accuracy, the much simpler equation given below may be used

$$f'_{hem} = \frac{pR_o^2}{2Rt}$$

The second criterion is imposed by the possibility of shell-buckling due to the external pressure loading. Shell thickness must be great enough to preclude budkling from taking place. For the cylindrical portion, the critical buckling pressure is:

$$p_{Cr_{cyl}} = \left(\frac{4E_t}{1-u^2}\right)\left(\frac{t}{D_o}\right)\left(\frac{t}{D}\right)^2$$

where:

E_t = Tangent modulus for the material, evaluated at the existing stress level

u = Poisson's ratio

t = Wall thickness (in.)

D = Mean diameter (in.)

D_o = Outer diameter (in.)

For the hemisphere:

$$p_{cr_{hem}} = 0.84\sqrt{E_t E_s}\left(\frac{t}{R_o}\right)^2$$

where E_s = secant modulus for the material, evaluated at the existing stress level, and other symbols as previously defined.

Mean radius for the hemisphere was made equal to the mean radius of the cylinder in every case to keep discontinuity stresses at the juncture of the two portions as low as possible by eliminating the eccentricity.

No actual calculations were performed for a glass pressure vessel. The attractive properties of some of the compositions of glass considered useful for this purpose include: fair strength in compression, light weight, a reasonable modulus of elasticity, and excellent resistance to corrosion. The major negative characteristic is the time and expense involved in mechanical design and development testing required to produce a suitable means of joining the two parts and including the required electrical receptacle penetration. Results obtained by calculation for materials 2 through 6 above are presented in Table 2. A sample calculation is included in Appendix B. Calculations were not performed for any of the medium strength steels because, at allowable yield strengths in the range up to that of the corrosion resistant (17-4PH) steel considered, there would be no strength advantage. Density and modulus of elasticity are nearly the same but the added thickness of material, required initially to compensate for attrition due to corrosion, would give a relatively large increase in weight. There is little advantage in considering use of some of the newer steel alloys in the strength range from 170,000 psi yield and up. This is because the modulus of elasticity does not increase. This minimum material thickness would still be required to provide buckling stability.

Table 2 shows that the hemispherical ends use the compressive strength properties much more fully than the cylindrical portions do. This is because the stability of a cylinder against buckling due to external pressure is lower than for a sphere of equal wall thickness and radius. In every case but one, wall thickness of the hemispheres was governed by the compression yield allowable for the material. For all the cylinders, except 6061-T6, buckling stability was the designing criterion. For the isolated case where 6061-T6 material was used, the compression yield allowable is so low that the required thickness is for more than enough for buckling stability. The efficiency of using a material based on compression yield allowable is also presented in Table 2. Separate figures are given for hemispheres and cylinders. The figures for cylinders are not too meaningful when based on compression yield but they do serve as a relative index.

The source of data used for material strength characteristics requires some explanation. Shell buckling instability is a function of modulus of elasticity (E). For values of stress above the material proportional limit ($F_{p.l.}$) actual values of the modulus of elasticity will be less than E by a figure which depends on the shape of the particular stress-strain curve of the given material. The reduced modulus to be used

Table 2. Comparison of Pressure Vessel Characteristics for Various Materials

Material	721 T6	621.8 T6	Berylco 165	6061-T6	17-4PH
Density (lb/in^3)	0.163	0.162	0.298	0.098	0.282
Weight (lb)	133	141	230	268	198
Compression Yield (psi)	111,000	100,000	120,000	36,000	165,000
Proportional Limit (psi)	85,200	72,500	74,800	30,700	131,700
Modulus of Elasticity (psi)	19.5×10^6	17.0×10^6	19.0×10^6	10.1×10^6	27.5×10^6
Cyl. Wall Thickness (in.)	1.032	1.182	0.910	6.420	0.710
Cyl. Max. Stress (psi)	98,500	52,500	49,670	36,000	47,700
Cyl. Struct. Effic. (%)	88.7	52.5	41.5	100.0	28.9
Hemisphere Wall (in.)	0.511	0.580	0.465	2.50	0.335
Hemisphere Max. Stress (psi)	111,000	100,000	120,000	36,000	163,000
Hemisphere Strut. Effic. (%)	100.0	100.0	100.0	100.0	98.8
Cyl. Outside Diam. (in.)	14.56	14.86	14.32	25.34	13.92

can take any one of several different forms. On the basis of correlation with test data, many authorities agree that, for buckling stability of cylinders, a reasonable critical buckling value may be found by using the tangent modulus (E_t) in place of E. For spherical shells, the reduced modulus recommended takes the form $\sqrt{E_t E_s}$, where E_s is the secant modulus. These quantities are defined by the accompanying sketch of a typical stress-strain curve.

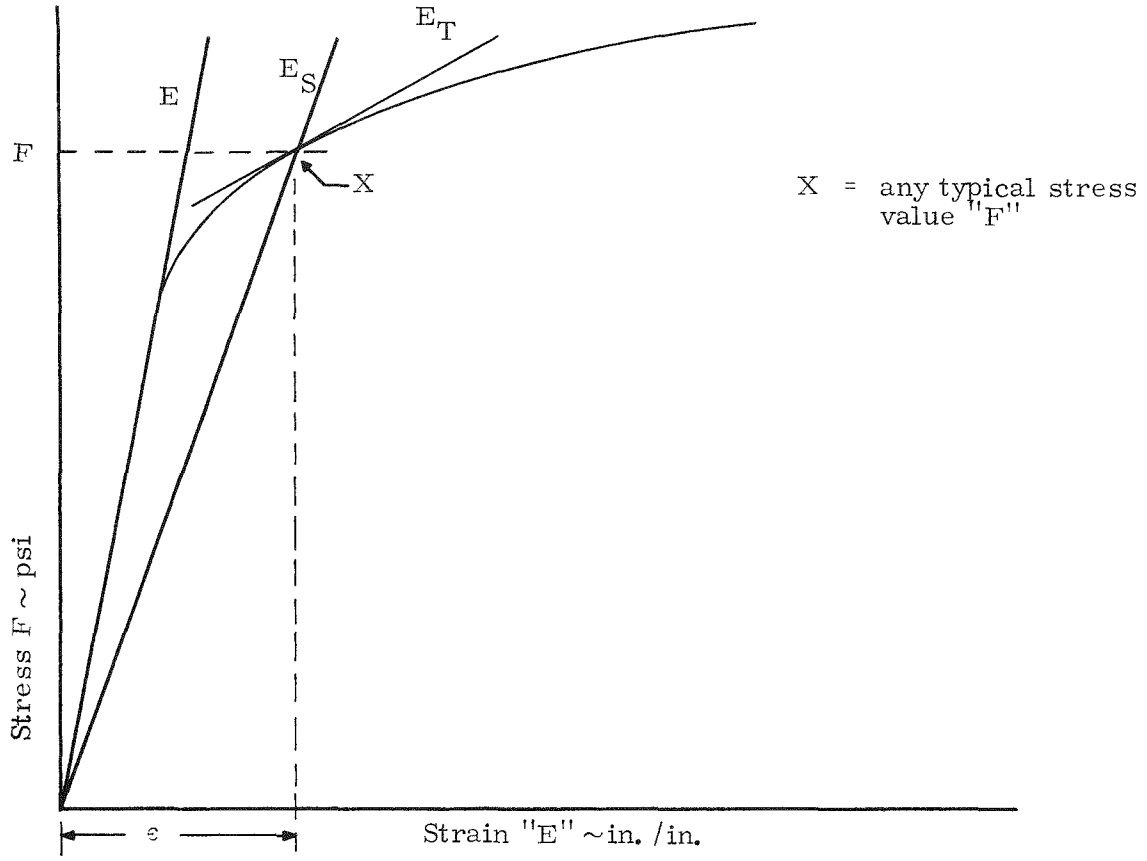

If an accurate stress-strain curve is readily available, E_s can be readily determined, but the slope of the tangent line, (E_t),is subject to some variation depending on the eye of the observer. Stress-strain curves are available from MIL-HDBK-5 and manufacturer's brochures. Material yield stress allowables, as obtained from manufacturer's brochures, are generally typical values. These values are based on a number of individual tests and represent the result of fitting a curve to the test data on probability basis. For design purposes we must work with minimum

guaranteed values, which lie on a curve through the lowest observed test points. Even then, it is necessary that the data used be the result of many tests. MIL-HDBK-5 gives both guaranteed minimum allowables and probability values (99 percent probability with 90 percent confidence levels) tabulated for many standard materials. Stress-strain curves and curves of E_s and E_t as given in the above source are based on the probability values and therefore should be modified for design purposes. A satisfactory method for providing design curves for stress vs. strain, and stress vs. E_s and E_t, is the analytical approach. Assuming that a probability based stress-strain curve is available, it is possible to draw a new curve through the desired yield point, affine to the original curve. The National Committee for Aeronautics T. N. 902, by Ramberg and Osgood, describes a method for writing analytical expressions for stress vs. strain based on three parameters. The method has been found to be quite accurate in relation to test data. The following sketch defines the three parameters used.

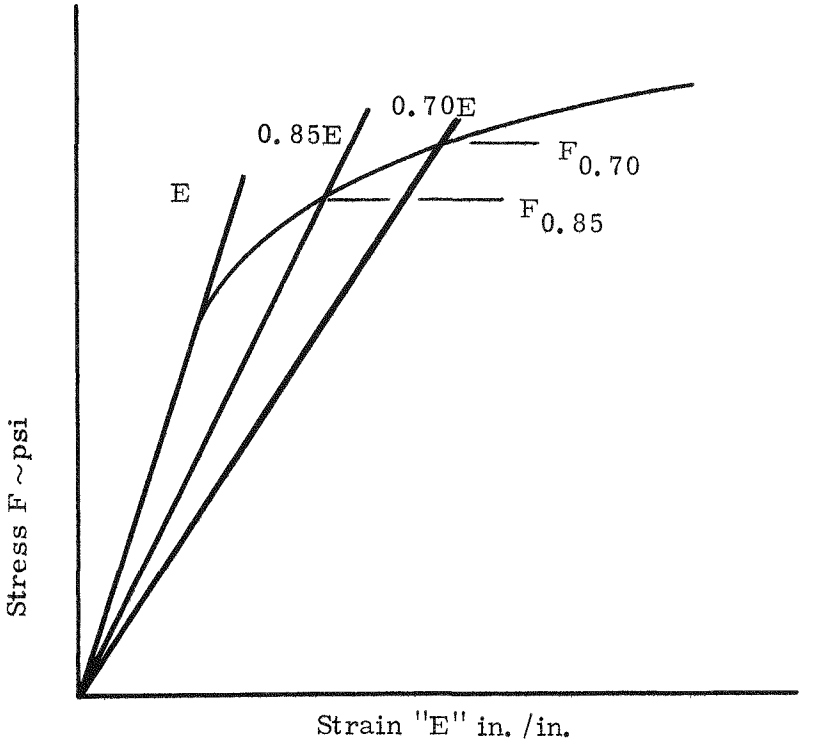

The three parameters used for defining the curves analytically are: E, $F_{0.85}$, and $F_{0.70}$. $F_{0.85}$ and $F_{0.70}$ are related by another factor defined as:

$$n = 1 + \frac{\ln \frac{17}{7}}{\ln\left(\frac{F_{0.70}}{F_{0.85}}\right)}$$

The desired relationship is given by:

$$E = \frac{F}{E}\left[1 + \frac{3}{7}\left(\frac{F}{F_{0.70}}\right)^{n-1}\right]$$

From the given stress-strain curve, "n" is determined by measuring values of $F_{0.70}$ and $F_{0.85}$ and computation from the defining equation. It is assumed that the affine curve will have the same shape defined by the original values of "E" and "n". In order for the design curve to pass through the design yield point (0.20 percent offset), values of E, n, F_y, and E_y are substituted into the stress-strain equation and the design value of $F_{0.70}$ is determined. In the event that a reliable stress-strain curve is not available, if two sets of values are given (as in the manufacturer's brochures), these values are used to write two equations which can be solved simultaneously to give n and $F_{0.70}$ and the new design equation can then be found as before. By analytical procedures, based on definitions, it is possible to write the following expressions:

$$E_t = \frac{E}{1 + \frac{3n}{7}\left(\frac{F}{F_{0.70}}\right)^{n-1}}$$

$$E_s = \frac{E}{1 + \frac{3}{7}\left(\frac{F}{F_{0.70}}\right)^{n-1}}$$

$$E_{p.l.} = \left[\frac{7}{3} E \times 10^{-4} (F_{0.70})^{n-1}\right]^{\frac{1}{n}}$$

In addition to the higher accuracy of analytical determination of E_t and E_s, the usual iterative procedure found necessary in determining allowable buckling values can be eliminated. The above formulas for E_t and E_s are substituted into the appropriate buckling equations and solutions can then be obtained without iteration.

The above general method has been used for thickness computations for the materials considered for pressure vessel use. Appendix B gives a more detailed analysis of the method and procedures used, the several stress-strain and modulus curves desired, and the defining equations. It should be pointed out that each material will have many different stress-strain curves depending on whether we are dealing with tension or compression, form of material (i.e., forged, drawn, rolled, cast, etc.) and thickness.

2.2.6 THERMOELECTRIC GENERATOR

2.2.6.1 Design and Analysis

During this quarter the design for the first four development generators of Phase II was completed and released. The design is basically the same as that of Phase I; however, design modifications have been made and incorporated to upgrade performance. These modifications are mostly in the areas of cold end heat transfer and thermoelectric couple electrical resistance.

Most of the design release occurred at the beginning of this quarter and since then several components have exposed problems in manufacture or inspection. The resulting Material Review Board (MRB) reports indicate that it may be desirable to re-evaluate certain areas for possible design changes to reduce these problems.

The generator case, long end, is a thin-walled cylinder with a circular section (0.005-0.006 in. thick) that is proving difficult to fabricate and inspect. Several nearly completed pieces have been scrapped because the thin wall has been damaged during fabrication or inspection. Another area to review would be interfaces between the following components: cold frame, short and long generator case, and the hot frame. This review could affect welding callouts as these are based on the present design. The fabrication of the spherical radius on the cold caps has been difficult, but present indications are that the requirement is necessary. The thermoelectric segments and legs are a problem during inspection and evaluation. It seems that the segment resistance and Seebeck voltage are slightly out of drawing tolerances. The evaluation of the leg cold joint resistance is also proving difficult. A new technique for evaluating the total resistance of segments and legs is being developed to better insure the use of acceptable couples.

A major effort this quarter was directed toward a study of the effects of generator performance as a result of making certain trade-offs. The evaluation is of a comparison nature, using a reference design as a base against which to make the comparisons. The reference design is as follows: basic Phase I configuration, argon atmosphere, MIN-K thermal insulation, ball and socket concept, copper cold frame, 0.500 in. deep follower hole and a Hastelloy-C generator case. The thermal requirements of this design is a hot junction temperature of 1100°F and a heat input of 153.5 watts. This heat flow through the SNAP-21 system provided a sink temperature of 70°F for the generator. Using present computer information, this indicated the design would produce 14.84 watts BOL or approximately 13 watts at EOL. Since one requirement for the dc to dc converter is that the generator produce a minimum of 11.8 watts, there is 1.2 watts of excess output. To reduce the excess output, two choices can be made: 1) lower heat input or 2) substitute less efficient, or less expensive components. Lowering the heat input by 10 watts produces a hot junction temperature of 1030°F with a corresponding output of approximately 12 watts electrical at EOL. The effects on generator performance of making single substitutions can be seen in Table 3. Justification for the use of micro-quartz or a 347 stainless steel generator case must be based on something other than efficiency. For example, the use of Hastelloy-C for the generator case means the manufacture would be very difficult and the cost would rise considerably. Considering the present problems with the thin wall section using 347 stainless steel, it is a logical substitution. The released design has the 2.213 inch-deep follower hole while the next design will use both the in-line concept and a follower hole that should be about 0.500 inch deep.

Table 3. Effects of Various Substitutions on Generator Performance

Xenon:	Output decreases 0.62 $watts_e$ Input decreases 4 $watts_{th}$
Micro-quartz:	Output unchanged Input increased 9 $watts_{th}$
In-Line:	Output increased 0.16$_e$ Input unchanged
Al Cold Frame:	Output decreased 0.49 $watts_e$ Input decreased 2 $watts_{th}$
2.213 in. Deep Hole:	Output decreased 0.15 $watts_e$ Input decreased 0.5 $watts_{th}$
347 Stainless Steel Case:	Output unchanged Input increased 4 $watts_{th}$

During this study it became evident that it was not possible to properly evaluate the effect of hardcoating in the spherical radius. Tests indicate that its removal creates conditions that approximate the temperature profile of reference design. When hardcoating is present, the cold junction is approximately 40°F higher, indicating that a change in contact area must take place. The hard surface of the hardcoated follower reduces surface deformation, thus there is less direct contact. Because gas conduction is less efficient, a higher temperature drop is produced. Since it is difficult to determine the amount of direct contact area, evaluation is not too reliable.

It must also be noted that the heat flow through micro-quartz filled with argon or xenon is subject to question. The suppliers (Johns-Manville) do not have any thermal conductivity values for micro-quartz in either atmosphere, but they did supply values for micro-quartz in a vacuum. These values were obtained from a

report released by GE, author unknown. A correlation of these values with those obtained from a study conducted for the SNAP-15C Program gave results which appeared reasonable with respect to each other and to air.

2.2.6.2 Test Equipment Design

During this period, the SNAP-21 generator test equipment design effort has been concentrated in the following areas:

- Preliminary design of the shock and vibration fixture, including heat source and insulation system, has been accomplished. The aluminum fixture consists of a base plate, side gussets, and an upright plate which provides for direct couple mounting of the generator and the heat source and insulation system.

  The heat source consists of five 200-watt electrical heating elements spaced within a cylindrical steel block. The block is supported mechanically within a cylindrical MIN-K insulation envelope.

- The cold end cooling system consists of a copper block sealed against the center of the generator cold frame with O-ring seals.

- All major test console components were specified and ordered during this period. The test console design includes a power control panel, a load panel, and a thermocouple selection panel. Layout drawings of these panels were begun during this period and component selection is in the final stages. These components will be put on order as soon as the selection is final. Several long-lead time items (elapsed time meters, thermocouple switches, power supplies, and special transformers) have been ordered to prevent schedule interruptions.

Requirements for the SNAP-21 thermoelectric generator test stations were established. These requirements were based on the current generator development program and test philosophy.

The eleven deployment generators to be fabricated will be subjected to the following types of testing:

1. Short-term Performance
2. Long-term Performance
3. Dynamic

The test sequence for the eleven thermoelectric generators will be as follows:

Unit	Test and Sequence
A10D1	Short-term performance, dynamic to destruction
A10D2	Short-term performance, dynamic and long-term test performance
A10D3	Short-term performance, to SNAP-21 system
A10D4	Short-term performance, and SNAP-21 system or long-term performance
A10D5	Same as for A10D1
A10D6	Same as for A10D2
A10D7	Same as for A10D3
A10D8	Undefined
A10D9	Undefined
A10D10	Qualification
A10D11	Qualification

After considering the test sequence and type of data that will be gathered, it was determined that seven universal test stations should be designed for use with units A10D1 through A10D9. The test stations will be designed to meet the following requirements:

- Tests will be run at constant temperature conditions. This will be accomplished by using an input power controller which will set the Q input for proper temperatures and then hold this Q constant.

The test station and controller will be designed to the controlling device will be portable and can be used on various test stations.

- All temperatures will be taken manually using rotary switches with digital readout. Both iron constantan and chromel alumel type thermocouples will be used.
- All voltages will be taken manually using rotary switches with digital readout. Both open and closed circuit voltages will be monitored.
- The load current will be measured using a calibrated shunt.
- All gas pressure readouts will be digital.
- The input power will be available for strip chart display.
- Time will be recorded by a resettable hour meter.
- A water flowmeter with line pressure regulation and in/out temperature measurement will be used to control cold side temperatures.
- All connections to services (air, water) will incorporate quick disconnects.
- The test station will be portable, not only within the laboratory but also for use at the dynamic testing facility.
- The thermoelectric generator will be mounted in the test station to permit easy removal from the panel for dynamic testing.
- Sufficient length of leads from thermoelectric generator to permit mounting of generator on dynamic test station without disconnection.

2.2.6.3 Generator Fabrication Development

During the last quarter, the development work on the fabrication of the SNAP-21 generator involved establishing rough parameters for brazing, soldering and welding, and procuring and installing new equipment to be used in building the

thermoelectric generators. The equipment which is being installed will require testing before being put into actual use.

a) Short Case to Cold Frame Brazing

The objectives in this operation were to develop and test existing materials and fabrication techniques to provide manufacturing with a process which would produce a quality bond and maintain a hermetic seal for generator life.

The tests that were run involved brazing simulated test blocks using three different braze alloys – Silvaloy 50, Handy Harmen Braze BT, and Handy Harmen Braze 603VTG. Early results showed Silvaloy 50 to be the most promising alloy. This choice was made from visual and rough metallographic examination.

A brazing fixture was designed to hold the short case in the cold frame during the brazing operation. This fixture not only would hold the short case in the cold frame, but would also keep the short case from becoming oval or out of round during the braze operation.

The next sample, which was the first sample that was full size except for the elimination of the high center hub on the cold frame, was brazed in a moving belt furnace using an inert gas as the atmosphere. This sample was brazed at 1300°F. The braze wire was pre-formed and placed on the inside of the short case and held in place with flux paste. This assembly was then put in the fixture and brazed. The appearance of this first unit was not quite what was expected – the braze ran in all directions and did a poor job of filleting on the outside of the short case. This was sectioned and, as expected, was not of good quality.

The second sample was a full-size unit. This sample was painted with braze stop-off before applying the braze wire. A visual examination of this sample after the braze operation showed good penetration of alloy, controlled braze flow, and adequate filleting. A leak check performed on this part indicated no detectable leaks. This sample, shown in Figure 2-15, was sent out to be fully machined to check out tooling and machining practice. Sample followers and couples will be used to assemble this unit with an out-of-spec long case and hot frame. The entire unit will be welded together, then sectioned and metallographically examined for results.

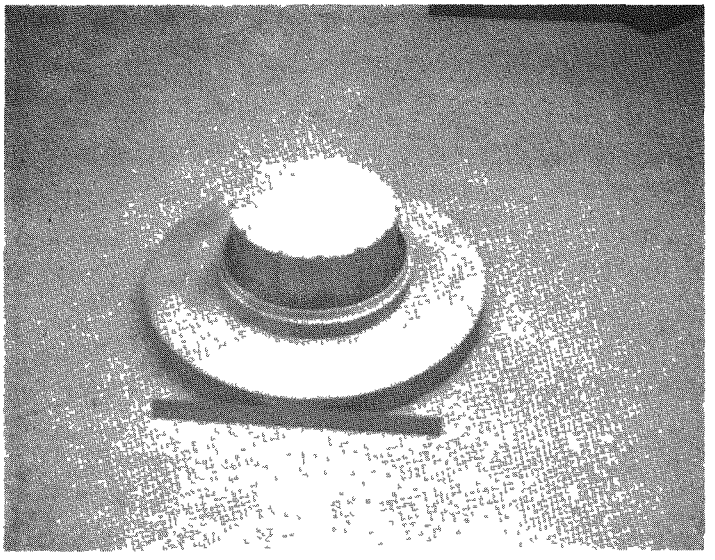

Figure 2-15. Brazed Short Case and Cold Frame Prior to Machining

b) Welding of Generator

The two welds which are required to seal the generator must be developed. To establish assembly and welding parameters, the revised assembly fixture which was redesigned from Phase I will require testing along with the new weld lathe.

During the first quarter, the primary effort was to procure and set up equipment. The lathe and assembly fixture were not delivered until late in the quarter. Very little development work was done. The drive motor on the lathe was replaced with a much slower gear motor which would give consistent and constant low speeds which will be required during the welding operation.

It is expected that the development parameters for the two welds will be established during the early part of the next quarter. This development will go hand-in-hand with equipment tryout.

c) Attachment of Instrumentation

The objective of developing techniques and parameters for attaching thermocouples to hot junction buttons and followers was to establish and document these parameters.

The instrumentation of the follower required that an iron-constantan thermocouple be soldered in place in a machined slot near the ball socket end of the follower. This was accomplished by soldering the couple to the follower with aluminum solder. Pull and electrical tests were performed with excellent results.

The instrumentation of the hot junction button required only the resistance spot welding of the iron-constantan thermocouple wires to the button. This was satisfactorily accomplished without any difficulty.

It was a straightforward approach and no problems were anticipated; however, from information on the Phase I Program, the life of these thermocouples is not adequate. A new approach, using shielded thermocouples, is now being investigated.

2.2.6.4 Fabrication

Efforts this quarter were concentrated on procurement of raw materials, selection of vendors and purchase or manufacture of finished hardware, preparation of Process Routings, updating Manufacturing Flow Plan, and tool tryout.

Cold frames, generator case short end, generator case, hot frame insulation and pinch-off tube were items of hardware that were built in 3M's shop facility. Other components, such as followers, cold caps, springs, hot junction buttons, hot junction electrodes and the assembly and welding fixture, were built by outside vendors. All hardware involving the first four generators has been ordered and, at this writing, approximately 85 percent is in-house.

Process Routings were written in March and the Manufacturing Flow Plan was updated and expanded. We now have a separate flow plan for the thermoelectric generator and for the cold frame assembly. Process Routings were written for all manufactured components, subassemblies and assemblies.

Specifications will be written, as Manufacturing Standard Instructions, to cover procedures and processes. The instructions covering welding and brazing techniques are being written as data is generated and becomes available from the development program.

The assembly and weld fixture was received and approved (Figure 2-16). The fixture concept is from Phase I tooling with modifications to improve reliability. Total assembly of the generator is completed in the fixture (Figure 2-17). Continuity checks can be made without removing the generator from the fixture and then the assembly will be placed in the lathe for welding at the cold end (Figure 2-18) and welding at the hot end (Figure 2-19). The completed generator will then be ready for processing.

2.2.6.5 System Quality Control

Quality Engineering is developing Quality Assurance Standard Instructions that will replace the Thermoelectric Product Inspection (TPI) documents now in use for specific inspection instruction purposes. The reason for this change is that a TPI cannot be revised and therefore any upgrading or revision requires assignment of another number. The Q.A. Standard is more versatile and can be revised by indication of a superceding date in the heading of the standard and with required approval. Use of the Q.A. Standard in conjunction with Manufacturing and Engineering Instructions will provide more compatible procedures. The Preliminary Linde Quality Control Plan has been issued with Addendum 1, and has been approved with corrections. The final Q.C. Plan will be updated during the development program and will be submitted by Linde at the final design review (FDR).

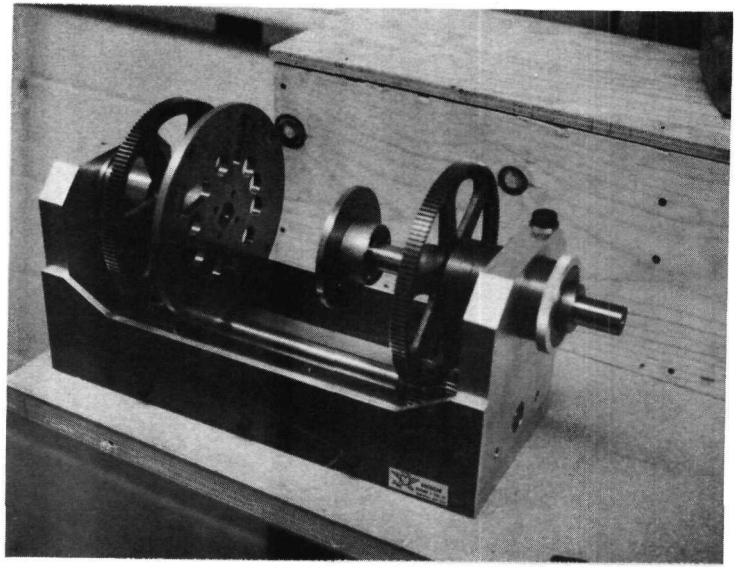

Figure 2-16. Assembly and Weld Fixture

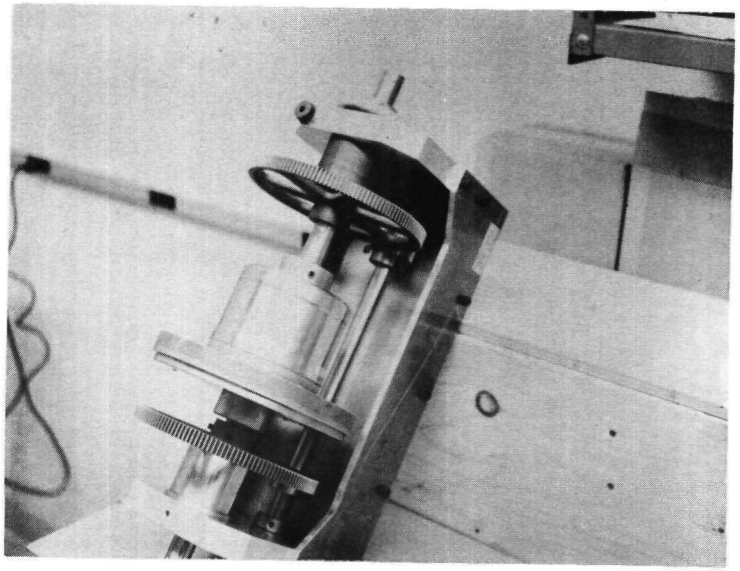

Figure 2-17. Assembly and Weld Fixture with Assembly

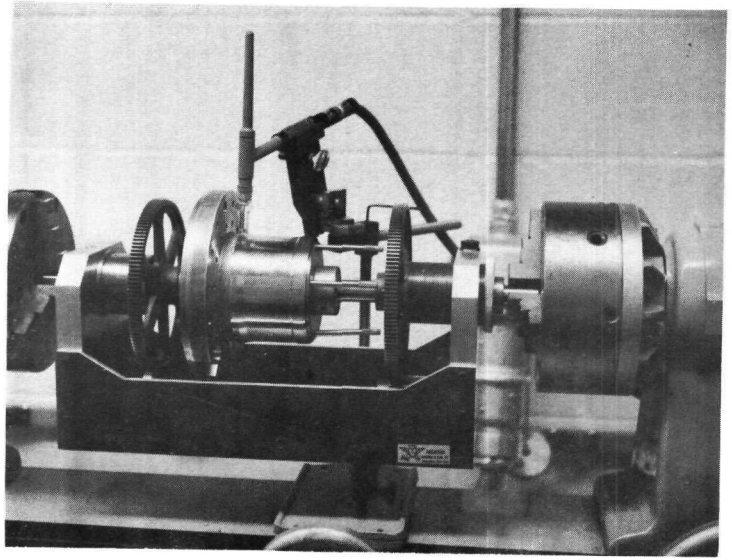

Figure 2-18. Fixture in Lathe Ready for Welding Cold End

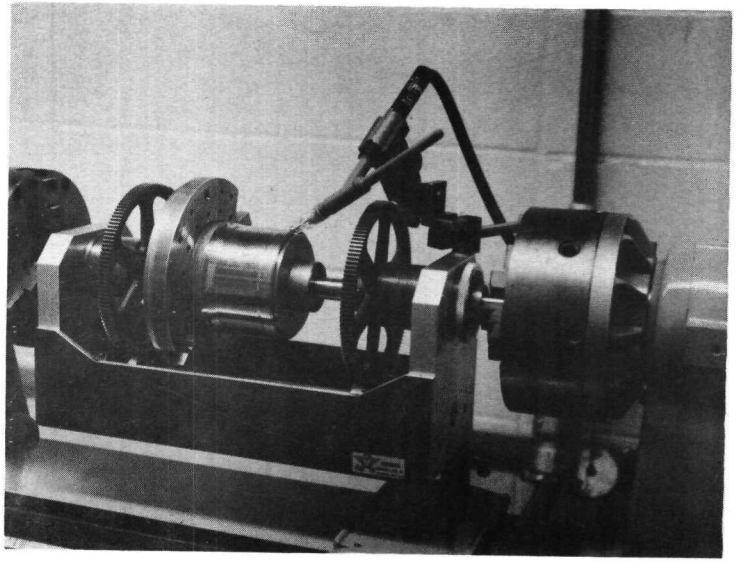

Figure 2-19. Fixture in Lathe Ready for Welding Hot End

Quality Control Surveys of vendors furnishing fabricated material for use in the program have been made to evaluate quality performance and service. Surveys will be a continuing activity while establishing new vendors.

Statistical analysis, variable data reporting and a classification of characteristics (critical, major, and minor) issued by Design Engineering are being used to provide a basis for allocating the quality inspection effort. From these procedures a sampling plan will be drawn up and used to establish the degree of inspection (100 percent, applicable sampling plans or objective evidence of quality history and proof of control based on criticality of the features). Phase II inspection results are presently being studied for application to all thermoelectric materials to be used in future phases of the SNAP-21 Program.

Non-conformance to drawing and specification requirements is resulting in a rising number of Material Review Board dispositions. Indications are that a number of factors, in addition to characteristic deviations, are responsible. This includes inadequate packaging procedures.

Manufacturing Process Routings for hot frame details and thermoelectric couple manufacture are in a review status prior to formal release. Engineering is reviewing the Process Routings for proper application of operations and equipment.

2.2.6.6 Thermoelectric Legs and Couples

During Phase I of the SNAP-21 Program five 48-couple prototype thermoelectric generators were fabricated, assembled and put on long-term electrical and thermal performance test. Four generators were put on bench test, the fifth was installed into the first prototype system.

The objective of the work performed during this period was to evaluate the data from these generators, identify those techniques which contributed to the change in performance and investigate means of improving generator performance.

A solution was proposed for the excessively high and unreproducible P-leg hot junction electrode electrical contact resistance experienced in Phase I generators.

The proposed solution uses a 3M Company proprietary P-leg hot junction electrode contacting technique. The short-term effectiveness of the proposed technique was demonstrated in a series of bell jar tests. Because of the results of these tests, and other favorable 3M experience in the use of the proposed contacting technique, it has been selected for use in the first four Phase II Development Generators. The long-term effectiveness of the contacting technique will be evaluated in at least two of the first four generators.

In addition to the evaluation of the P-leg contacting technique, the feasibility of a new P- and N-leg manufacturing technique was demonstrated. It is felt that the new method of leg manufacture, coupled with the proposed P-leg contacting technique, will result in the degree of electrical reproducibility desired in the SNAP-21 thermoelectric generators. In addition to reproducibility, the new leg manufacturing technique (XTPO-193A) is expected to result in the P- and N-type thermoelectric materials being used to a degree which more nearly approaches their theoretical capability.

a) Data Evaluation

Examination of experimental test data from these generators shows that all generators have undesirable internal resistance characteristics. In most generators the initial internal resistance was close to design expectations; however, some improvement in initial internal resistance is desirable in terms of both magnitude and reproducibility. Most generators experienced an undesirable internal resistance increase during the first 2,000 to 4,000 hours of operation.

In general, the largest undesirable internal resistance traits can be traced to the P-leg. The major contributor to this resistance change is the P-leg hot junction electrode electrical contact. However, improvements in initial resistance remain to be realized within the leg itself.

The initial variability of couple electrical resistance is shown in Table 4. In this table extraneous resistance is defined as all resistance in excess of the computer predicted thermoelectric material resistance. This necessarily includes all hardware and contact resistances. The extraneous resistances shown in Table 4 were determined by dividing the total generator internal resistance by the number of couples and subtracting the computer predicted thermoelectric material resistance.

Table 4. Couple Extraneous Resistance

Unit	Time (Hours)	Extraneous Resistance per Couple (mΩ)
Six couple Module A1	192	9
Six couple Module A3	72	12
Six couple Module A4	240	9
Prototype Generator P3	96	2
Prototype Generator P5	24	13
Prototype Generator P6	24	4
Prototype Generator P7	168	6

Of the extraneous resistances shown in Table 4, 1 to 2 milliohms can be accounted for in cold junction electrode hardware, and 0 to 1 milliohms in N-leg hot junction electrode electrical contact resistance. The remainder of the coupld extraneous resistance is associated with the P-leg. The extraneous resistance associated with the P-leg is divided between hot junction electrode electrical contact and excess material resistance (above "book" value). However, previous experience has shown that the major portion of the P-leg extraneous resistance is associated with the hot junction electrode contact rather than the material.

b) Phase I Technology Evaluation

In the manufacture of segmented P-legs for the SNAP-21 Phase I prototype generators, several problems existed which were not resolved. Two methods of manufacture of segmented P-legs were used and, while satisfactory legs could be manufactured by either process, the controls required to do so were very sensitive and the possibility of inclusion of legs of somewhat lower quality than desired in a device was possible. The methods used are briefly described in the following paragraphs.

One method of manufacturing segmented P-legs consisted of forming the two segment sections separately and then joining the segments to an interposing stainless

steel wafer by a welding process. A two-step process was employed in which the hot segment material was first bonded to the disc. No difficulty was encountered in this operation. In the next operation, in which the cold segment was bonded to the disc, the temperature control for bonding was very critical. If the temperature was slightly too high, sufficient segment contamination in the zone of the weld would occur which would seriously affect the thermoelectric properties of the leg.

Unfortunately, this contamination principly affects the Seebeck coefficient and the tests to determine the Seebeck coefficient are destructive to the legs. In view of this difficulty, the process was abandoned and a method of joining the segments in one operation (XTPO-25) was employed. Some compromises were made to produce legs by this method:

1. The desirable operations required for the two segment materials is quite different. Due to die ejection problems, it was necessary to compromise the two operations. This results in a cold segment material density which is considerably lower than optimum.

2. The required sintering temperature for the two segment materials is substantially different. To overcome this problem, a sintering agent had to be introduced into the hot segment material to provide sufficient sintering at the maximum cold segment material sintering temperature. The introduction of this sintering agent results in the loss of some thermoelectric quality of the hot segment, even under ideal conditions. Also, cross contamination of the legs during sintering is difficult to prevent because the sintering agent used in the hot segment material is a modifying agent for the cold segment material. Again, adequacy of leg manufacture can only be fully verified by destructive testing of the leg.

c) Performance Improvement Evaluation

Between phases of the SNAP-21 Program, a manufacturing method was developed which permits the individual segments to be processed independently, that is, to be pressed and sintered in a manner which bests satisfies each segment's specific requirements. This processing removes the need for a sintering agent

in the hot segment material and allows optimum pressing conditions for both segments. The segments can then be joined by bonding (XTPO-193-A), a method which results in minimum joint contamination. The test results on legs so manufactured have been extremely encouraging.

A similar bonding method (XTPO-193-A) can be used for the production of segmented N-legs. Although there are currently no chemical problems involved for the N-legs, some densification improvement is possible which will result in slightly improved (by approximately 5 percent) resistance characteristics for legs produced per XTPO-193-A.

d) Bell Jar Tests

The following is a brief description of the SNAP-21 bell jar testing conducted during this period:

Test No. 1

Test No. 1 used 3P material unsegmented legs. One half of the test legs contained XTPM-81 material at the hot end. The purpose of this material is to deform at temperature to produce an intimate, resistance free, interface at the contacting surface. This constitutes the 3M proprietary P-leg hot junction electrode electrical contacting technique discussed in the introduction. For future discussion, all P-type thermoelectric legs incorporating the proprietary contacting materials will be referred to as "soft nosed" legs.

The purpose of the test was to evaluate the performance of 3P material thermoelectric legs of the type used in the SNAP-21 Phase I thermoelectric generators and 3P material thermoelectric legs incorporating the proprietary contacting material. Both batches of legs were as nearly identical as possible (both series from the same batch of thermoelectric material, sintered and processed together) except for the soft nose section. This material is introduced in operation XTPO-189.

The tests were conducted in a bell jar test fixture under the following conditions:

- T_h = hot electrode temperature: 1100°F following a 1 hour "seat in" at 1200°F
- T_c = cold electrode temperature: 150°F
- Atmosphere - Argon + 5 percent He
- Insulation - Micro-quartz
- Hardware - SNAP-21, Phase I cold end hardware. Hot end hardware was Fe plated copper strap with a mild steel connecting button designed to conform to the test fixture cold block.

The following conditions were monitored during the test:

- Hot junction temperature
- Cold junction temperature
- Open circuit voltage
- Closed circuit voltage (1 amp current from constant current source)
- Resistance from connecting button to cold cap.

The electrical characteristics of the legs as taken before and after the test to determine if any significant change had occurred during the 500-hour test period.

The important results from this test may be summarized as follows:

> All soft nose legs performed with consistent resistance values. The maximum deviation was 0.8 milliohm for the soft nose legs and 11.0 milliohm for the conventional legs.

The essential test information is displayed in Figures 2-20 and 2-21 along with the "book values" of properties. ("Book values" are the computer properties of the thermoelectric materials at the measured temperatures). The initial

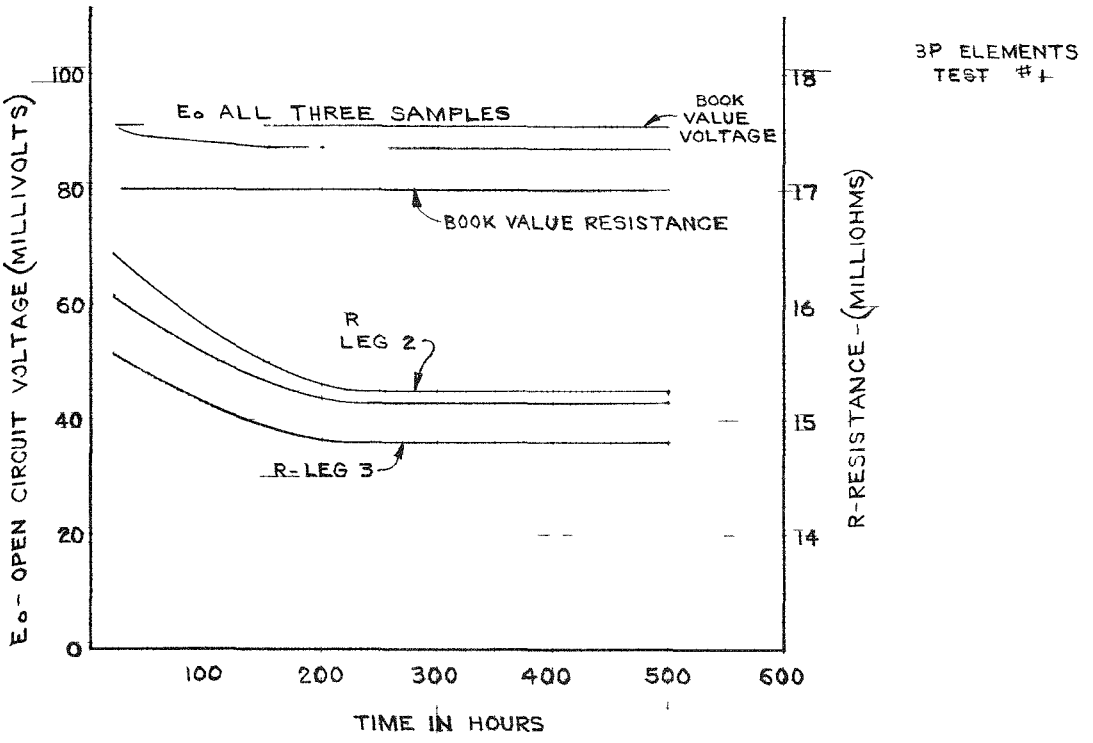

Figure 2-20. Observed Electrical Characteristics of Unsegmented "Soft-Nosed" Legs

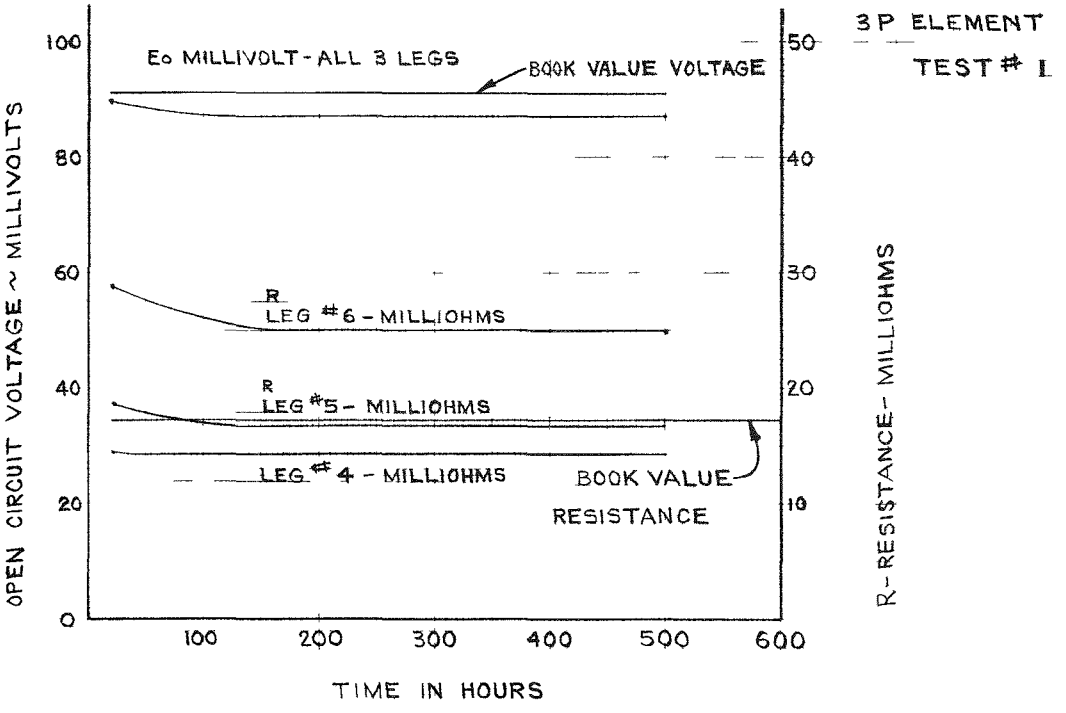

Figure 2-21. Observed Electrical Characteristics of Unsegmented Conventional Legs

variability of leg electrical resistance is shown in Table 5. The same nomenclature is applicable for this table as was defined for Table 4.

The fact that the resistance observed for some of the legs is lower than the assigned book value can be attributed to the following:

1. Present processing of legs has been upgraded by improved sintering controls since the book values were determined.

2. The book value of resistance assumes one dimensional heat flow. This cannot be maintained in the test fixture. Since heat is unavoidably lost from the sides of the element, the mean temperature is lower than the book value, and, since the resistance of the legs increases with the temperature, the average resistance is lower due to the lower average temperature.

Comparison of the data in Table 5 with that in Table 4 clearly reveals the effectiveness of the soft nose contacting technique.

Table 5. Leg Extraneous Resistance

Leg No.	Contact	Time (hours)	Extraneous Resistance (mΩ)
1	Soft Nose	10 500	-0.9 -1.8
2	Soft Nose	10 500	-0.5 -1.7
3	Soft Nose	10 500	-1.4 -2.1
4	Conventional	25 500	-1.0 -2.5
5	Conventional	25 500	+4.0 0.0
6	Conventional	25	+11.5 + 7.0

As can be seen from Figures 2-20 and 2-21, the Seebeck and resistivity values decreased during the test. This data is shown in Figure 2-22.

There are two factors which tend to influence the Seebeck and Resistivity properties of the 3P material at high temperature:

1. The presence of moisture or oxygen will reduce the Seebeck coefficient and resistivity.

2. Even with the absence of moisture or oxygen, the equilibrium solubility characteristics for 3P material are such that the doping concentration is higher at high temperature than when the element is equilibrated to room temperature. It is felt that some of the solubility factors are long-term and require several hundred hours at temperature to achieve their final state. It is analytically impossible and experimentally impractical to treat the case of solubility dependence to obtain book value properties.

Test No. 2

Test No. 2 was a test devised to determine if any advantage in N-leg properties could be obtained from individually pressed and sintered segments bonded together as specified in XTPO-193-A as opposed to legs fabricated according to XTPO-24. The test consisted of taking four N-legs of each fabrication method and operating them in a bell jar fixture.

After an initial heat up to 1200°F for 2 hours, the legs were operated at T_h = 1100°F, T_c = 130°F. The resistance of the legs fabricated according to XTPO-24 averages a little more than 1 milliohm/leg higher in resistance:

Average R (per XTPO-24) = 20.2 mΩ

Average R (per XTPO-193-A) = 19.0 mΩ

This is undoubtedly due to better densification of material effected by pressing the segments separately rather than the technique used in XTPO-24.

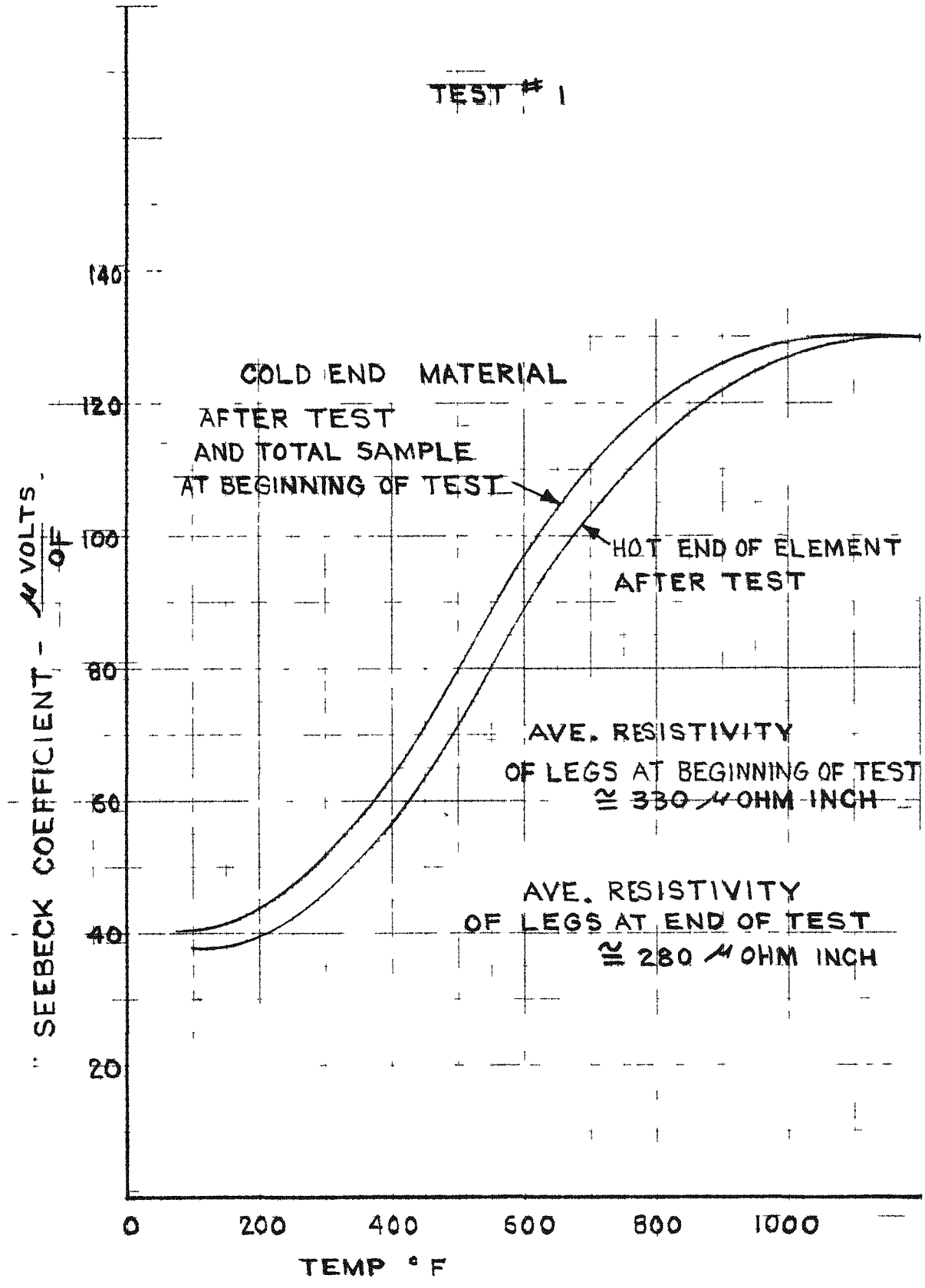

Figure 2-22. Seebeck Coefficient vs Temperature, Before and After Test No. 1

The test was continued for 720 hours with no variation in E_o or R greater than experimental error on any of the eight legs under test.

The use of N-legs bonded according to XTPO-193-A is recommended on the basis of the resistance improvement of the legs as well as the improved quality control possible for the leg components.

Test No. 3

The third test of the series was an attempt to demonstrate the combined effectiveness of the soft nosed P-elements and legs fabricated according to XTPO-193-A to produce a high performance, reproducible, thermoelectric couple. Five couples were tested. All N- and P-legs were fabricated as specified in XTPO-193-A. Two of the five P-legs were "conventional" (couples 1 and 2), and three were of the soft nose variety (couples 3, 4 and 5). The leg geometries used were identical to those used in the SNAP-21, Phase I, prototype generators 3, 4 and 5. Table 6 summarizes the dimensional characteristics of the elements used in this test. All N- and P-segment materials were also the same as those used in the Phase I prototype generators. The only differences in the thermoelectric legs used in this test and those used in Phase I prototype generators 3, 4, and 5, are the soft nose on three of the P-legs and the method of manufacture, as described above.

Table 6. Test No. 3 Element Dimensions

Leg	L	D	Lc/L	L/A
N	0.600	0.188	0.383	21.73
P	0.446	0.188	0.455	16.15

L = Total leg length (inch)
Lc = Cold segment length (inch)
D = Leg diameter (inch)
A = Leg cross sectional area $(inch)^2$

The test conditions were as follows:

- T_h = 1100°F
- T_c = 120°F
- Power to heater = 175 watts
- Atmosphere - Argon + 5% He
- Insulation - Micro-quartz
- Hardware -

  Cold Junction - As in original SNAP-21

  Hot Junction - Plated copper strap. (TPF-5)
  Hot junction button, mild steel designed
  to conform to test fixture cold block.

The conditions monitored during the test were:

- Hot junction temperature
- Cold junction temperature
- Open voltage/leg/couple
- Closed voltage/leg/couple
- Leg resistance
- Power under optimum load

The results of this test are summarized in Figures 2-23 to 2-32. In Figures 2-23 and 2-24 the electrical characteristics of the couples are shown, and in Figures 2-25 to 2-32 the electrical characteristics of the individual legs of couples 1, 2, 4, and 5 are shown. Instrumentation limitations prevented obtaining individual leg data from couple #3.

Examination of the data in Figures 2-23 and 2-24 again clearly reveals the effectiveness of the soft nose contacting technique. This is substantiated by the data in Figures 2-25 to 2-28. It is apparent that benefits can be realized in terms of leg and couple reproducibility and that the magnitude of the resistance associated with the P-leg is consistently reduced substantially with the use of the soft nose

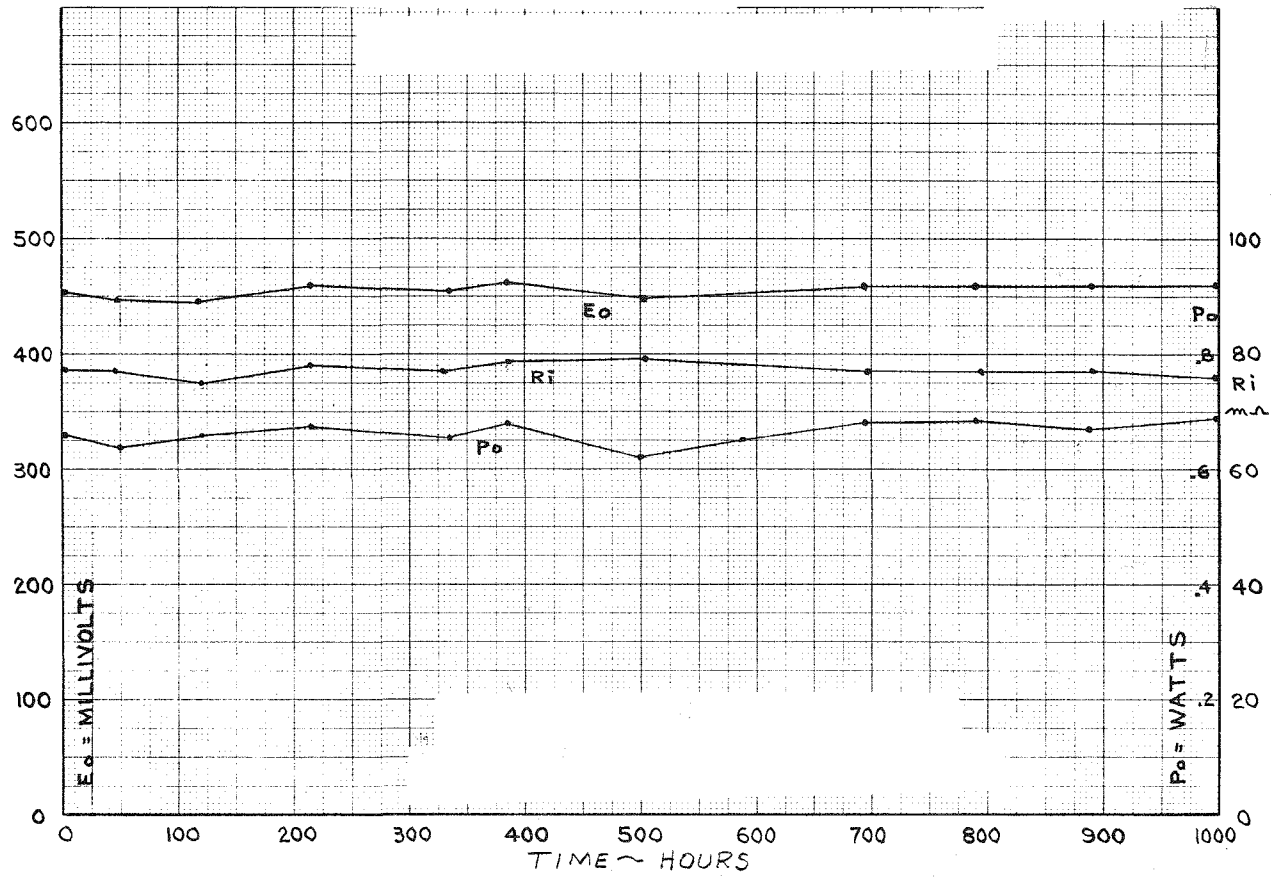

Figure 2-23. Test No. 3: Electrical Characteristics of Couple Nos. 1 and 2, Conventional P-Legs

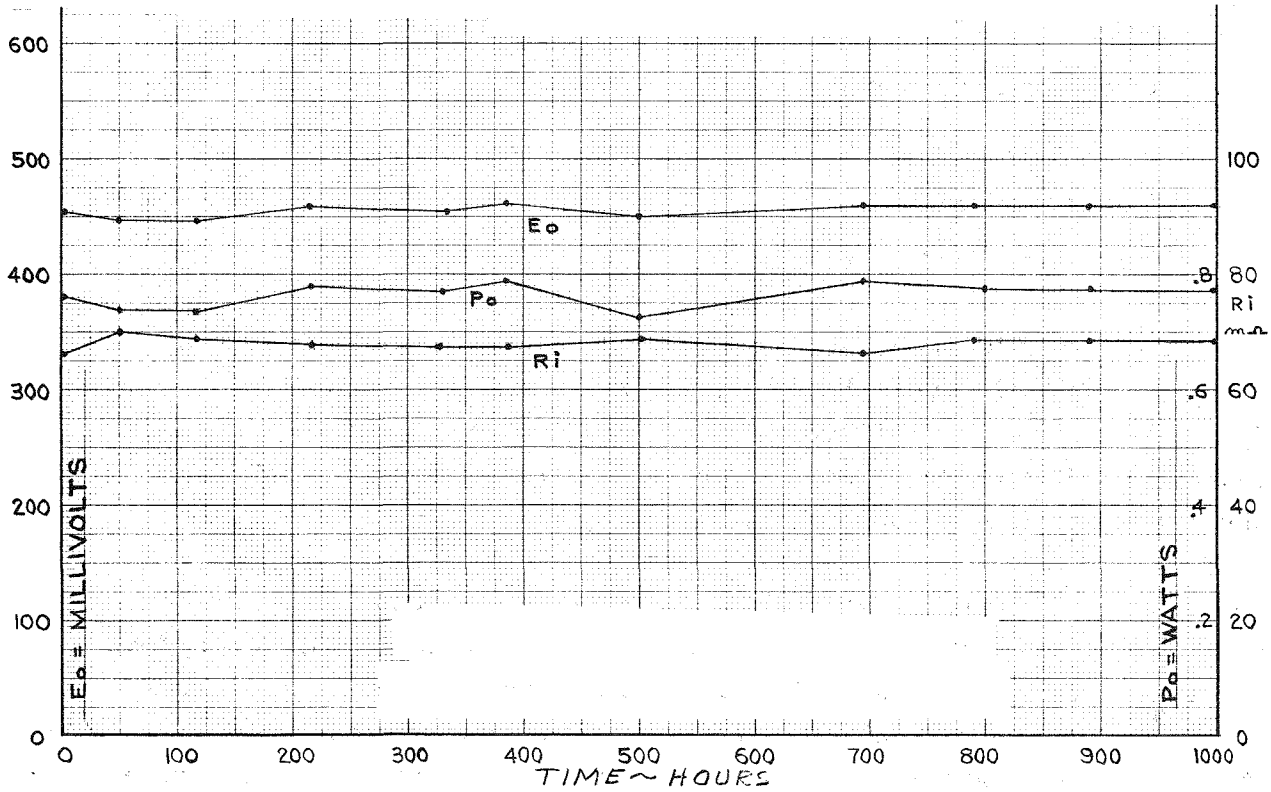

Figure 2-24. Test No. 3: Electrical Characteristics of Couple Nos. 4 and 5, Soft-Nose P-Legs

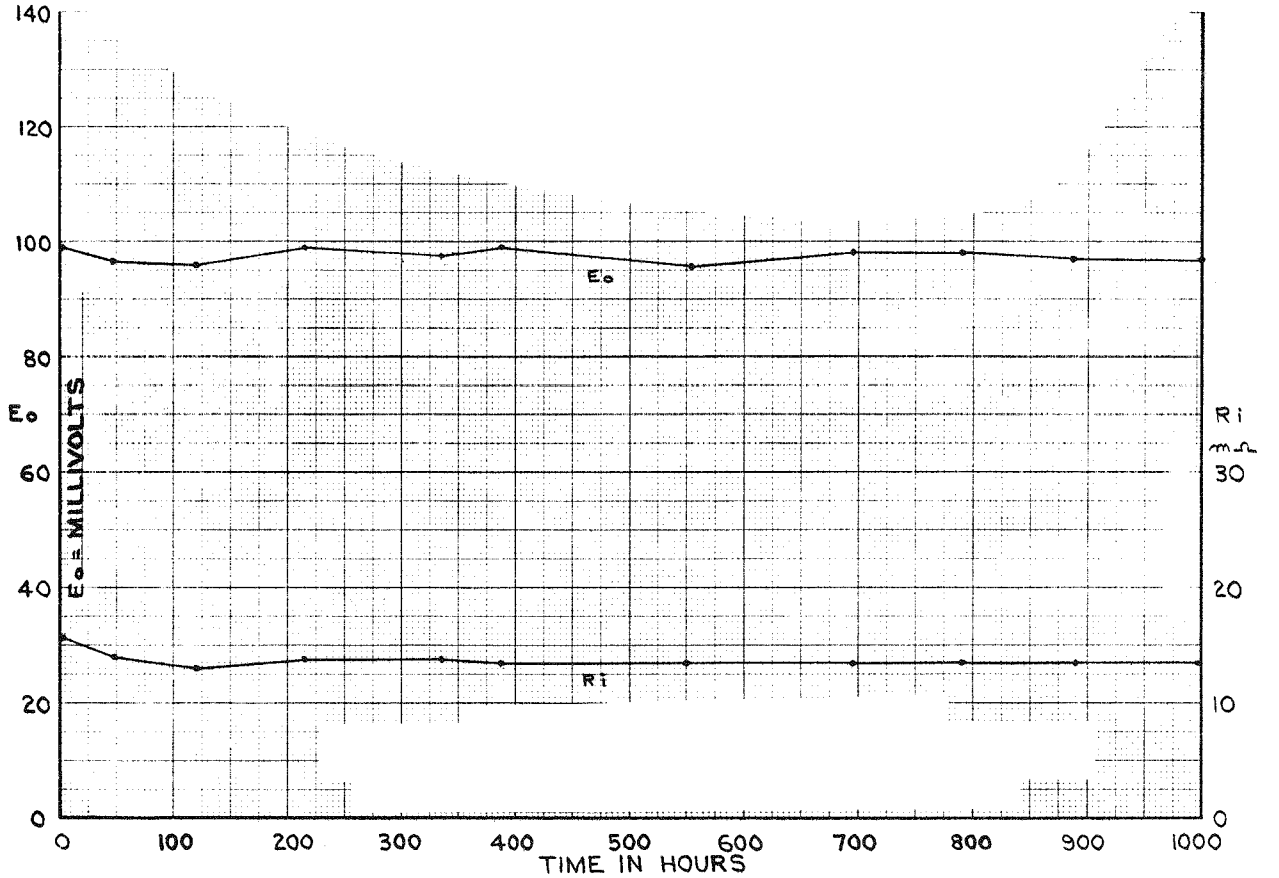

Figure 2-25. Test No. 3: Electrical Characteristics of P-Leg Couple No. 1

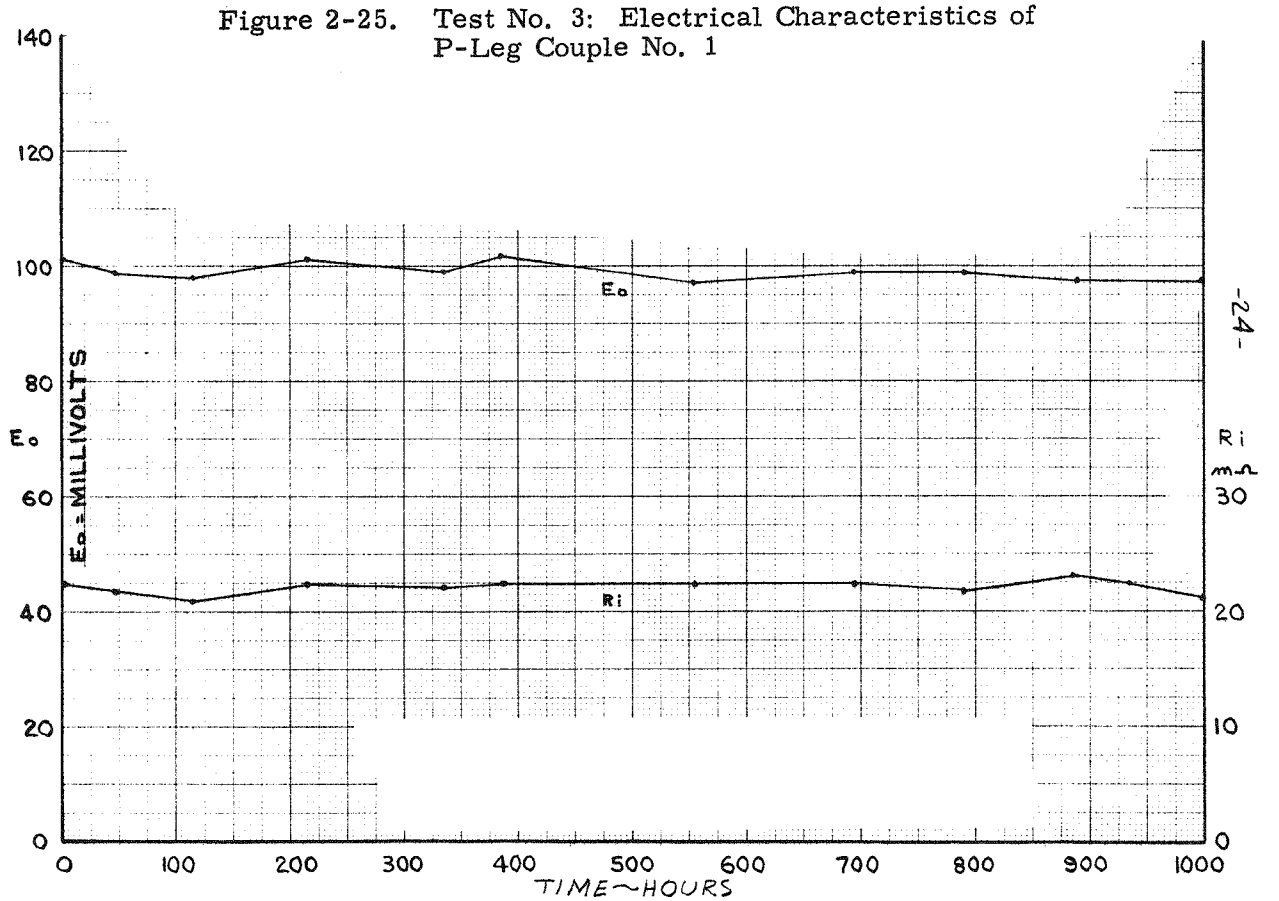

Figure 2-26. Test No. 3: Electrical Characteristics of P-Leg, Couple No. 2

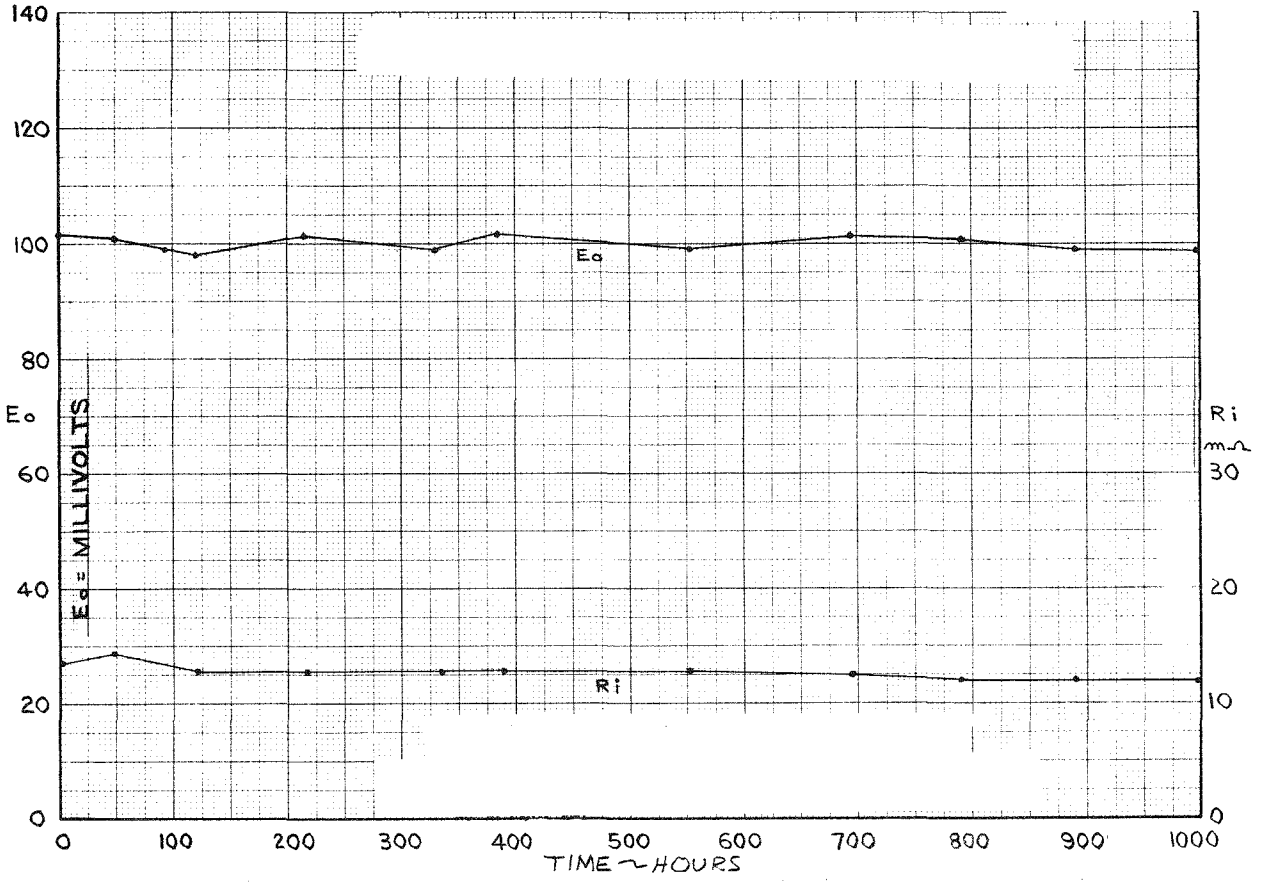

Figure 2-27. Test No. 3: Electrical Characteristics of P-Leg, Couple No. 4

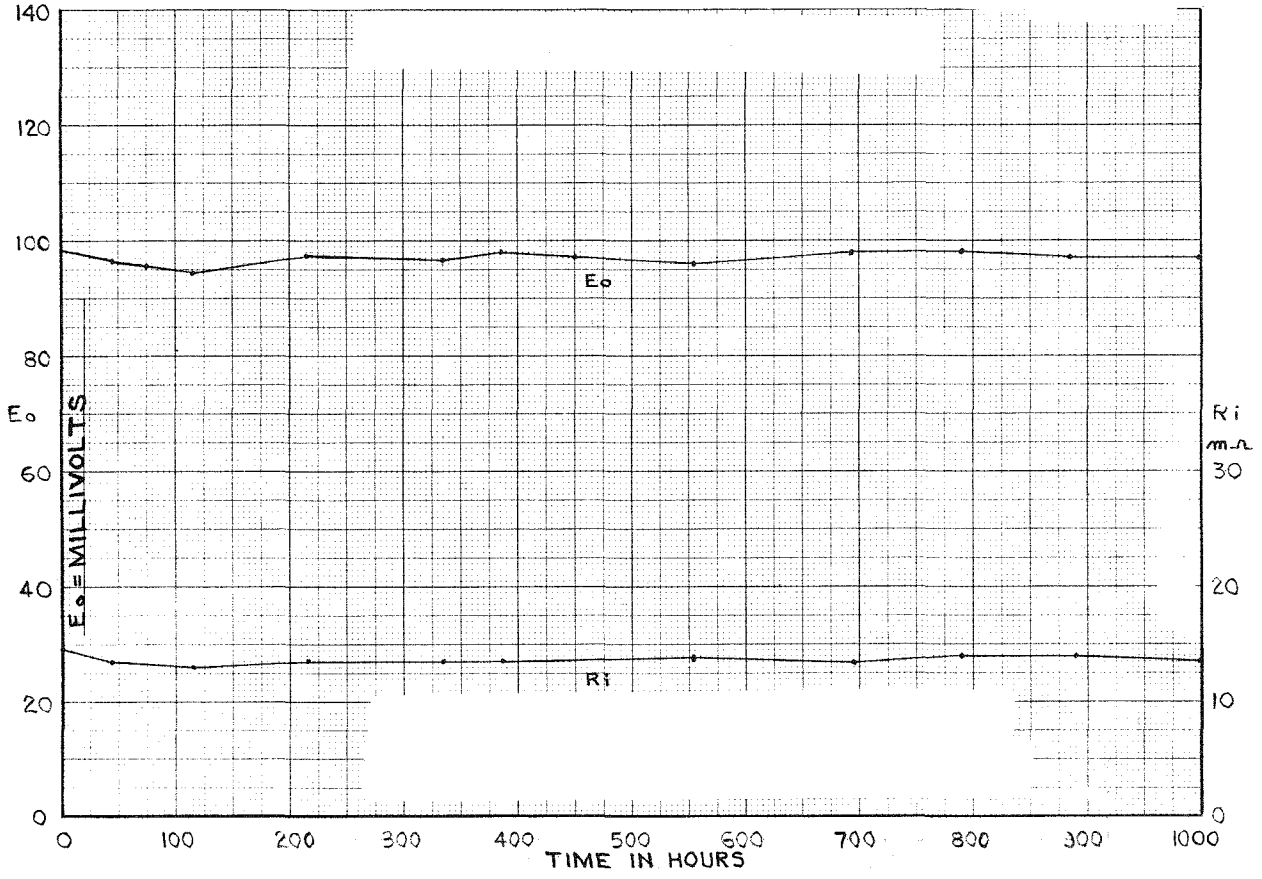

Figure 2-28. Test No. 3: Electrical Characteristics of P-Leg, Couple No. 5

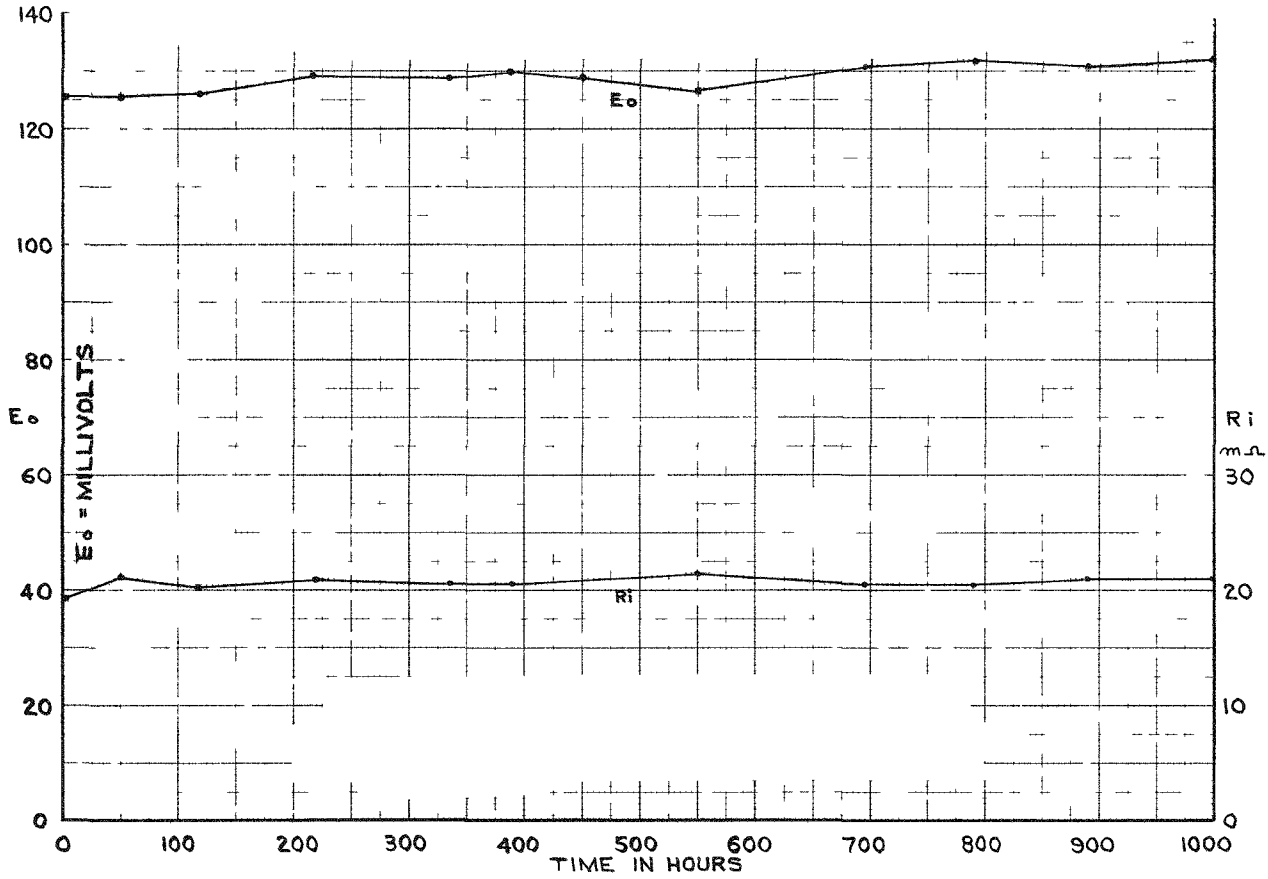

Figure 2-29. Test No. 3: Electrical Characteristics of N-Leg, Couple No. 1

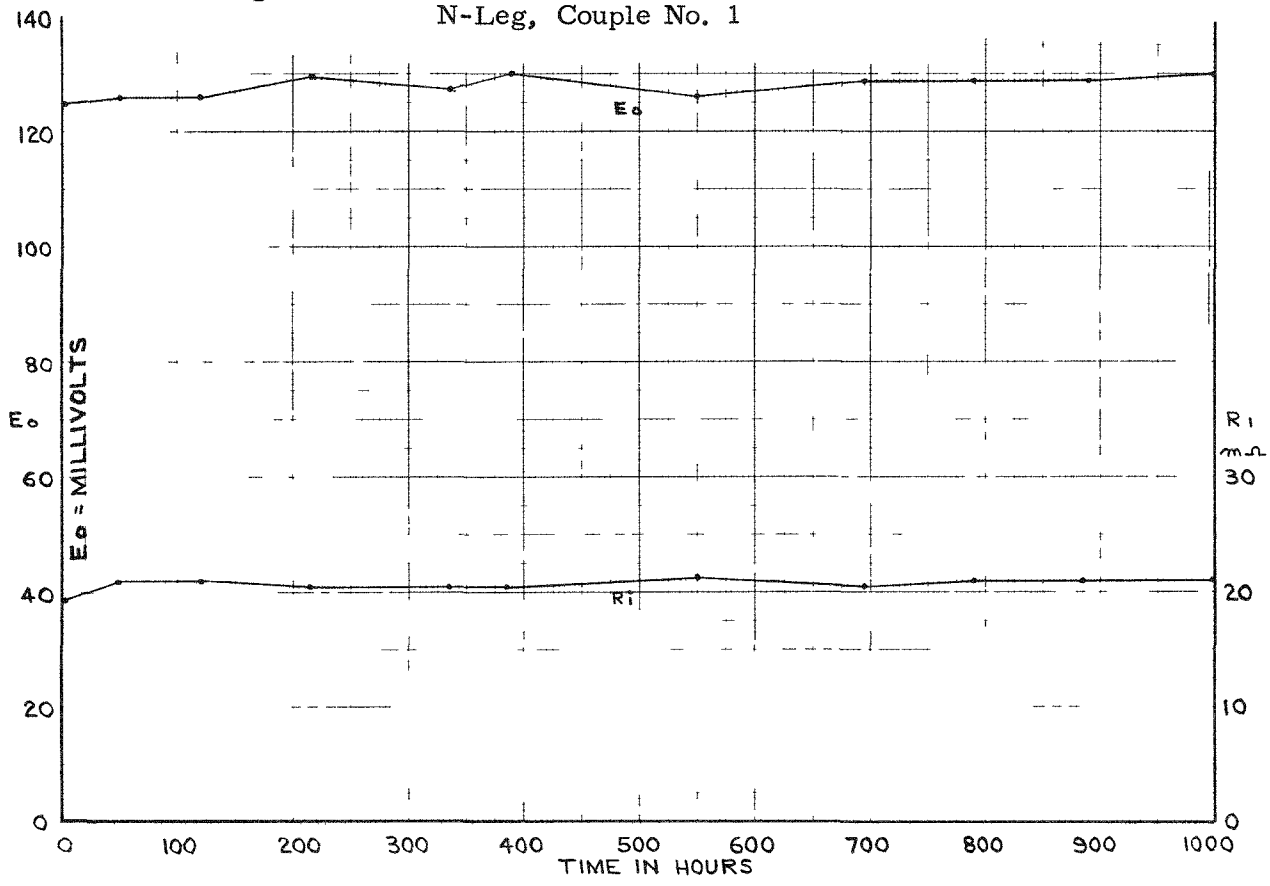

Figure 2-30. Test No. 3: Electrical Characteristics of N-Leg, Couple No. 2

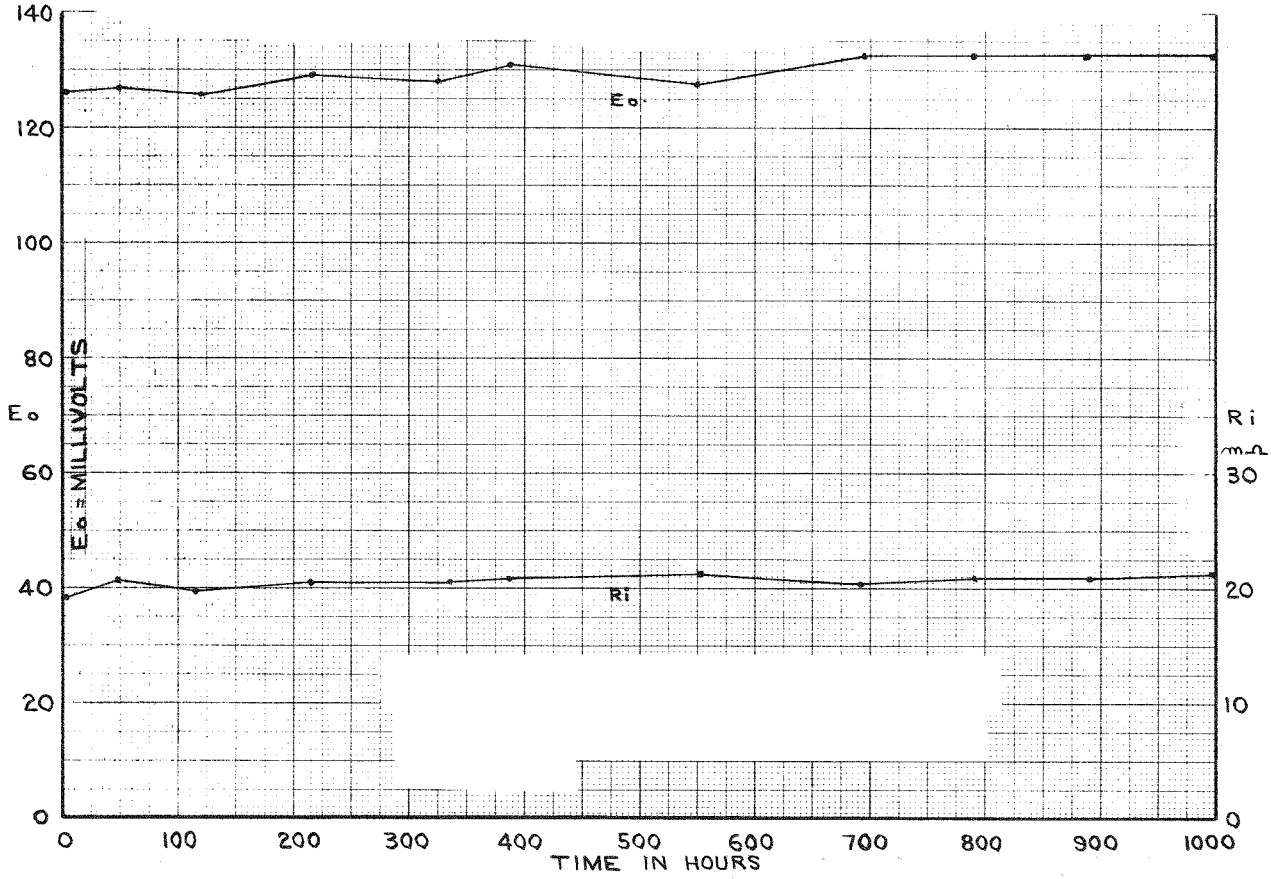

Figure 2-31. Test No. 3: Electrical Characteristics of N-Leg, Couple No. 4

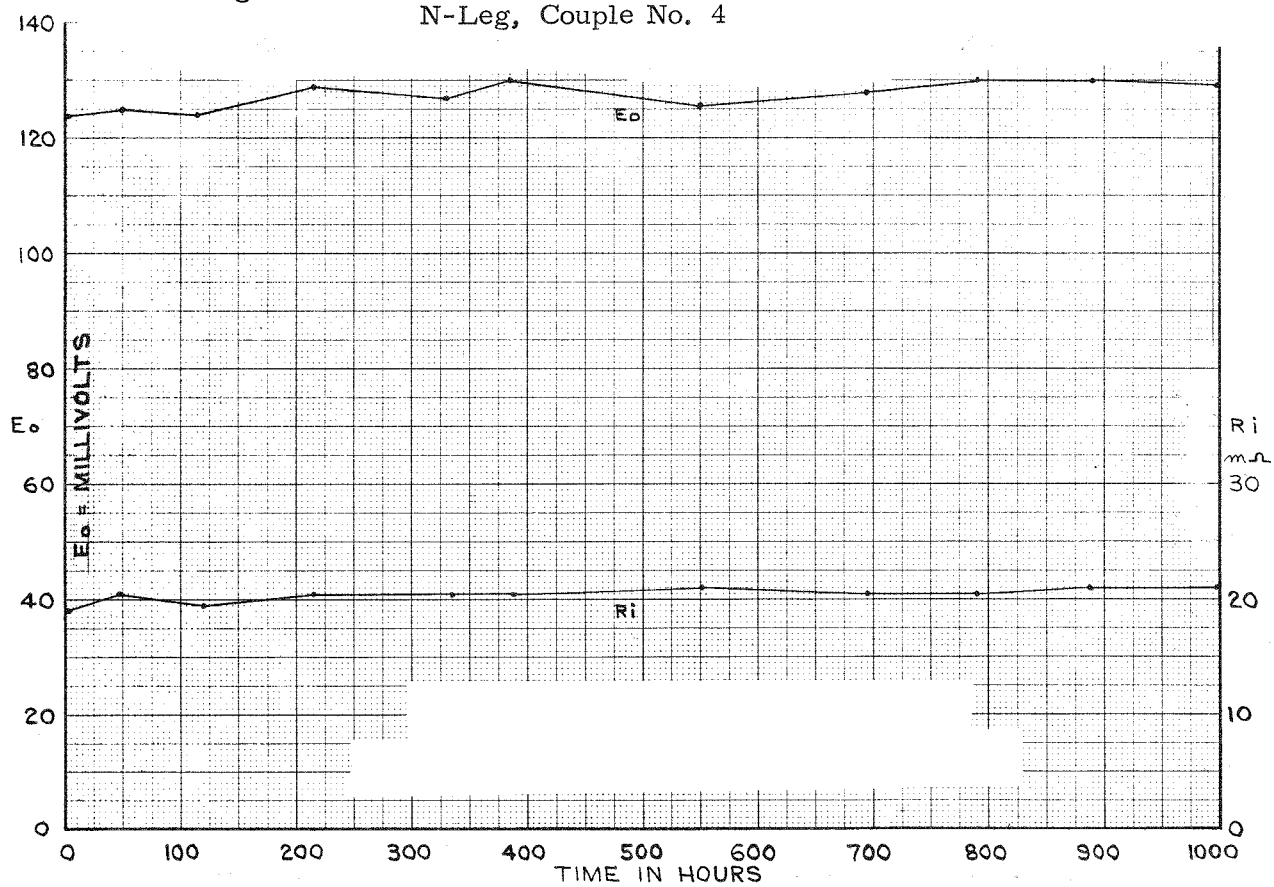

Figure 2-32. Test No. 3: Electrical Characteristics of N-Leg, Couple No. 5

material. Figures 2-29 to 2-32 show a very reproducible N-leg; however, the resistance is slightly higher than that observed in Test No. 2.

As can be seen in the graphs of legs and couple characteristics, minor variations in properties are observed from reading to reading. This is because the cooling water temperature and flow rate are subject to building water supply variations.

From the previous data for temperatures of 1100°F at the hot junction and 120°F at the cold junction, the output of a 48-couple generator using this type couple would be approximately 17 watts.

Reasonable average values observed in test are:

$N\ E_o$ = 129 millivolts

Leg R_i = 21 milliohms

$P\ E_o$ = 98 millivolts

Leg R_i = 13 milliohms

For the couples:

E_o = 227 millivolts

R_i = 36 milliohms (including hardware)

P opt Ld = 0.360 watts/couple

Therefore the power for a 48-couple device = 17.5 watts.

If the P-leg were designed so N L/A = P L/A = 21.73 then the N-leg would be as above and the P-leg:

E_o = 98

R_i = 17.7 milliohms

For a couple:

E_o = 227

R_i = 41

P_c = 0.32 watts/couple

or, for a 48-couple device the power/generator = 15.2 watts at 1100/120.

It can be reasonably expected that the sacrifice of power output caused by lengthening the P-leg would be more than compensated for by increased leg efficiency, since the legs' electrical loading would be more nearly optimum.

Leg Bonding

Fixtures for bonding both N- and P-legs according to XTPO-193-A were developed, evaluated, tested, and manufacturing techniques established for the first four generators. Other promising techniques for bonding legs are being investigated. Figure 2-33 shows P-type legs before and after bonding.

Bonding Conclusions

The bonding techniques (XTPO-193-A) are satisfactory for limited production and laboratory use and will be used for bonding the thermoelectric legs for the first four generators. Other new and promising fabrication techniques are being investigated. These techniques will be evaluated against the present methods of XTPO-193-A and the best technique picked for all future leg fabrication.

Thermoelectric Couple Development

(1) Brazing Caps to Wires

An experimental batch process was investigated for bonding cold caps and jumper wires in a reducing atmosphere. Difficulties were encountered during assembly and positioning of parts. This method was therefore abandoned and the established induction-heater-continuous feed method was adopted.

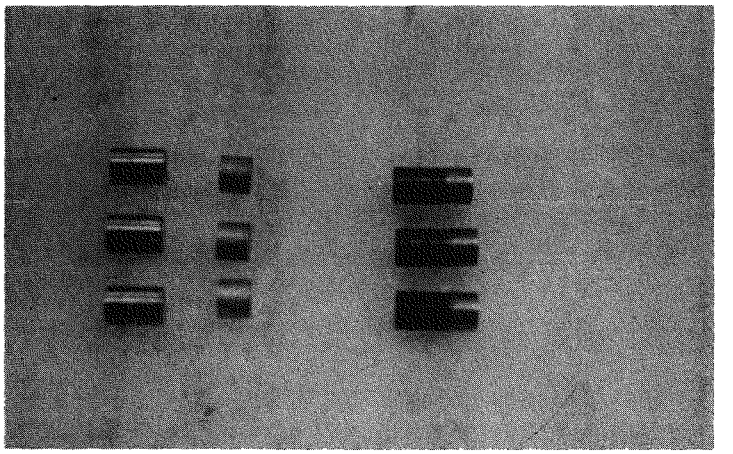

Figure 2-33. P-Legs Before and After Bonding

Bonding molds for holding and positioning parts were designed and fabricated. Satisfactory brazing was accomplished using No. 1801 eutectic silver solder and introducing it through the locating hole at the top of the cap. No flux was required since a reducing atmosphere was introduced in the heating chamber. Figure 2-34 shows a typical brazed wire to cap assembly. Instrumented caps were brazed by using the same process; these are shown in Figure 2-35.

(2) Soldering Legs to Cold End Hardware

Over the past few years, many couples have been fabricated by soldering with pure tin. Development work was required to establish the machine settings to give the correct temperature and time at temperature and amount of tin used on each leg.

Since the cold end segment of the P-leg reacts with the solder, it is the critical factor. Settings of power input and rate of speed through the heating unit have been established. A tin disc 0.002 inch thick will be used on the N-leg, and approximately 0.004 to 0.006 inch will be used on the P-leg. Figure 2-36 shows thermoelectric couple hardware prior to complete assembly as shown in Figure 2-37.

The following table lists the hardware produced during this period:

N-type segments:		P-type segments:			
Hot	1733	Hot	736	P-type legs:	378
Cold	2068	Cold	1300	N-type legs:	350
				Cold cap assemblies:	196

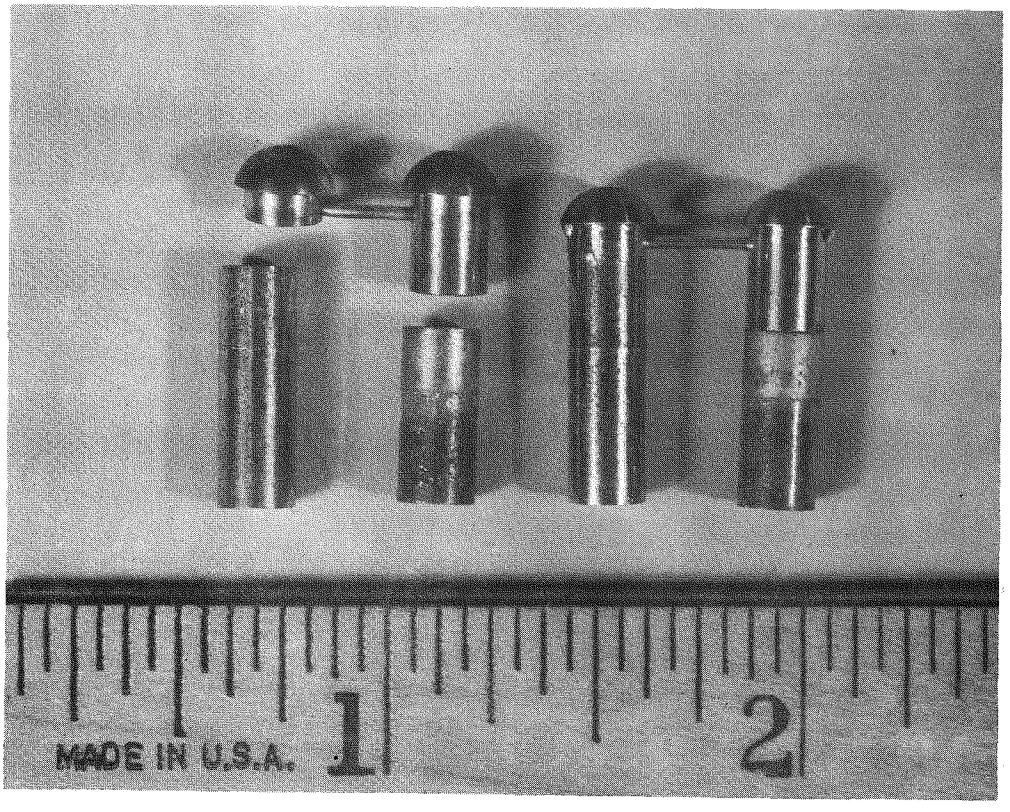

Figure 2-34. Typical Brazed Wire to Cold Cap Assembly

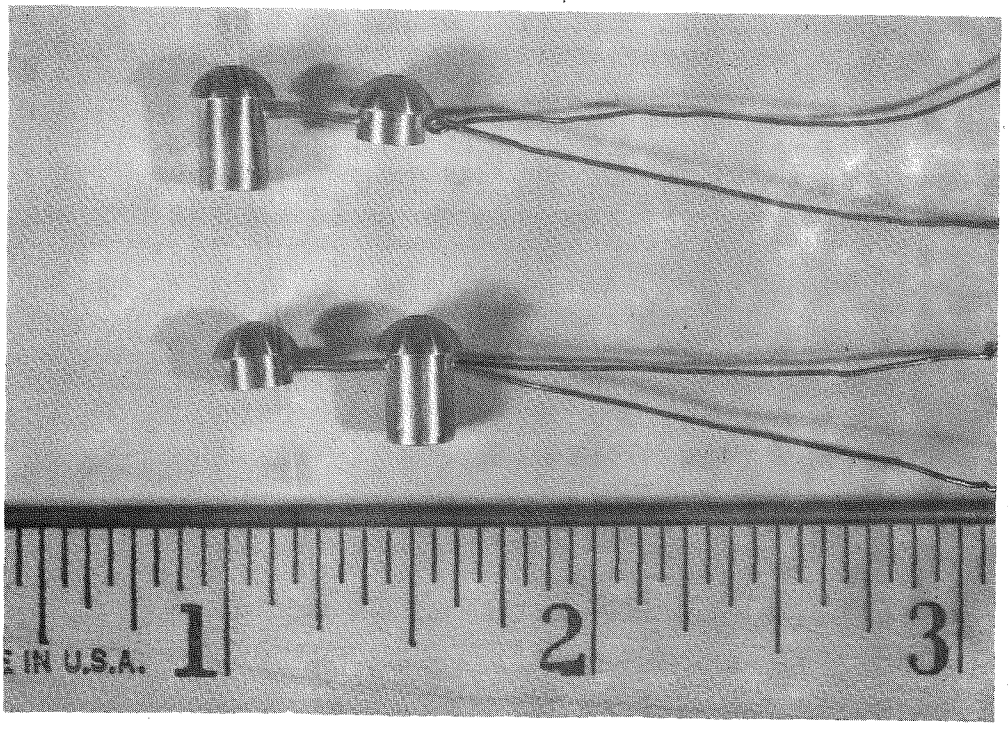

Figure 2-35. Instrumented Cold Caps, Brazed

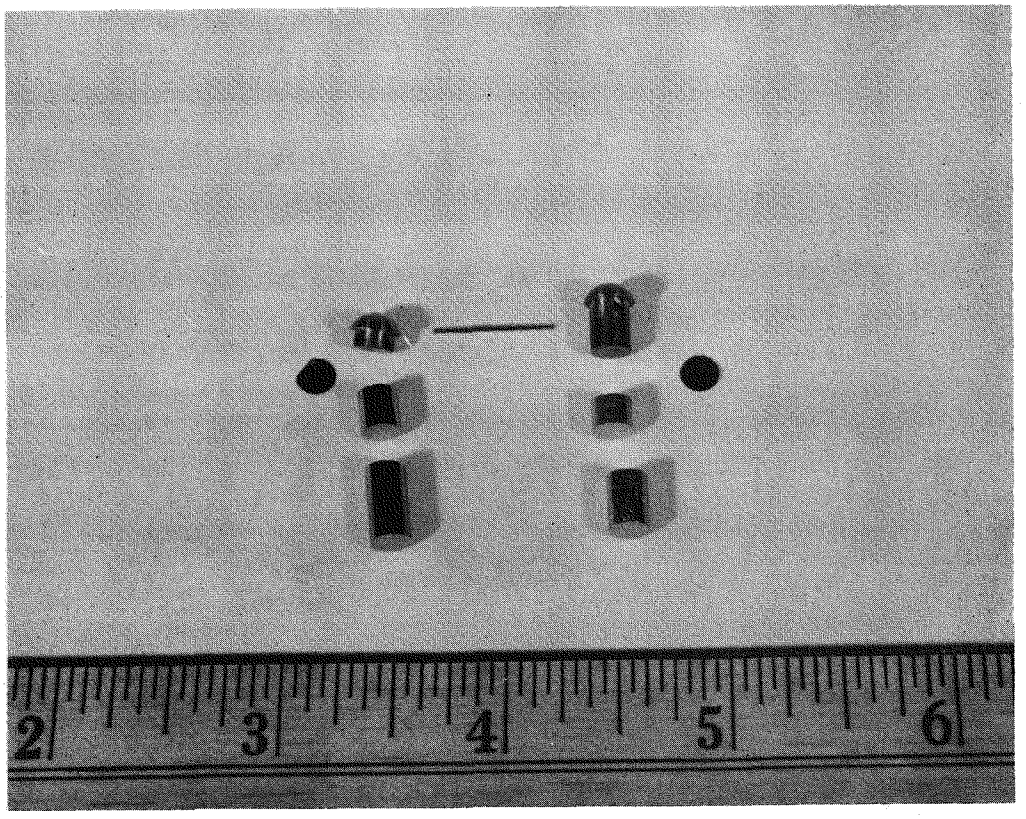

Figure 2-36. Thermoelectric Couple Hardware Before Assembly

2.3 COMPONENT AND SUBASSEMBLY TESTING

2.3.1 FUEL CAPSULE

The Naval Radiological Defense Laboratory has completed general test plans for conducting ocean exposure studies of electrically heated SNAP-21 fuel capsules, laboratory corrosion testing of SNAP-21 materials, and fueled capsule ocean exposure tests. Conceptual designs for the electrically heated fuel capsule, the marine fouling system, the galvanic coupling system mock-up specimens, and fueled capsule exposure chamber specimens are shown in Figures 2-37, 2-38, and 2-39. Detailed designs will be completed during the next work period.

Samples of Hastelloy-C, depleted uranium-8 molybdenum and titanium-621.8 have been supplied for laboratory corrosion studies.

Pacific Northwest Laboratory has started ultrasonic testing of the first set of development fuel capsules. Results, however, will not be available until early in the next report period.

2.3.2 BIOLOGICAL SHIELD

Candidate materials for use as the inner liner-shield compatibility barrier were ordered for compatibility testing. Columbium, molybdenum, and tantalum foils, 0.020 inch thick, will be used for the tests.

Arrangements have been made to conduct biological shield radiation tests in May. The residual Phase I shield being incorporated into the Linde Super Insulation System will be used. ORNL has a 200-watt strontium oxide source available for this test. While a plug will be required to complete shielding, it is not necessary that it be encapsulated. Such encapsulation is only required for oxidation protection of the shield plug alloy when at operating temperature and, due to the short time required for this test, these temperatures will not be reached.

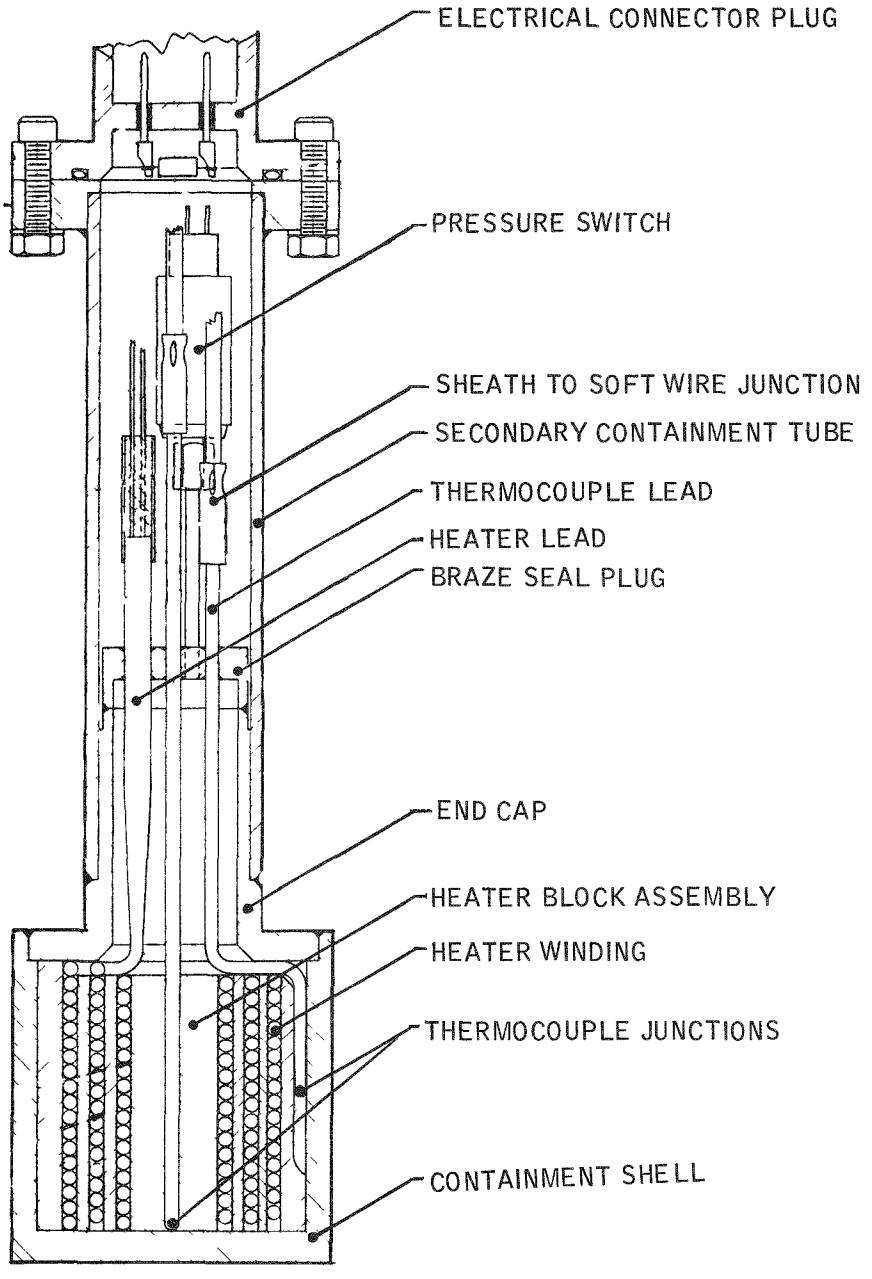

Figure 2-37. Electrically Heated SNAP-21 Fuel Capsule Mock-Up (Conceptual)

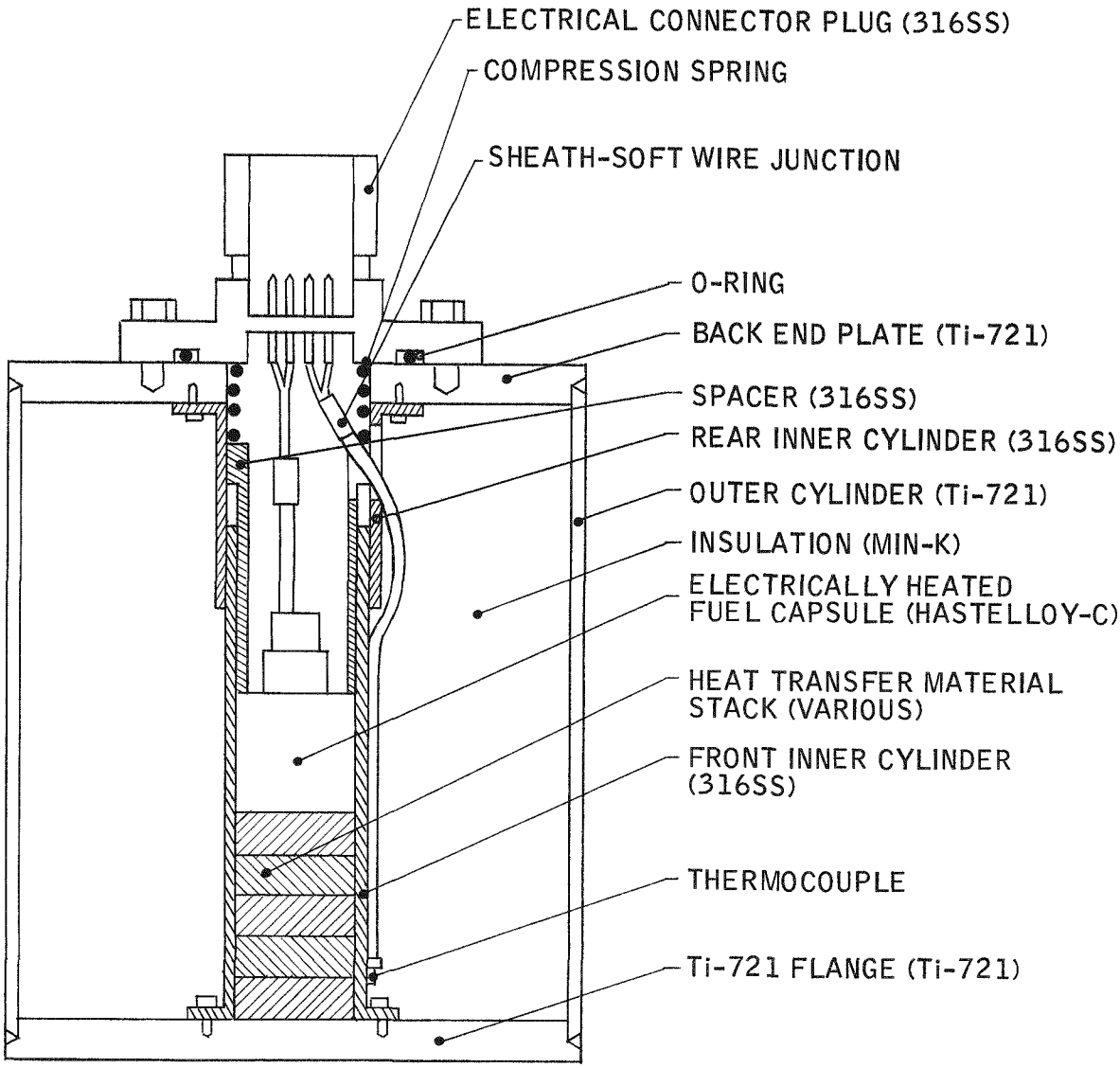

Figure 2-38. Marine Fouling Systems Test Mock-up (Conceptual)

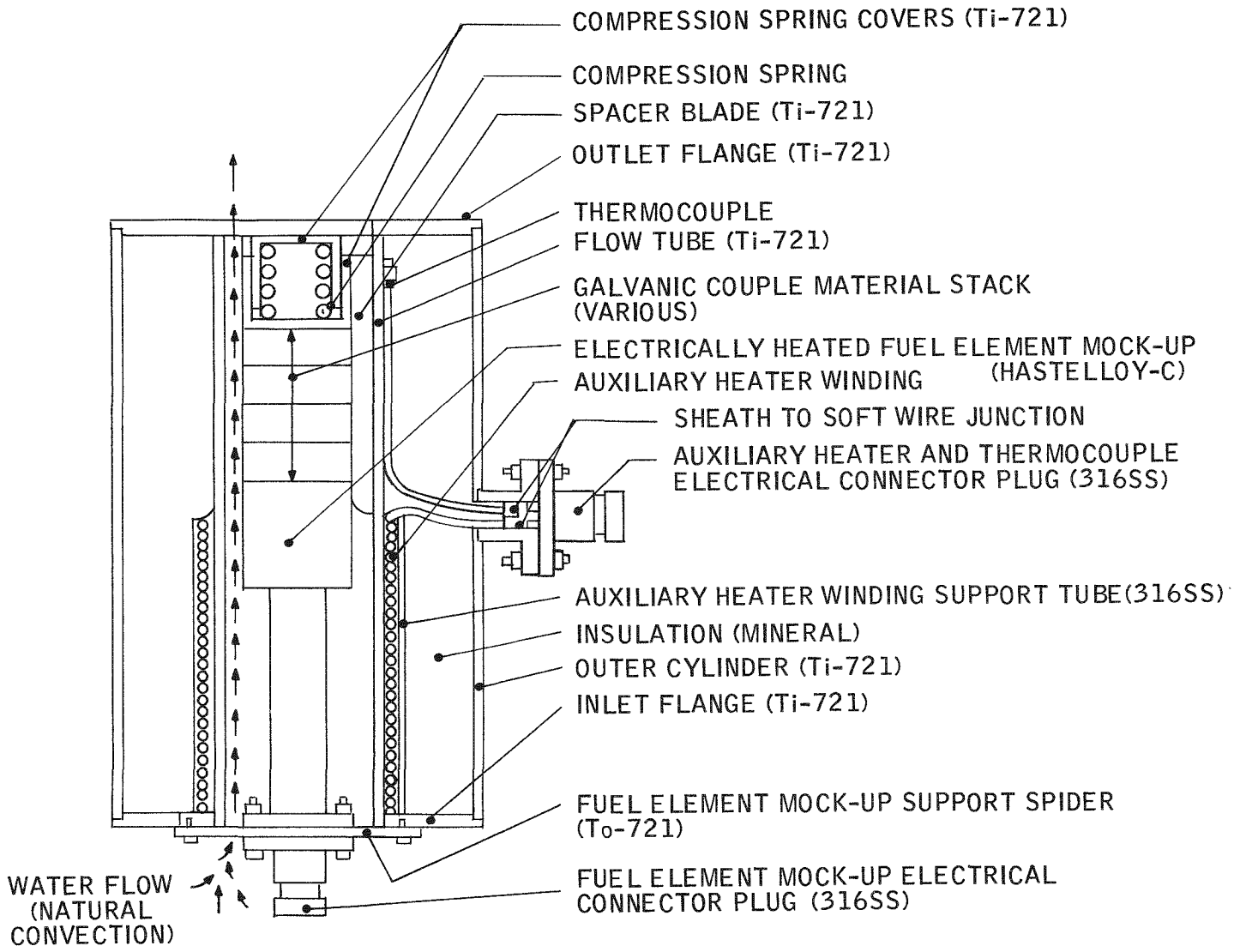

Figure 2-39. Galvanic Coupling Test System Mock-up (Conceptual)

2.3.3 INSULATION SYSTEM

2.3.3.1 Offgassing Investigation

During this reporting period offgassing tests to determine the offgassing rate and gas composition were conducted on the neck tube material (Hastelloy-X), biological shield material, and quartz paper. The offgassing test chamber was fabricated from a Hastelloy-X tube and a vacuum seal flange. Prior to starting the Hastelloy-X offgassing test, the empty chamber (as fabricated and wiped with a cloth) was maintained at 1550°F for 64 hours while evacuating. This was done to provide initial degassing and cleanup.

The pressures shown in Figures 2-40 and 2-41 are as measured. They have not been corrected for gauge calibration or hydrogen content in the sample. Following the outgassing tests, the vacuum gauge will be recalibrated and the curves appropriately corrected. At this time the outgassing rates will be calculated. From the preliminary curves, however, it is apparent that the outgassing rates will be quite low. The curves also indicate that the gas composition from the Hastelloy-X sample does not appear to contain a significant amount of any gas which will cause a problem during gettering.

Fifteen samples, 1/2 inch diameter x 3 inches long (copper coated, depleted uranium - 8 molybdenum), were prepared for the offgassing test of the biological shield material. The samples were cleaned with isopropyl alcohol, loaded into the test chamber, and tested. Figure 2-42 (bottom) shows the offgassing cycle; the pressure versus time curves for cycles E and F are shown on Figure 2-43. The additional 16-1/2 hours of conditioning at 1550°F further conditioned the sample, as evidenced by the cycle F curve being lower than the cycle E curve. The empty chamber pressure rise characteristics prior to the test are also plotted on Figure 2-44 (cycle B of December 14 and cycle C of December 15). When comparing the pressure cycles of the chamber with the sample with those of the empty chamber, (E with B and F with C), it is noted that the sample curves are lower than the empty chamber curves in both cases, indicating that the biological shield material is an absorber rather than an offgasser. Apparently some of the offgassing from the chamber wall is being absorbed by the sample.

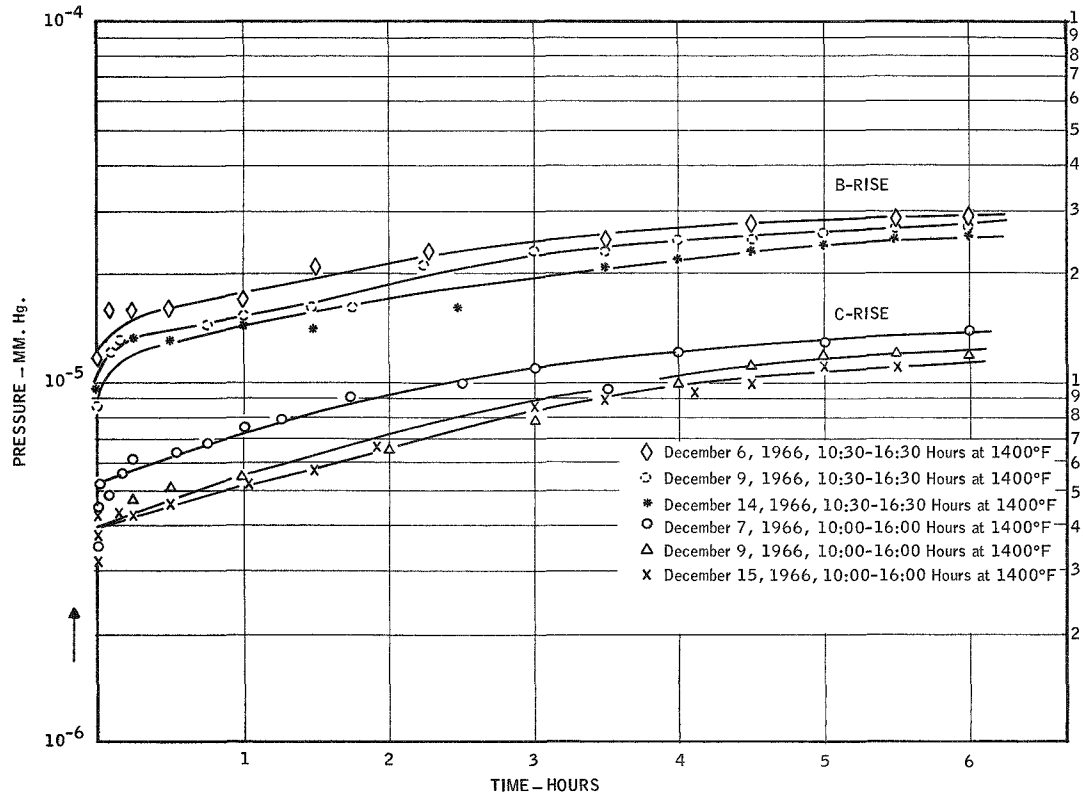

Figure 2-40. Empty Chamber Run: Pressure Rise (mm of Hg) vs Time (hours)

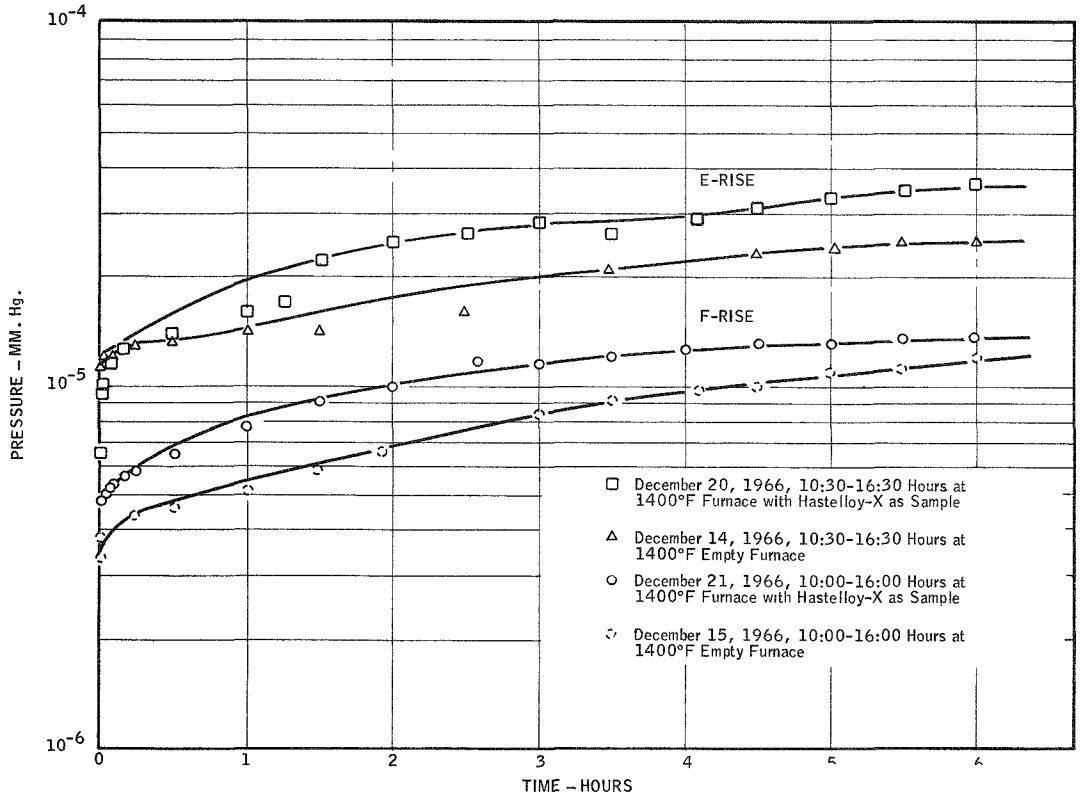

Figure 2-41. Pressure Rise Curves for Hastelloy-X and Empty Chamber

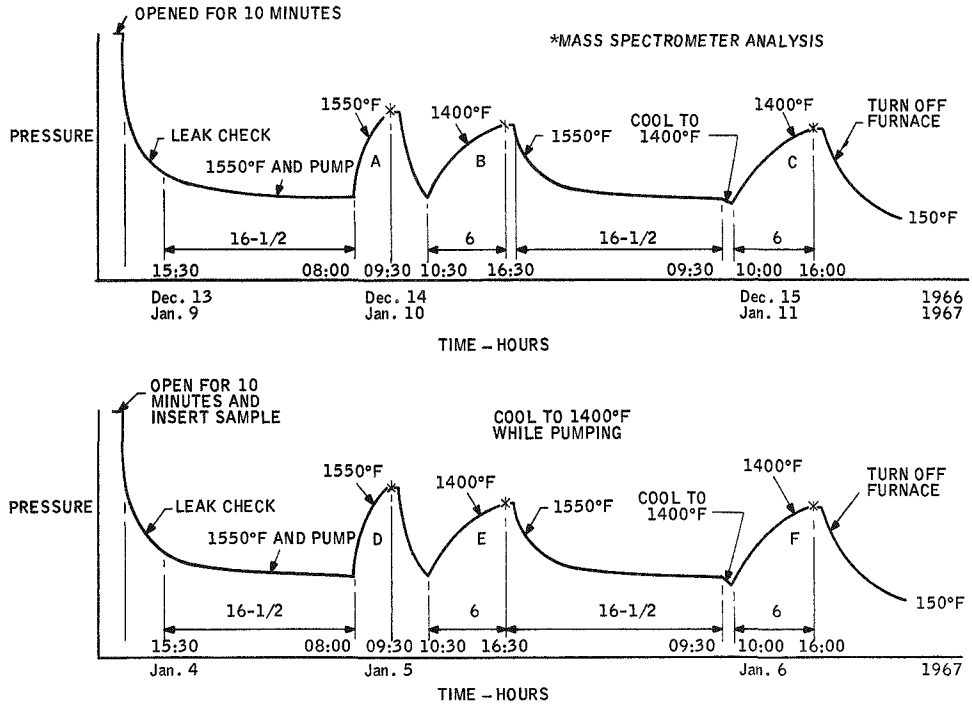

Figure 2-42. Offgassing Cycle for Empty Chamber and Chamber with Radiation Shield Material as Sample

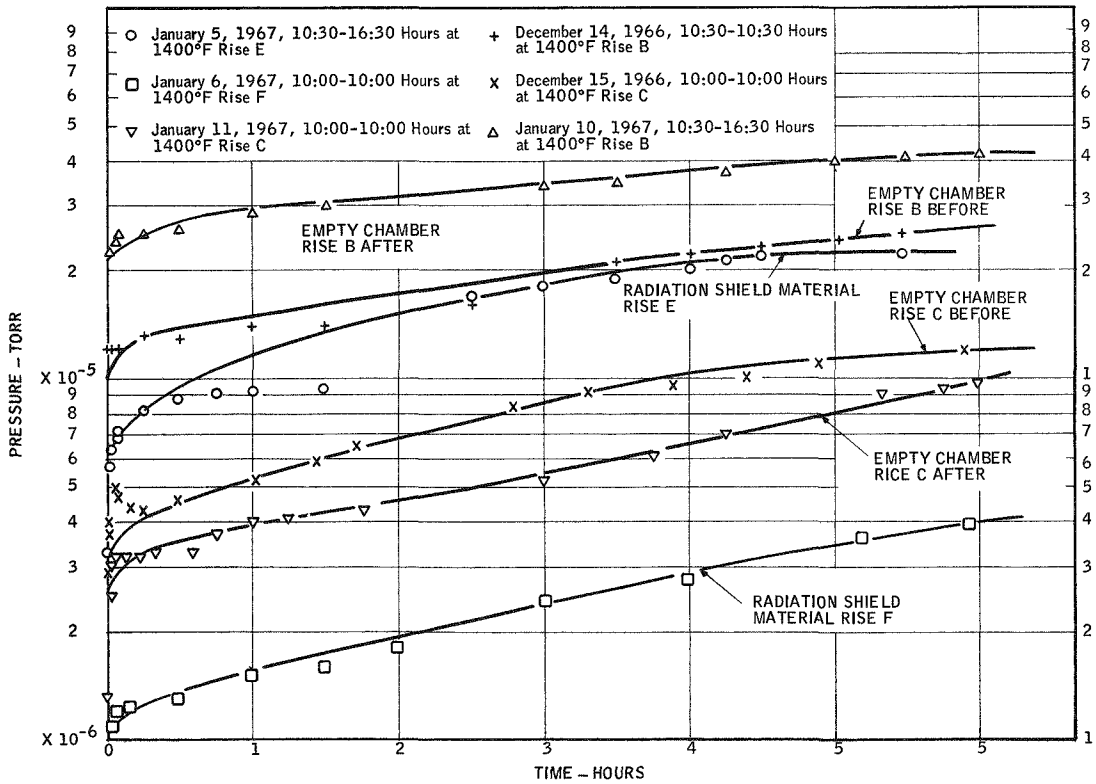

Figure 2-43. Pressure Rise Curves for Empty Chamber and Chamber with Nuclear Material

The mass spectrometer analysis of the gas components taken during the biological shield offgassing cycle and the empty chamber offgassing cycle is presented in Table 7.

During the performance of offgassing work on the Linde-AEC contract (AT(30-1)-3632), it was found that the quartz paper, while being conditioned at 1900°F and tested at 1800°F, had an unacceptable offgassing rate. The main components of the offgassing were carbon monoxide and hydrocarbons (methane, etc.). Since the SNAP-21B prototype unit currently being insulated contains a large amount of quartz paper radiation shield separator material, it was felt that an offgassing test should be conducted at 1400°F to determine if this material will cause an offgassing problem. An 80-square-foot sample of processed quartz paper, as used on the prototype unit, was evaluated for offgassing using a stainless steel chamber. The offgassing cycle was the same as used for the Hastelloy-X sample (Figure 2-44) and the biological shield sample. Following the quartz paper offgassing cycle, an empty chamber cycle was performed to determine the base pressure rise characteristics of the chamber.

The pressure versus time for the sample cycles E and F are shown on Figure 2-46 along with the corresponding empty chamber cycles B and C. After 16-1/2 hours of conditioning at 1550°F, the pressure cycle curve (cycle E) with the quartz paper was only slightly higher than the empty chamber pressure cycle (cycle B). This indicates that the sample is exhibiting a low offgassing rate. The rate will be calculated after the vacuum gauge is recalibrated and the corresponding pressures are corrected for the calibration and the gas composition. After 33 hours of conditioning at 1550°F, the sample pressure cycle curve (cycle F) was lower than the empty chamber pressure cycle curve (cycle C). This indicates that the additional 16-1/2 hours of conditioning have apparently caused the quartz paper to become an absorber, thereby absorbing some of the empty chamber offgassing.

The mass spectrometer analysis of the gas components taken during the paper offgassing cycle and the empty chamber of offgassing cycle is presented in Table 8.

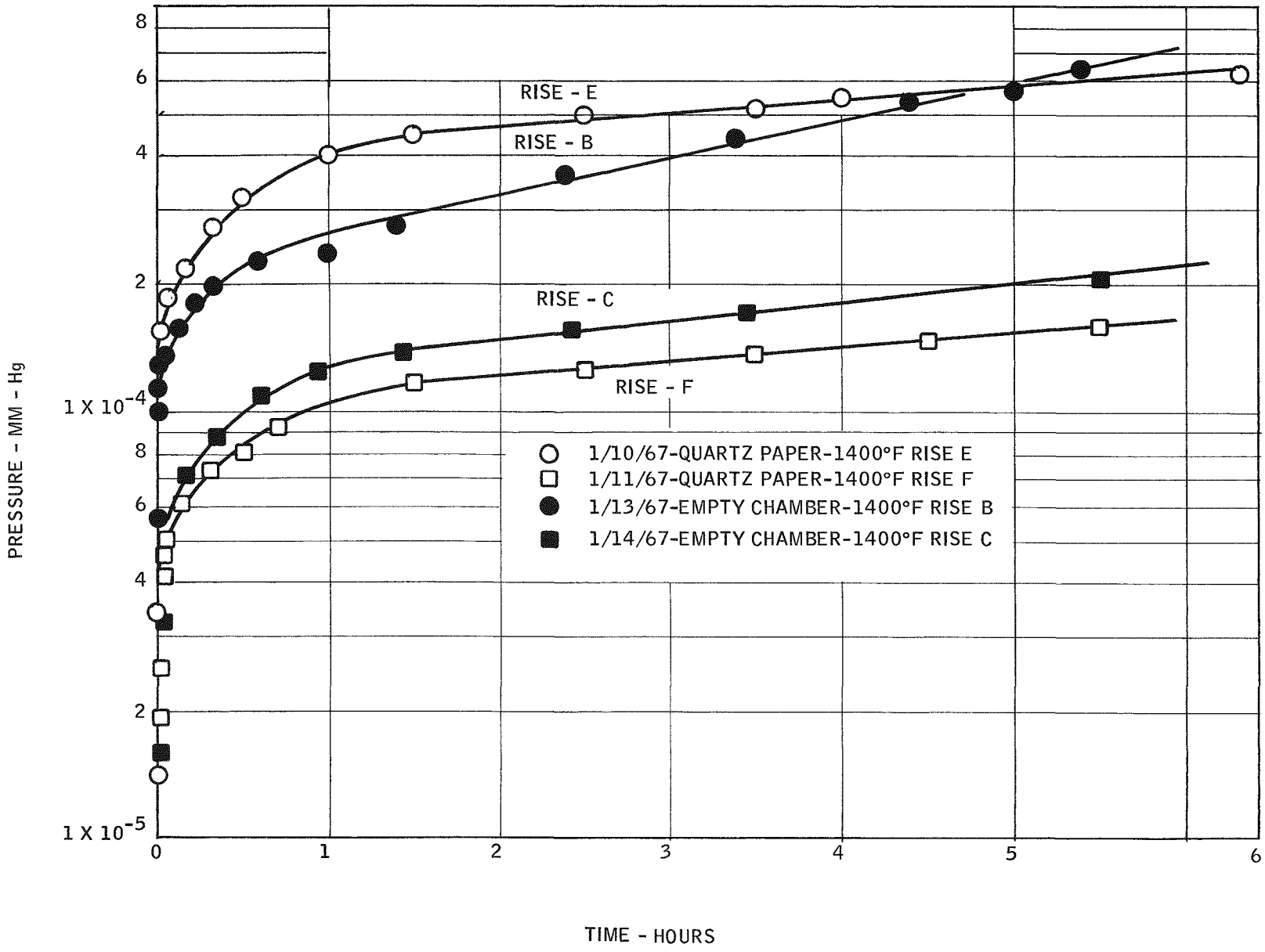

Figure 2-44. Pressure Rise Curves for Chamber with Quartz Paper Sample and Empty Chamber

Table 7. Data from Mass Spectrometer Analysis (see Figure 2-43 for Cycle Identification)

Date	Time	Temp.	Percent Composition					Hydro-carbons	Remarks
			CO_2 (%)	H_2 (%)	Ar (%)	H_2O (%)	N_2-CO (%)		
January 5, 1967	9:30 a.m.	1550° F	--	46.90	16.53	24.89	11.66	--	Biological Shield
January 5, 1967	4:30 p. m.	1400° F	--	85.32	5.16	8.5	0.65	0.354	Biological Shield
January 6, 1967	4:00 p. m.	1400° F	--	81.78	4.79	11.86	1.56	--	Biological Shield
January 10, 1967	9:30 a. m.	1550° F	0.713	76.23	3.74	9.82	8.8	0.68	Empty Chamber
January 10, 1967	4:30 p. m.	1400° F	--	88.68	5.308	3.96	1.76	0.27	Empty Chamber
January 11, 1967	4:00 p. m.	1400° F	0.473	64.12	7.57	23.25	3.8	0.701	Empty Chamber

Table 8. Data from Mass Spectrometer Analysis of Offgassing Constituents

Date	Time	Temp.	Percent Composition					Hydro-carbons	Remarks
			CO_2 (%)	H_2 (%)	Ar* (%)	H_2O (%)	N_2-CO (%)		
January 10, 1967	4:30 p. m.	1400° F	0.21	82.98	3.26	8.33	4.44	0.77	Quartz Paper
January 11, 1967	4:00 p. m.	1400° F	0.22	82.06	1.25	8.90	6.48	1.09	Quartz Paper
January 13, 1967	4:30 p. m.	1400° F	0.09	89.63	0.59	4.13	4.23	1.33	Empty Chamber
January 14, 1967	4:00 p. m.	1400° F	0.11	89.19	0.42	4.44	4.60	1.25	Empty Chamber

*Lines and furnace purged with argon.

2.3.3.2 Vacuum Seal Off and Getter Retention

In the Quarterly Report No. 2, (MMM 3691-12), it was stated that the torque required to effect a vacuum tight seal with the gold O-ring in the seal-off device varied from 17 to 95 ft-lbs. In an effort to obtain a more constant seal-off torque, the gold wire was annealed before it was formed. The point in the ring where the ends of the wire were flame welded was not uniform. Eight rings were checked. The torque required for sealing varied from 22 to 37.5 ft-lbs. A schematic diagram of the apparatus used to evaluate the seal is shown in Figure 2-45. Gold O-rings will be purchased and tested to determine whether rings with uniform cross section have a more uniform sealing torque.

A sample of 347 stainless steel powder pressed plate, 0.050 inches thick, with wire mesh was purchased as a candiate for the getter retainer material. The pore size of this plate was 11 microns. A gas conductance test was run. Figure 2-46 is a schematic of the test apparatus for determining the gas conductance through a porous metal sheet. The 347 stainless steel proved satisfactory from a vacuum conductance standpoint. A vibration test was then performed, using the test fixture shown in Figure 2-47. After the test, the clear plastic sheet was examined and no trace of the simulated getter could be found. An attempt was made to weld this material into a 1/4-inch thick 304 stainless steel plate. The weld was not satisfactory. A satisfactory weld was obtained, however, when the porous metal sheet was welded to a 304 stainless plate 1/16-inch thick. The 1/16-inch thick plate was then welded to the 1/4-inch thick plate.

2.3.3.3 Evaluation of MIN-K 1301

The work done on the performance tradeoff study this quarter consisted of determining the feasibility of developing an alternate to the present insulation system.

The criteria for the insulation material considered for this system is that it must have a low coefficient of thermal conductivity and remain stable at high temperatures over long periods of time.

MIN-K 1301, manufactured by Johns-Manville Corporation, was analyzed for heat loss. The analysis was done for MIN-K 1301 in different forms and in different

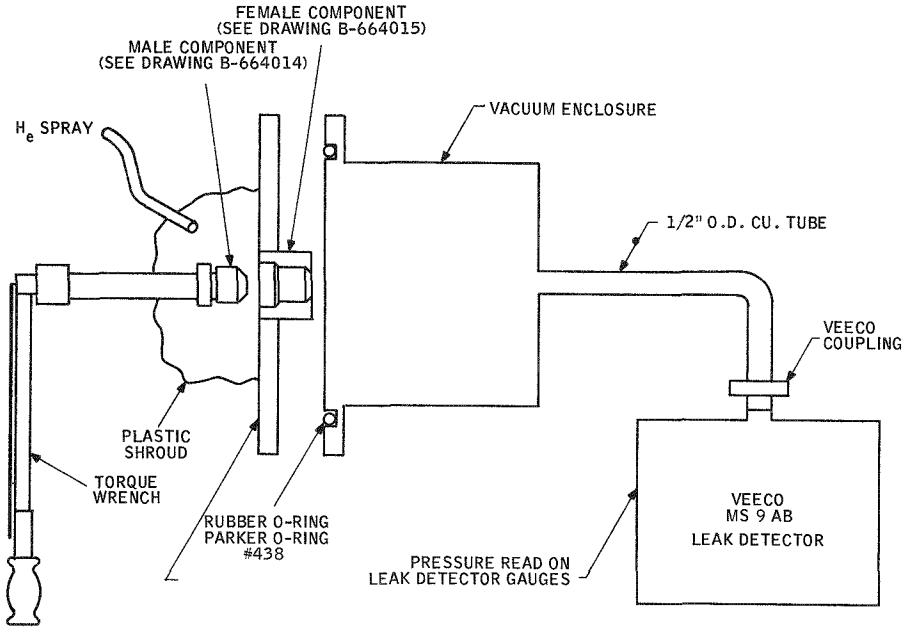

Figure 2-45. Schematic of Gold O-Ring Seal-Off Test Apparatus

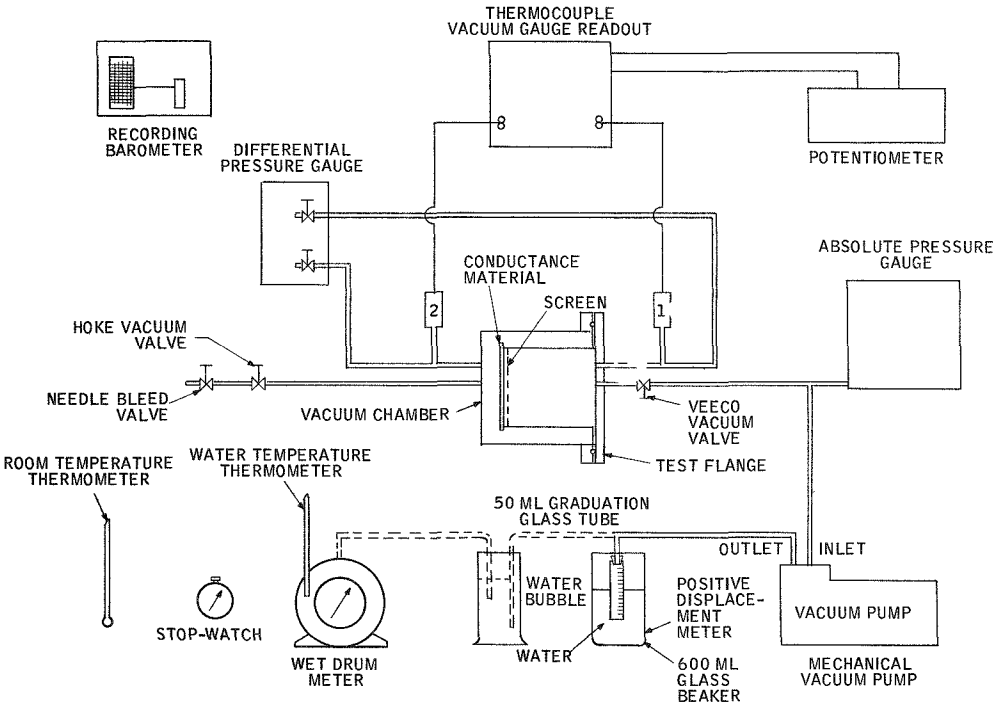

Figure 2-46. Schematic of Test Apparatus for Determining Gas Conductance through a Porous Metal Sheet

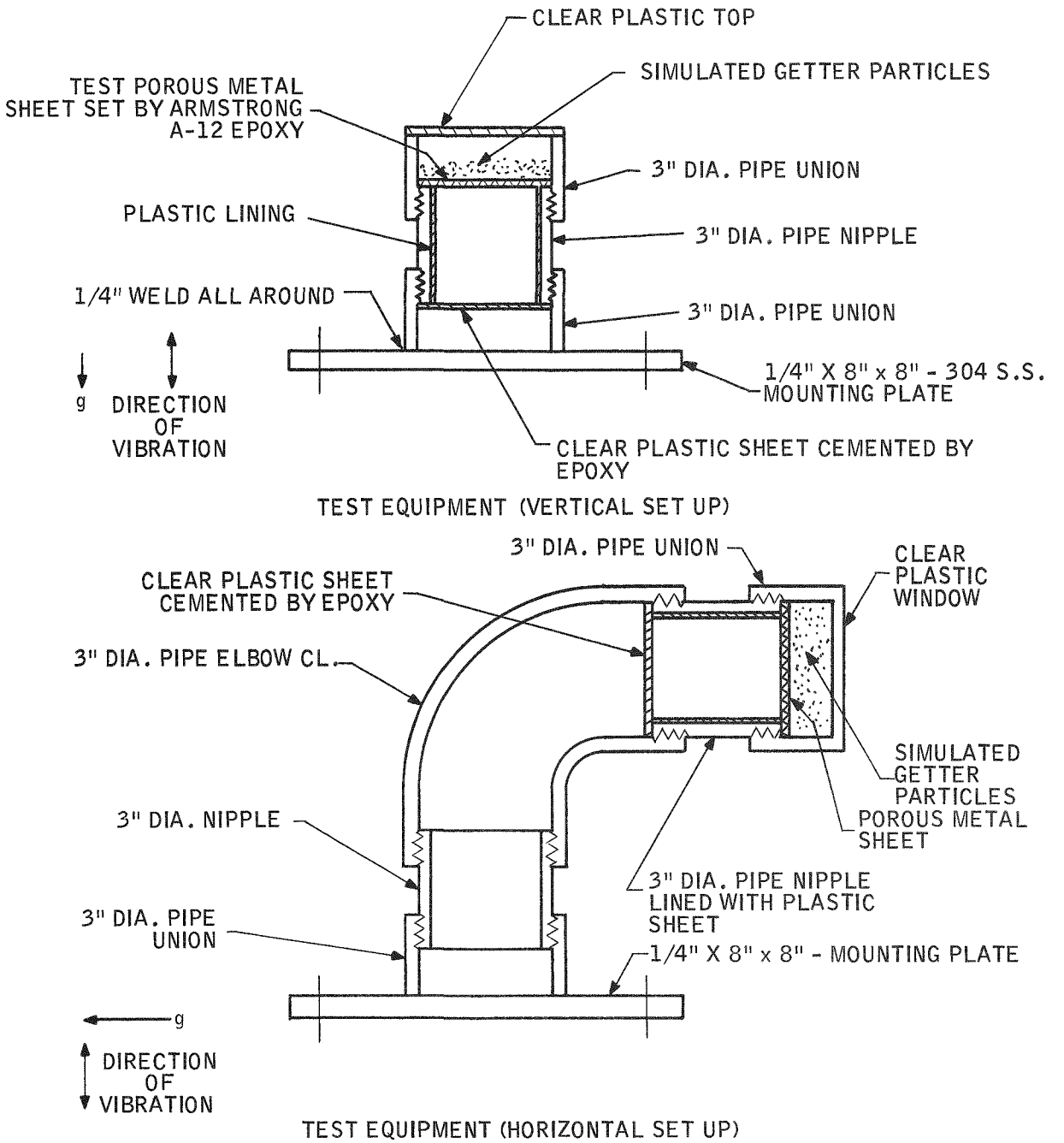

Figure 2-47. Test Fixture for Retainer Vibration Tests

atmospheres. The results are shown graphically in Figure 2-48. The insulation thickness was selected to be 2 inches minimum and 4 inches maximum. Less than a 2-inch thickness would permit too much heat loss; more than a 4-inch thickness would cause the size to exceed specifications. Heat losses for the various configurations are shown in Figure 2-49 and summarized in Table 9.

Table 9 shows that the desired insulation configuration would be 4 inches of block MIN-K in air at 55 mm Hg. This would be with a neck tube which is increased to 4 inches in length and using three 0.187-inch diameter tension rods to support the biological shield. The total heat loss would be 79.5 watts, 34.5 watts over the specified 45-watt system. This is based on the tension rods being inclined at 30° from the horizontal to support the biological shield without inducing thermal stresses in the rods under hot and cold conditions.

The detailed calculations for the tension rod diameters versus neck tube length are contained in Appendix B of Quarterly Report No. 2, MMM 3691-12. The total heat loss through the tension rods and neck tube is summarized in Figure 2-50 for different length neck tubes and rods.

Due to the increased heat loss, the fuel load and shield weight increases. The weight of the shield with 203 watts input is 252 pounds; the weight with 253 watts input is 268 pounds. The increased shield weight will not increase the stress in the rods or neck tube beyond the present allowable stresses. This is verified by calculations contained in Appendix B of Quarterly Report No. 2.

If the insulation envelope configuration were to use the existing 2.497-inch neck tube with 4-inch thick insulation on the bottom and sides, the overall heat leak would be increased to 92 watts, since the neck tube heat leak would increase from 15.9 watts to 26.50 watts and the MIN-K heat leak would increase from 3.45 watts to about 5.5 watts.

The time saved in the assembly of a MIN-K insulation system over the present web and foil system would be about one month, thus reducing the cost. However, since this system does not meet the specification, the decision was made to use the foil insulation system.

A representative heat leak calculation is presented in Appendix C.

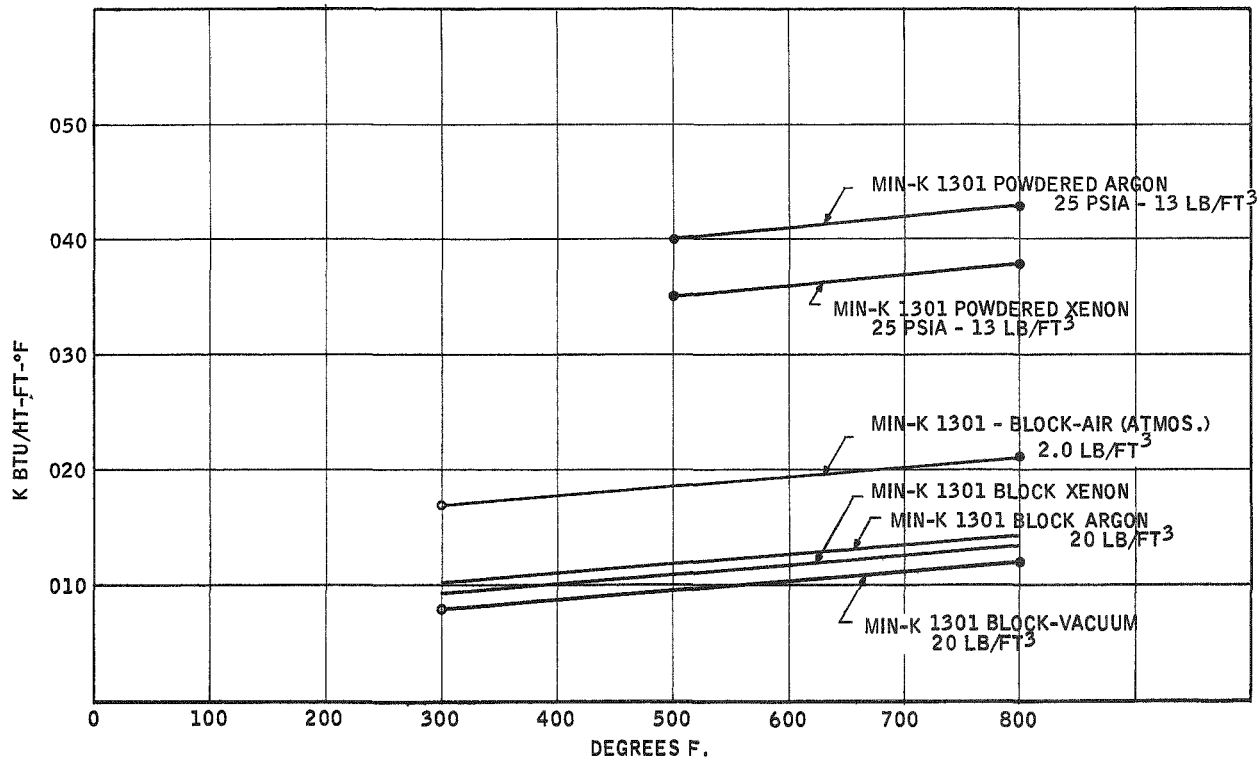

Figure 2-48. MIN-K Tests: Thermal Conductivity vs Temperature

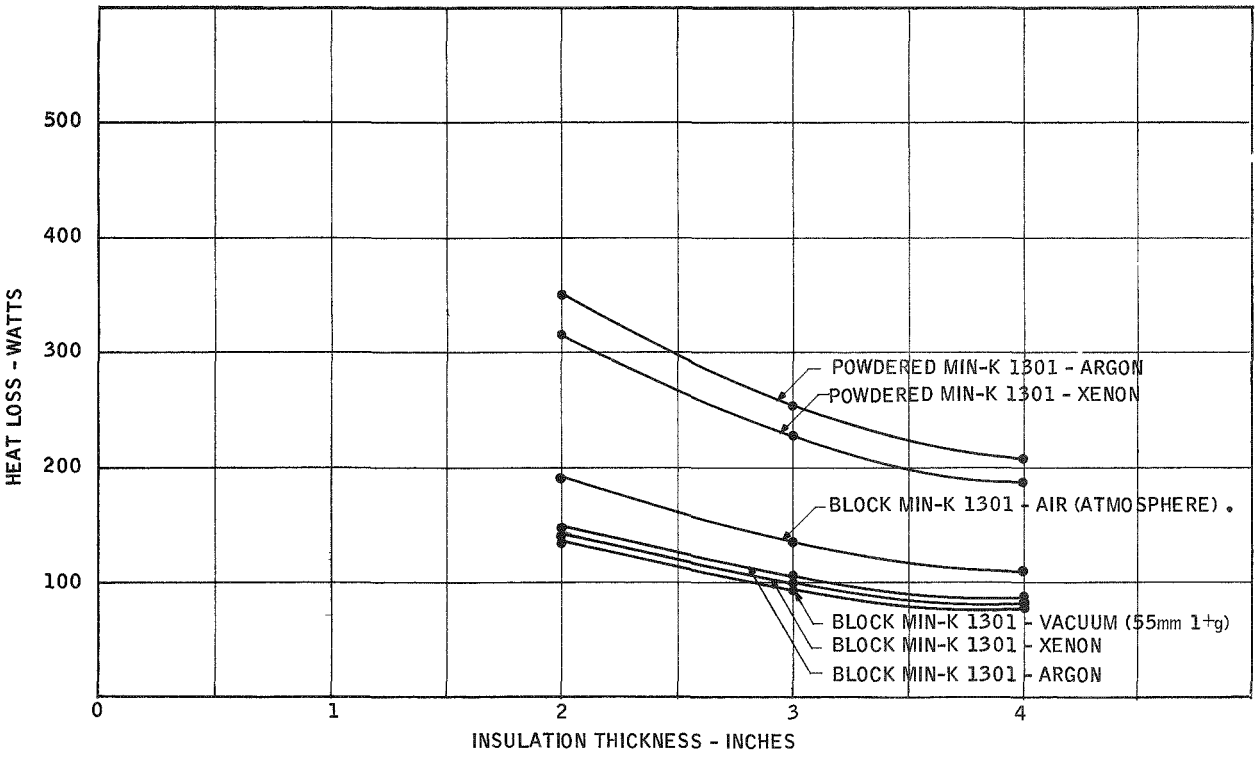

Figure 2-49. SNAP-21 Insulation System Heat Loss

Table 9. MIN-K Insulation Test Summary

Insulation Configuration	Insulation Thickness	Neck Tube Length	Tension Rod Length	Heat Leak (Watts)			Total Heat Leak (Watts)
				Neck Tube	Tension Rods	Ins.	
Powdered MIN-K 1301 Argon Backfilled	4	4	4	15.9	9.0	165	209.9
	3	3	3	21.2	12.0	222.3	255.5
	2	2	2	31.8	18.1	301.2	351.1
Powdered MIN-K 1301 Xenon Backfilled	4	4	4	15.9	9.0	163.5	188.4
	3	3	3	21.2	12.0	197.5	230.7
	2	2	2	31.8	18.1	265.8	315.7
Block MIN-K 1301 Air Atmosphere	4	4	4	15.9	9.0	86.5	111.4
	3	3	3	21.2	12.0	106.0	139.2
	2	2	2	31.8	18.1	144.0	192.9
Block MIN-K 1301	4	4	4	15.9	9.0	54.56	79.46
	3	3	3	21.2	12.0	66.47	99.67
	2	2	2	31.8	18.1	89.2	139.10
Block MIN-K 1301 Argon Backfilled	4	4	4	15.9	9.0	58.5	83.4
	3	3	3	21.2	12.0	71.0	104.2
	2	2	2	31.8	18.1	96.0	145.9
Block MIN-K 1301 Xenon Backfilled	4	4	4	15.9	9.0	56.6	81.5
	3	3	3	21.2	12.0	69.0	102.2
	2	2	2	31.8	18.1	92.5	142.4

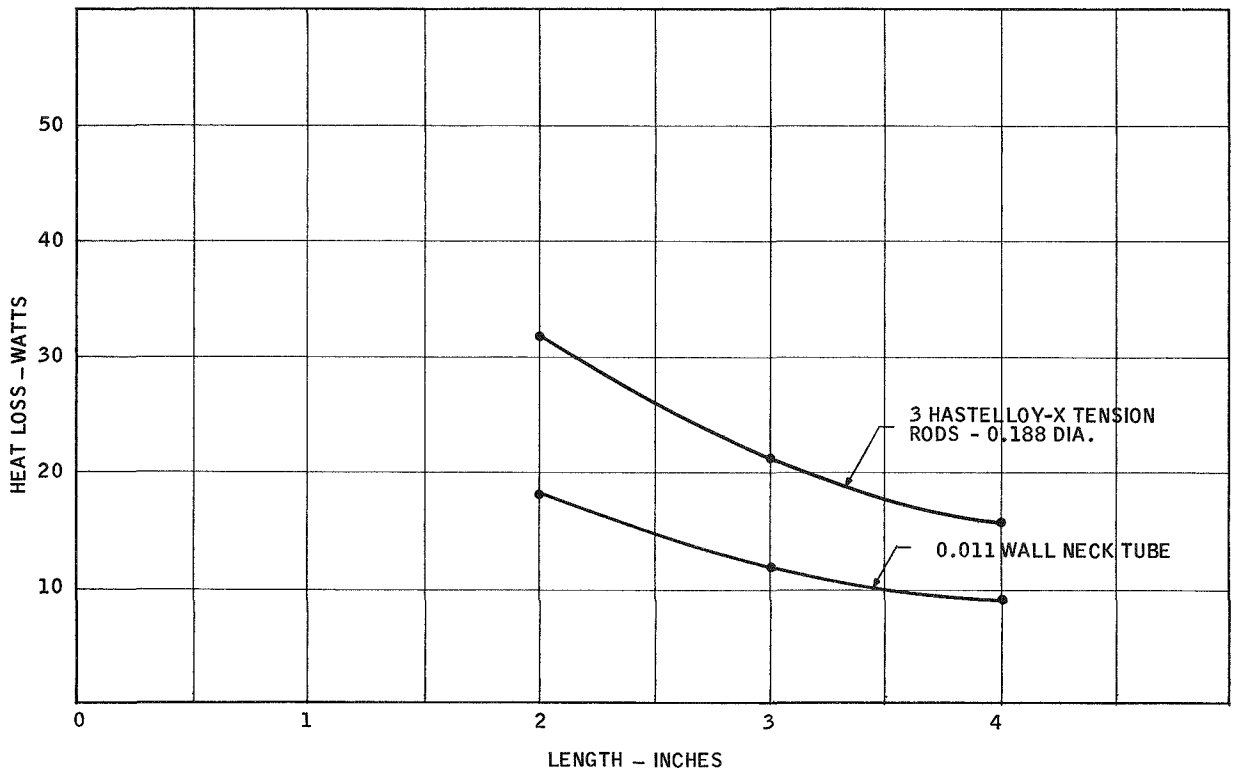

Figure 2-50. Neck Tube and Tension Rod Heat Leak

2.3.4 SEGMENTED HOLD DOWN RING

A study was made to determine the best method to test the segmented ring to ensure that it will meet its intended function. The study consisted of determining the type of materials which would closely simulate the shield mass and center of gravity of the actual shield and insulation system. The mock-up shield would be a combination of two metals, lead and steel. The enclosure would be of existing residual upper and lower sections of the outer envelope and fabricated by welding into an insulation envelope. Experimental testing could then be performed to determine segmented hold down ring capabilities under simulated dynamic loads experienced by the system.

2.3.5 PRESSURE VESSEL

No effort expended on this subtask during this report period.

2.3.6 THERMOELECTRIC GENERATOR

2.3.6.1 Cold End Heat Transfer Testing

Development effort was continued to improve the heat transfer efficiency between the cold end of the leg and the cold frame. This effort consisted of:

- Further investigation into comparative fitting of spherical radii.
- Investigation into the effect of various metallic foils in the spherical interface.
- Procurement of in-line followers in various lengths and diameters. The in-line followers ordered were 0.2495 inch, 0.2485 inch, and 0.2465 inch in diameter and 0.50, 0.75, and 1.10 inch in length. By varying diameter and length, it would be possible to find a design flexible enough for ease of assembly and resistance to shock and vibration without too great a temperature difference between the leg-follower junction and the cold frame.
- Initial testing of in-line hardware.

The following paragraphs describe the tests completed this quarter.

a) Test #4 used 0.001-inch lead foil between cold caps and followers and compared Phase I cold end hardware with that of SNAP-27 spherical precision. Legs #1 and #3 used cold end hardware with improved spherical precision; legs #2 and 4 used residual Phase I cold caps and followers. The test showed that the use of 0.001-inch lead foil in the interface between the follower and cold cap increases the effective heat transfer coefficient across the interface by about 100% (comparing the results leg-for-leg with test #2).

b) Test #5 used 0.001-inch gold foil (annealed at 600° F) between the cold caps and followers. Except for the use of a different type of foil, the hardware used was that of test #4. Unprocessed MIN-K insulation was inadvertently used, hence the test results are felt to be invalid.

c) Test #6 was the same as test #5 except for the use of processed MIN-K.

Test #6 showed that using 0.001-inch gold foil in the interface between the follower and cold cap increases the effective heat transfer coefficient across the interface by less than 20 percent with the improved precision hardware (legs #1 and #3), and by about 50 percent in the case of the Phase I residual hardware (legs #2 and #4). This difference between pairs of legs is probably caused by the inability of the gold foil (even after annealing) to cup smoothly in the followers. Comparing test #6 with test #4, the gold foil is decidely inferior to the lead foil. The slightly higher cold frame temperature in test #6 was caused by a piece of microquartz insulation which lodged between the cold frame and cooling block during assembly.

d) Test #7 was the same as test #6 except for the use of 0.002-inch indium foil between cold caps and followers. This increased the effective heat transfer coefficient across the interface by an average of about 200 percent. Comparing tests #4, #6, and #7, the indium foil is superior to either the gold or the lead foils.

e) Test #8 was the same as test #7 escept that legs #1 and #3 used followers with no hardcoating on the spherical surface. The test indicated an increase in the effective heat transfer coefficient across the interface by more than 250 percent, in the case of the Phase I residual hardware (legs #2 and #4), and by about 100 percent with the nonhardcoated followers (legs #1 and #3).

f) Test #9 used four nonhardcoated, high-precision followers with legs #1 and #3 having cold caps with SNAP-27 finishes and tolerances and legs #2 and #4 having Phase I residual cold caps. The 1.5-mil radial mismatch of legs #2 and #4 decreased the effective heat transfer coefficient across the follower-cold cap interface by about 60 percent.

g) Test #10 used 0.001-inch aluminum foil between cold caps and followers and compared Phase I cold end hardware with that having SNAP-27 spherical precision. The cold end hardware used was similar to that of test #2 (refer to Quarterly Report No. 2, MMM 3691-12). Legs #1 and #3 used cold end hardware with improved spherical precision. Legs #2 and #4 used residual SNAP-21 Phase I cold caps and followers.

   The results of test #10 show that the use of 0.001-inch aluminum foil in the interface between the follower and cold cap results in negligible improvement in the effective heat transfer coefficient across the interface in the case of the improved precision hardware (legs #1 and #3). The validity of the data on legs #2 and #4 is doubtful since, upon disassembly, it was discovered that the thermocouples on #2 cold cap and #4 follower had come loose from their mountings.

h) Test #11 was similar to test #10 except for the use 0.001-inch silver foil (annealed at 600° F) between cold caps and followers. The results of test #11 show that the use of 0.001-inch silver foil in the interface between the follower and cold cap increases the effective heat transfer coefficient across the interface by about 70 percent with the Phase I residual hardware. In the case of the improved precision hardware, use of the foil decreased the coefficient by about 20 percent. It is felt that these phenomena resulted from a lack of foil malleability, even after annealing. Hence, with a poor fit (Phase I hardware) the conformability of the foil is greater than the conformability of the ball to the socket (exclusive of foil)

resulting in an overall improvement in fit. Conversely, with a relatively good fit, the foil's conformability is less than the conformability of the ball to the socket (exclusive of foil) resulting in an overall degradation in fit.

i) Test #12 used heat transfer grease (Dow Corning #340 Silicone Heat Sink Compound) between the follower and cold frame. The hardware was similar to that used in test #11 except that no foil was used.

The results of test #12 show that the use of heat transfer grease at the interface increases the effective heat transfer coefficient across the interface by 100 percent.

j) Test #13 was similar to test #12 except that at different heat transfer grease (Wakefield Type 120 Thermal Joint Compound) was used in the follower-cold frame interface. This test was also the initial use of the newly procured alternate two-couple test fixture.

The results of test #13 show that both the Dow Corning and the Wakefield greases offer the same degree of improvement on heat transfer. Position #4 in this test also demonstrates that if grease is used, the follower-to-hole clearance can be opened up appreciably without adverse thermal effects.

k) Test #14 used two in-line follower legs 0.2494 inch in diameter by 0.749 inch in length, and two 0.2495-inch diameter by 1.112-inch long followers soldered to four standard SNAP-21 legs. This allowed a diameteral clearance of 0.005 inch between the follower and cold frame, allowing very little flexibility and making assembly difficult and tedious. After the test, on disassembly, three of the legs were found broken just above the solder joint. The results of the test were thus felt to be invalid.

l) Test #15 was run with legs of the same dimensions as those of test #14, except that the 1.112-inch long followers were replaced with 0.499-inch long ones. Since the diameter was still large, the rod which protrudes from the hot shoe into the hot electrode strap was filed off to give flexibility at the hot end. These legs remained intact. The effect of length on temperature drop is evident in this test, as the average drop is 23° F less with the longer follower.

Tables 10, 11, and 12 summarize the cold end heat transfer testing for the first quarter of 1967.

Future in-line testing will include smaller diameter followers and effects of various greases. After this, it is felt that more tests are needed in mismatch of spherical surfaces. Since indium foil showed great promise, indium plating is also being investigated. Assembly is made quite difficult with the foils.

2.3.6.2 Leg Inspection Development Testing

During this report period, development effort was expended to improve the testing method used to evaluate both the physical and electrical bond integrity of segmented N-legs. This effort consisted of:

- Evaluation of the historical method used to evaluate bond integrity (R vs L)
- New approach
- Application
- Results
- Future development and application

The following paragraphs describe the problem of evaluating bond integrity of SNAP-21 segmented N-legs and the approach to the solution. (Additional tests are planned for the next report period which will further refine this test method and increase its application to include the bond integrity of segmented P-legs and direct, nondestructive measurement of the resistivity of individual hot and cold N- and P-segments.)

a) Historical evaluation of bond integrity (R vs L)

The R vs L method yields a total resistivity trace for the entire length of the segmented leg.

Table 10. Ball and Socket Cold End Heat Transfer Tests Performed During First Quarter of 1967 (Couples)

Leg No.	Follower Spring Pressure 150 psi (on leg) Test Description and Number	Follower to Hole Clearance (Diam.) In.	Follower Spherical Radius, In.	Follower Spherical Surface Finish μ In.	Cold Cap Spherical Radius, In.	Cold Cap Spherical Surface Finish μ In.	Hot Button Temp T_h (°F)	Cold Cap Temp T_c (°F)	Follower Temp T_f (°F)	Ave. Cold Frame Temp T_{cf} (°F)	Seebeck Voltage (MV)	$T_c - T_f$ °F	$T_f - T_{cf}$ °F	$T_c - T_{cf}$ °F	Internal Gas Pressure, psig
1	Test No. 4	+0.0012	0.12535	8	0.1250	< 32	1101.5	102.0	79.0	73.5	128.25	23.0	5.5	28.5	3.0
2	Same as Test #1 with 0.001" Lead Foil in Cold Cap-to-Follower Gap	+0.0010	0.1274	16	0.1235	32	1101.5	122.0	77.5	73.5	125.55	44.5	4.0	48.5	↓
3		+0.0011	0.12535	8	0.1250	< 32	1099.5	101.5	80.5	73.5	127.15	21.0	7.0	28.0	
4		+0.0012	0.1275	16	0.1235	32	1098.5	105.5	81.0	73.5	126.20	24.5	7.5	32.0	3.0
1	Test No. 6	+0.0013	0.12535	8	0.1250	< 32	1098.0	127.0	91.5	84.0	126.40	35.5	7.5	43.0	2.55
2	Same as Test #1 with 0.001" Gold Foil in Cold Cap-to-Follower Gap	+0.0010	0.1274	16	0.1235	32	1100.0	137.5	94.0	84.0	124.50	43.5	10.0	53.5	↓
3		+0.0009	0.12535	8	0.1250	< 32	1098.0	123.0	93.0	84.0	125.65	30.0	9.0	39.0	
4		+0.0012	0.1275	16	0.1235	32	1100.0	125.0	91.0	84.0	124.75	34.0	7.0	41.0	2.55
1	Test No. 7	+0.0013	0.12535	8	0.1250	< 32	1101.5	94.0	82.5	73.0	129.25	11.5	9.5	21.0	3.2
2	Same as Test #1 with 0.002" Indium Foil in Cold Cap-to-Follower Gap	+0.0010	0.1275	16	0.1235	32	1100.5	108.0	80.0	73.0	126.25	28.0	7.0	35.0	↓
3		+0.009	0.12535	8	0.1250	< 32	1099.5	91.0	84.0	73.0	128.40	7.0	11.0	18.0	
4		+0.0012	0.1275	16	0.1235	32	1102.5	91.0	82.0	73.0	127.65	9.0	9.0	18.0	3.2
1	Test No. 8	+0.0014	0.1250	4	0.1250	< 32	1101.0	90.0	83.0	74.0	129.40	7.0	9.0	16.0	3.1
2	Same as Test #7 Non-Hardcoated Follower Socket and Phase I Residual Parts (see text)	+0.0009	0.1273	16	0.1235	32	1102.0	97.0	81.0	74.0	127.30	16.0	7.0	23.0	↓
3		+0.0011	0.1250	4	0.1250	< 32	1099.0	83.5	85.0	74.0	128.85	-1.5	11.0	9.5	
4		+0.0012	0.1275	16	0.1235	32	1103.0	91.0	82.0	74.0	127.60	9.0	8.0	17.0	3.1
1	Test No. 9	+0.0014	0.1250	4	0.1250	< 32	1099.5	90.5	84.0	75.0	127.60	6.5	9.0	15.5	3.25
2	Non-Hardcoated Follower Sockets (see text for full description)	+0.0008	0.1250	4	0.1235	< 32	1100.0	102.0	84.5	75.0	127.35	17.5	9.5	27.0	↓
3		+0.0012	0.1252	4	0.1250	< 32	1099.0	88.5	83.0	75.0	129.20	5.5	8.0	13.5	
4		+0.0009	0.1250	4	0.1235	< 32	1103.0	99.5	81.5	75.0	126.40	18.0	6.5	24.5	3.25

Table 11. Ball and Socket Cold End Heat Transfer Tests Performed During First Quarter of 1967 (Legs)

Test No.	Leg No.	Follower Spring Pressure 150 psi (on leg)	Follower to Hole Clearance (Diam.) In.	Follower Spherical Radius, In.	Follower Spherical Surface Finish μ In.	Cold Cap Spherical Radius, In.	Cold Cap Spherical Surface Finish μ In.	Hot Button Temp. T_h (°F)	Cold Cap Temp. T_c (°F)	Follower Temp T_f (°F)	Ave Cold Frame T_{cf} (°F)	Seebeck Voltage (MV)	$T_c - T_f$ °F	$T_f - T_{cf}$ °F	$T_c - T_{cf}$ °F	Internal Gas Pressure Psig
10	1		+0.0013	0.12535	8	0.1250	< 32	1099.0	120.0	81.5	74.5	125.65	38.5	7.0	45.5	2.8
	2		+0.0009	0.1273	16	0.1235	32	1100.5	106.0	81.5		127.00	24.5	7.0	31.5	↓
	3		+0.0010	0.12535	8	0.1250	< 32	1100.5	117.0	81.5		127.05	35.5	7.0	42.5	↓
	4		+0.0012	0.1275	16	0.1235	32	1100.0	117.0	108.0		125.35	9.0	33.5	42.5	2.8
11	1		+0.0013	0.12535	8	0.1250	<32	1100.0	129.0	84.0	74.0	125.00	45.0	10.0	55.0	3.25
	2		+0.0009	0.1273	16	0.1235	32	1102.5	110.5	82.5		126.70	28.0	8.5	36.5	↓
	3		+0.0010	0.12535	8	0.1250	< 32	1100.5	130.5	83.5		126.10	47.0	9.5	56.5	↓
	4		+0.0012	0.1275	16	0.1235	32	1100.0	121.0	82.0		125.05	39.0	8.0	47.0	3.25
12	1		+0.0013	0.12535	8	0.1250	< 32	1094.5	123.5	79.5	74.5	125.15	44.0	5.0	49.0	2.9
	2		+0.0009	0.1273	16	0.1235	32	1099.5	135.0	79.0		124.85	56.0	4.5	60.5	↓
	3		+0.0010	0.12535	8	0.1250	< 32	1100.0	111.5	79.0		127.55	32.5	4.5	37.0	↓
	4		+0.0012	0.1275	16	0.1235	32	1099.5	149.5	78.5		123.15	71.0	4.0	75.0	2.9
13	1		+0.0006	0.12535	8	0.1250	< 32	1099.5	123.0	80.0	76.0	125.10	43.0	4.0	47.0	3.40
	2		+0.0006	0.1273	16	0.1235	32	1101.5	136.5	80.5		123.30	56.0	4.5	60.5	↓
	3		+0.0005	0.12535	8	0.1250	< 32	1099.0	115.5	80.5		126.80	35.0	4.5	39.5	↓
	4		+0.0027	0.1275	16	0.1235	32	1100.0	148.5	79.5		120.80	70.0	3.5	72.5	3.40

T_c - Cold Cap Temp. ~ °F

T_f - Follower Temp. ~ °F

T_{cf} - Average Cold Frame Temp. ~ °F

Table 12. In-Line Cold End Heat Transfer Testing Performed During First Quarter of 1967

Leg No.	Follower Spring Pressure 150 psi (on leg) Test Description and Number	Follower to Hole Clearance (Diam.) In.	Follower Length (In.)	Follower Diam. (In.)	Hot Button Temp T_h (°F)	Leg Follower Interface Temp T_c (°F)	Ave. Cold Frame Temp T_{cf} (°F)	See-beck Volt-age (MV)	$T-T_{cf}$ (°F)	Internal Gas Pressure psig
1	Test #15	0.0013	0.748	0.2492	1103	94.0	74.5	127.1	19.5	3.30
2		0.0010	0.499	0.2493	1108	120.0	74.5	125.8	45.5	3.30
3	In-Line Test for	0.0011	0.749	0.2494	1094	101	74.5	127.15		3.30
4	Length Effects, 0.2495 diam	0.0010	0.498	0.2495	1098	121.5	74.5	123.75	47.0	3.30

Example

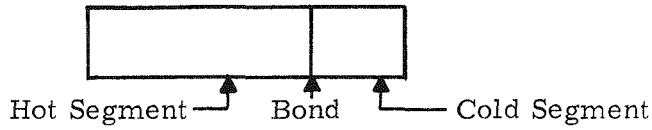

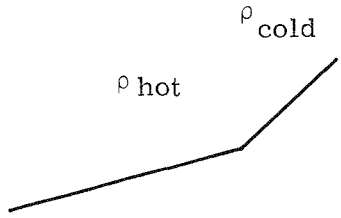

Trace #1

The resistivity ρ is actually an incremental trace of a voltage drop over an element of a known length and area

$$\left(\rho = \frac{E\,A}{I\,1} \right)$$

ρ = resistivity
E = voltage
I = current
A = area of segment
1 = length of segment

The slope of the trace increases as the element or segment is traversed and the resistance, measured as a voltage drop per unit length, increases. In the case of the segmented leg, each segment has a different resistivity and is identified by a different slope at the point of bonding, as indicated by trace #1. Trace #1 is an example of a bonded segmented leg possessing a zero bond resistance. The slope change identifies the hot-cold segment interface. The trace of a bonded segmented leg possessing a finite bond resistance is illustrated in trace #2.

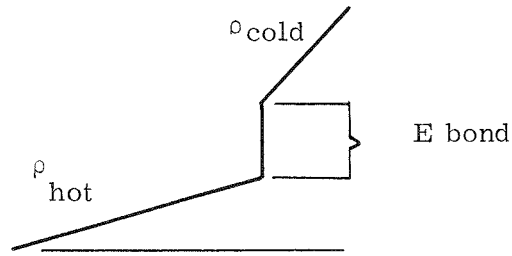

Trace #2

The finite bond resistance (E bond) is a voltage drop with an incremental length of zero, as indicated by a vertical line. The vertical line identifies the hot-cold segment interface with an electrical bond resistance.

Using the method described above for the evaluation of bond integrity, it was found that the trace yielded interface information for only the actual area of the trace. Additional traces traversed at various radial locations of the same element yielded a variety of voltage drop jumps, each an evaluation of the bond condition in the area of its individual trace. It was further noted that a physical misalignment of the hot and cold segments also caused a vertical jump which possessed no correlation to the actual electrical integrity of the bond.

b) Approach

Using a direct current power source and discounting end effects* caused by the short length elements, the following was considered:

$$\rho = \frac{E\,A}{I\,1}$$

ρ = resistivity
E = voltage
A = area of segmented leg
1 = length of segmented leg
I = current

*This assumption is valid because all elements are essentially the same with respect to length, diameter, density and material.

In the case of an individual type of a segmented leg, the area and the length are constants and do not effect any change in the resistivity values for segmented legs of the same type; therefore, only R_{total} was evaluated.

$R_t = \frac{E}{I}$ (Ohms Law)

E = voltage
I = current
R = resistance

$\therefore$ R = E if the current is set at 1 ampere resistivity equals resistance.

This approach produced a total resistance value for each segmented leg. Assuming that the resistance of the hot segment plus the resistance of the cold segment would equal the total resistance of the segmented legs, any variation in total resistance would be the value introduced by the bond resistance.

c) Application

A direct resistance device was designed using voltage probes which contacted the test specimen at each end, exactly at the center. The current probes contacted each end of the element in an annular pattern at a finite distance centrally located from the voltage probe. (See sketch below.)

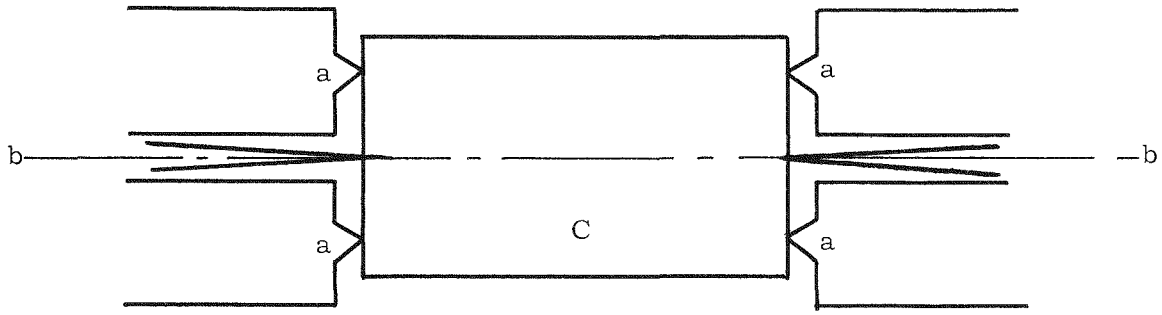

a - current probes
b - voltage probe
c - segmented leg

The voltage probe was a spring-loaded needle which in operation broke through the surface of each end of the segmented leg to eliminate spurious readings caused by a possible oxide film. A mechanical attachment was designed to locate the centerline of the segmented leg coincident with the centerline of the voltage and current probes. The segmented leg was held in place by a spring pressure sufficient in magnitude to force the annular current probes through any oxide film. A block diagram of the test set-up is depicted below:

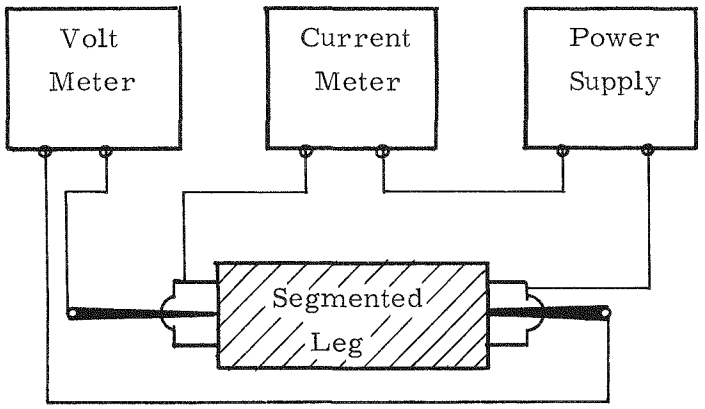

d) Results

Exhaustive tests (over 300) of the above system indicated it to yield reproducible resistances within ±2 percent on individual SNAP-21 segmented N-legs. Resolution of the resistance variations was found to be accurate enough to predict the physical strength of the bond between the hot and cold segments and to indicate temperature variations used to perform the bonding operation.

e) Future Development and Application

During the next reporting period this device will be refined to the extent that the resistivity read on each segmented leg will be the actual resistance of that leg. This will be accomplished by determining a correction factor which will eliminate the error introduced by the "end effect". The device will then be applied to the nondestructive test evaluation of the room temperature resistivity of SNAP-21 elements.

2.3.6.3 Phase I Continuation Testing

Long term testing of thermoelectric devices initiated during Phase I continued during this report period. The units on test are:

a) Three 6-couple test modules; A1, A3, and A4

b) Four prototype generators; P3, P5, P6 and P7

All units are performing normally with no significant changes. Performance data of these units are shown in Figures 2-51 through 2-54.

2.3.6.4 Phase II Generator Development Testing

No effort was expended in this area during this reporting period.

2.3.7 POWER CONDITIONER

Late in this report period, an analysis of power conditioner test data was initiated. The results of the analysis will be used for additional power conditioner study and recommendations for specific areas of redesign in the forthcoming SNAP-21 systems.

Life tests of the Phase I electronic components (power conditioner, regulators, and automatic selector switch) are continuing. Test data shows no significant change in performance over test durations of from 15,000 to 20,000 hours.

2.3.8 ELECTRICAL RECEPTACLE

No effort was expended on this component for the report period.

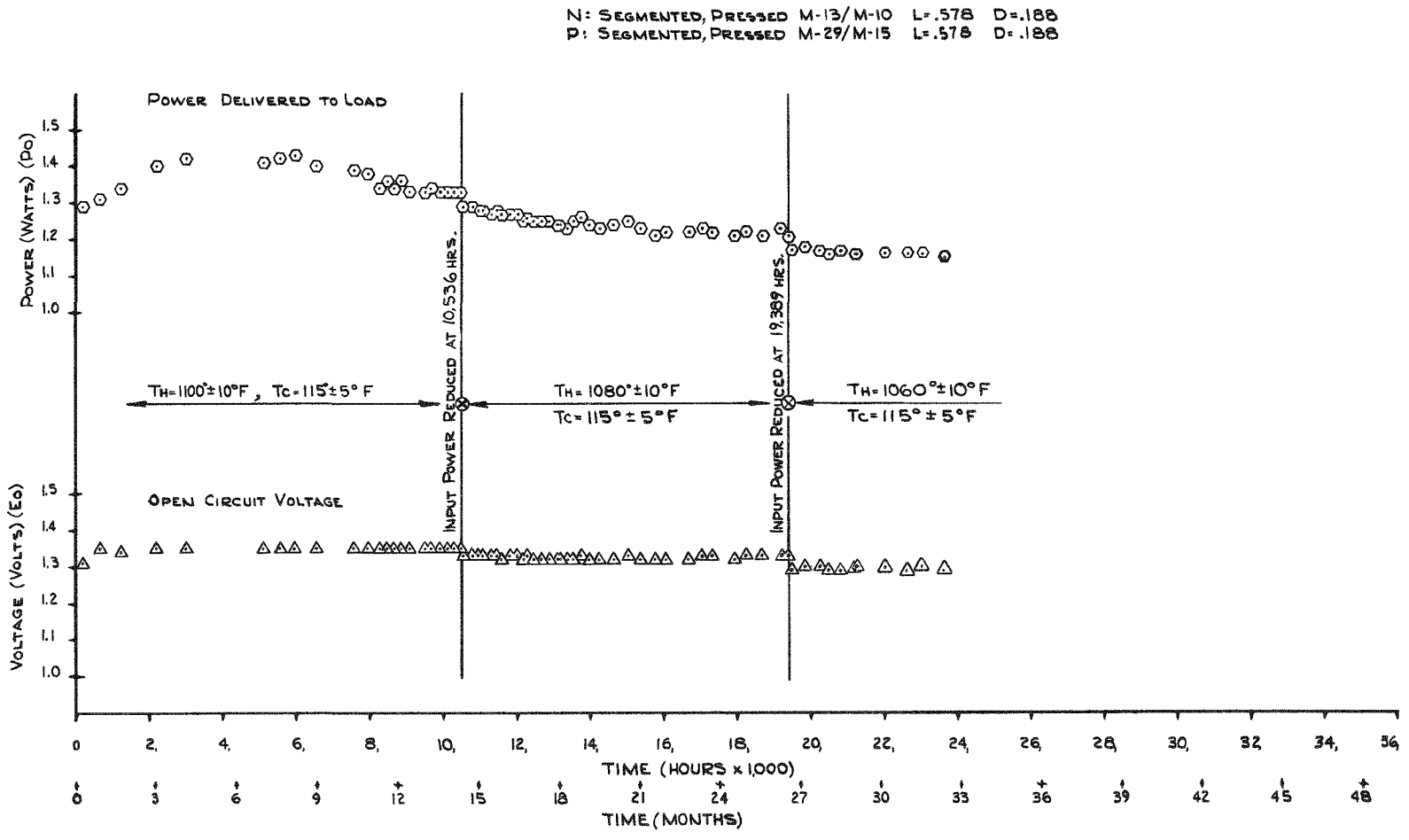

Figure 2-51. Performance Data, SNAP-21B 6-Couple Module A1

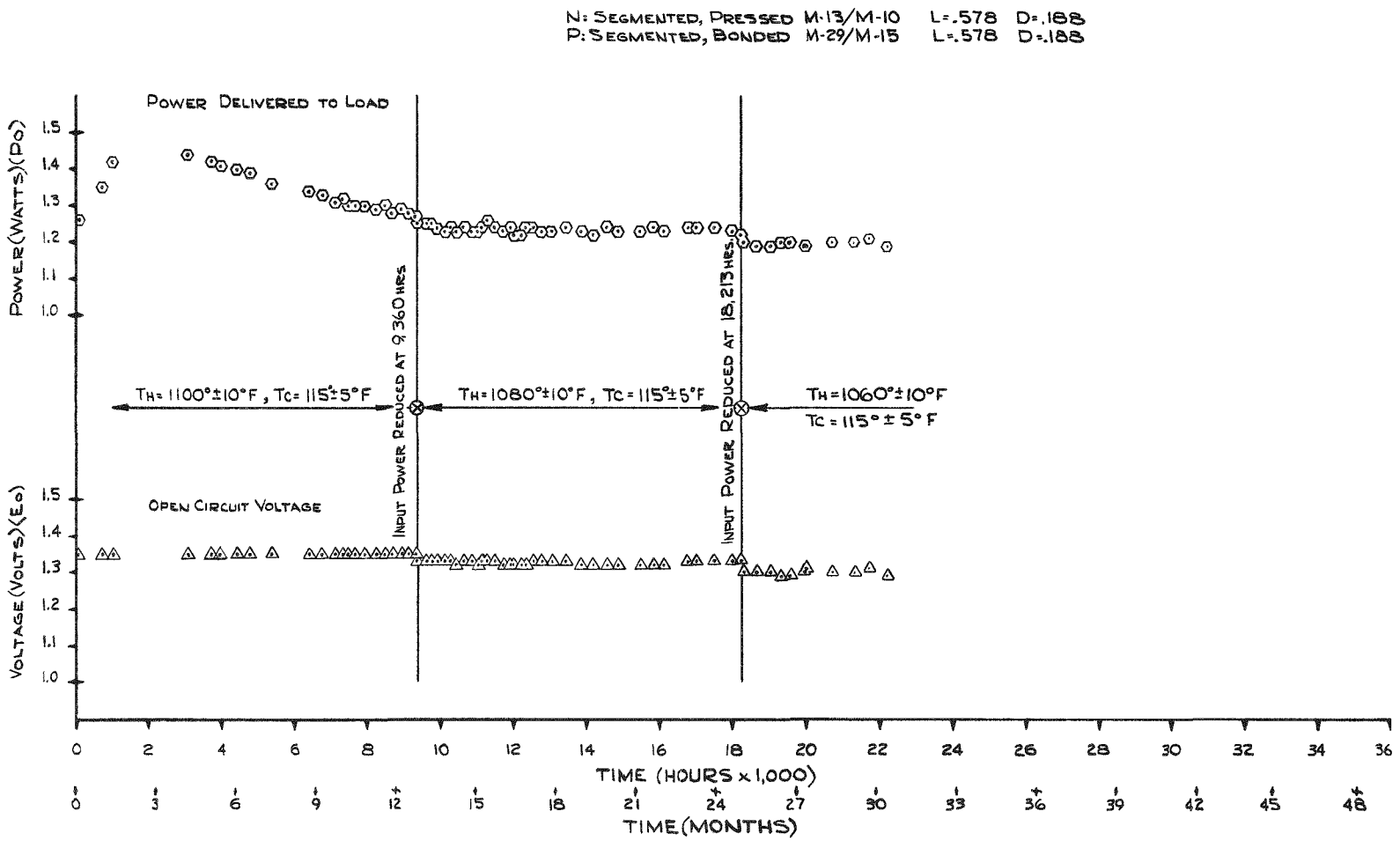

Figure 2-52. Performance Data, SNAP-21B 6-Couple Module A3

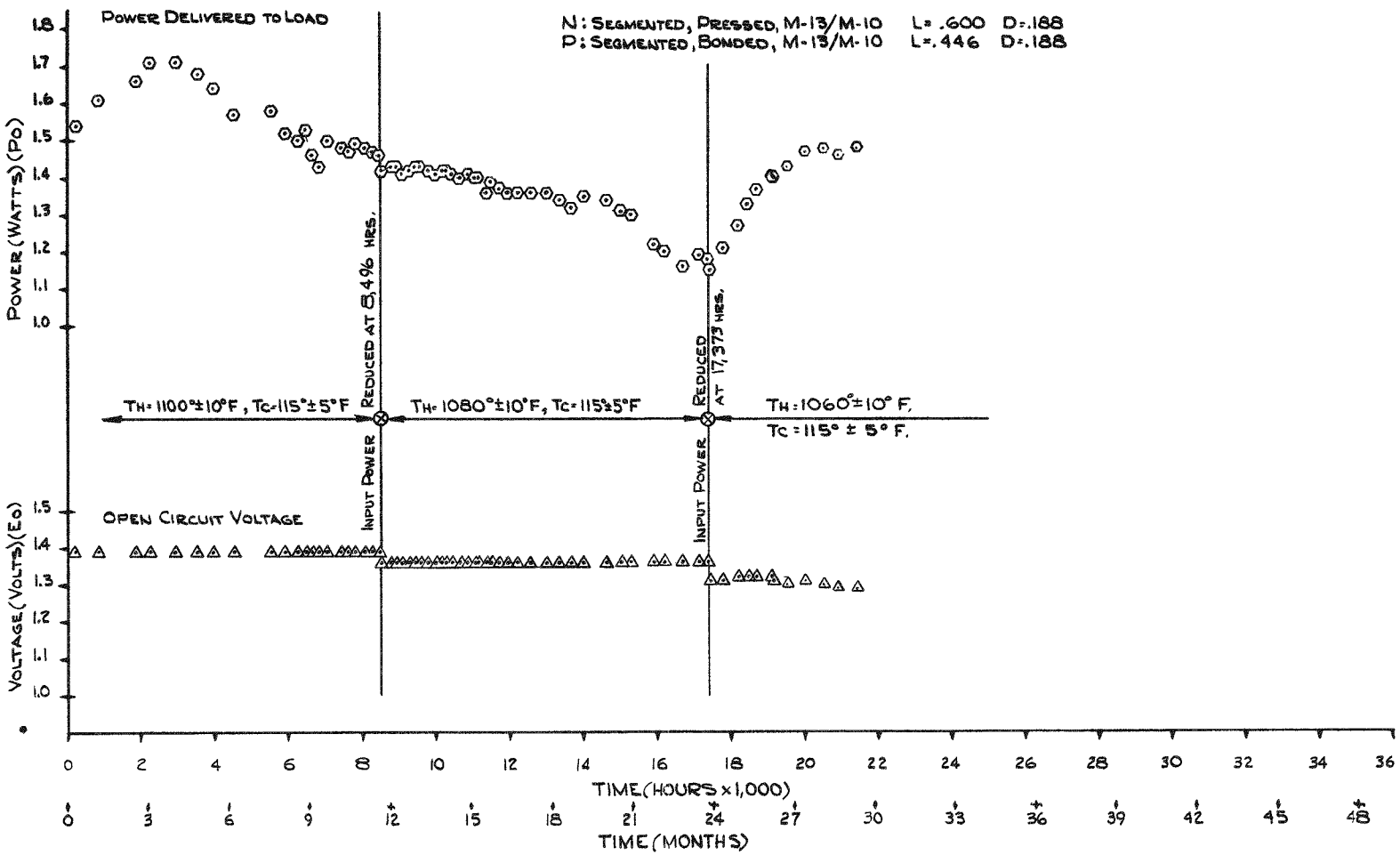

Figure 2-53. Performance Data, SNAP-21B 6-Couple Module A4

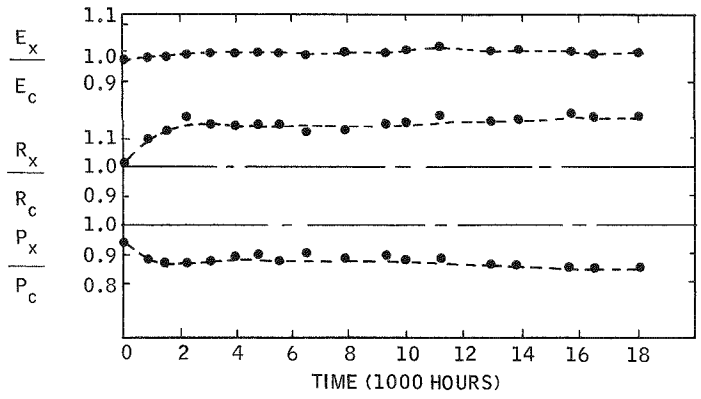

Prototype 3M-37-P3

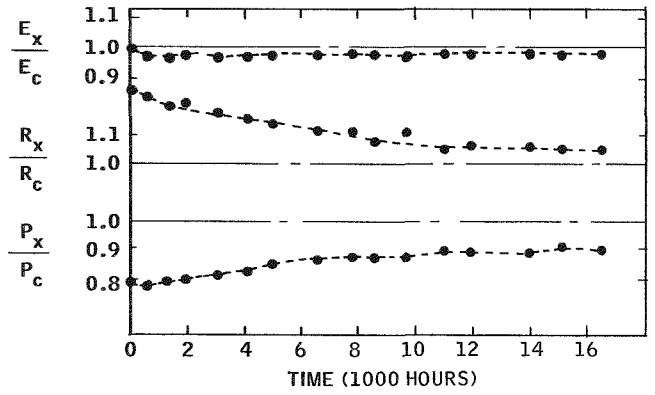

Prototype 3M-37-P5

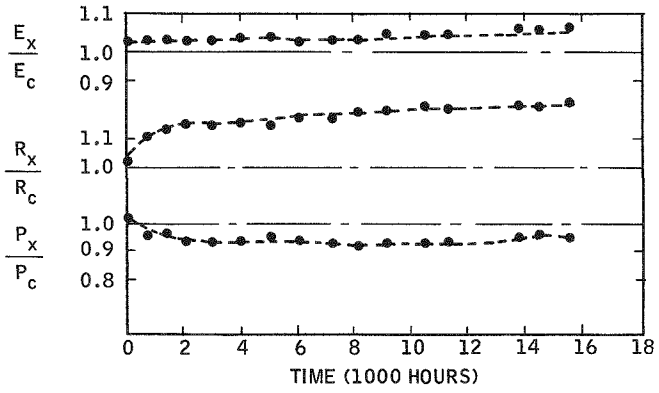

Prototype 3M-37-P6

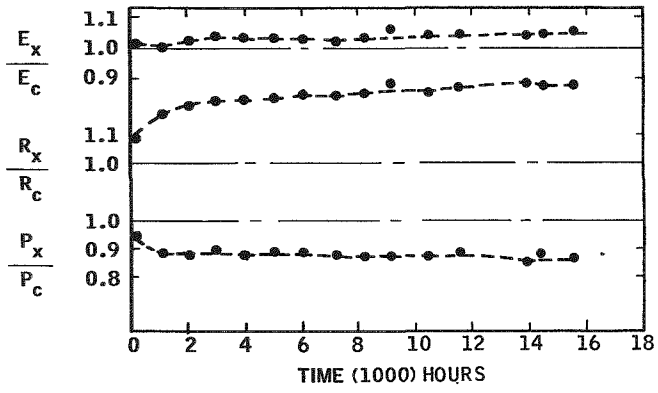

Prototype 3M-37-P7

Figure 2-54. Performance of Prototype 48-Couple Generators 3M-37-P3, P5, P6, P7 (E = voltage, R = resistance, P = power, x = experimental, C = computer)

2.4 PHASE II SYSTEM

No effort was expended in this area during the past report period.

2.5 SAFETY ANALYSIS AND TESTING

2.5.1 COMPARISON OF FUEL FORMS

Safety considerations require a thorough examination of fuel properties. Strontium titanate has been previously regarded as the most desirable fuel form with considerable import attached to its insolubility. However, more recent data shows an appreciable solubility for highly radioactive titanate. The philosophy of complete containment (demonstrated capability) under all credible accident and operating conditions makes the SrO fuel equally acceptable from a safety standpoint. ORNL is planning to conduct additional compatibility tests on both fuel forms in the near future. Both fuels are prepared by a hot press technique using a platinum jacket. This approach eliminates the need for double encapsulation. Recently the AEC has announced plans to conduct extensive tests on SNAP-7A, a 5-watt $SrTiO_3$ fueled system which has been in service for 5-1/2 years. Analysis of the fuel and fuel capsule should provide valuable data on material compatibility, weld quality, dimensional stability, isotope purity, and fuel solubility. This work will be done at ORNL and will take about 6 months.

2.5.2 BIOLOGICAL SHIELD RADIATION TEST

Arrangements have been made to conduct biological shield radiation tests in May. The residual Phase I biological shield being incorporated in a Linde Super Insulation System will be used. ORNL has a 200-watt SrO source available for this test. While a plug will be required to complete shielding, it is not necessary that it be encapsulated. Such encapsulation is only required for oxidation protection of the shield plug alloy when at operating temperature. Due to the short time required for this test, these temperatures will not be reached (see Figure 2-55).

Because of the fragile nature of this particular insulation system, great care must be exercised during its handling. Preliminary plans have been drafted which cover shipping, handling, and test procedures. Actual radiation mapping will be relatively simple. Both survey type readings and more precise dosimeter measurements will be taken. The test system will closely simulate an operational unit. A titanium pressure vessel and dummy copper cold frame will be used to provide similar radiation attenuation.

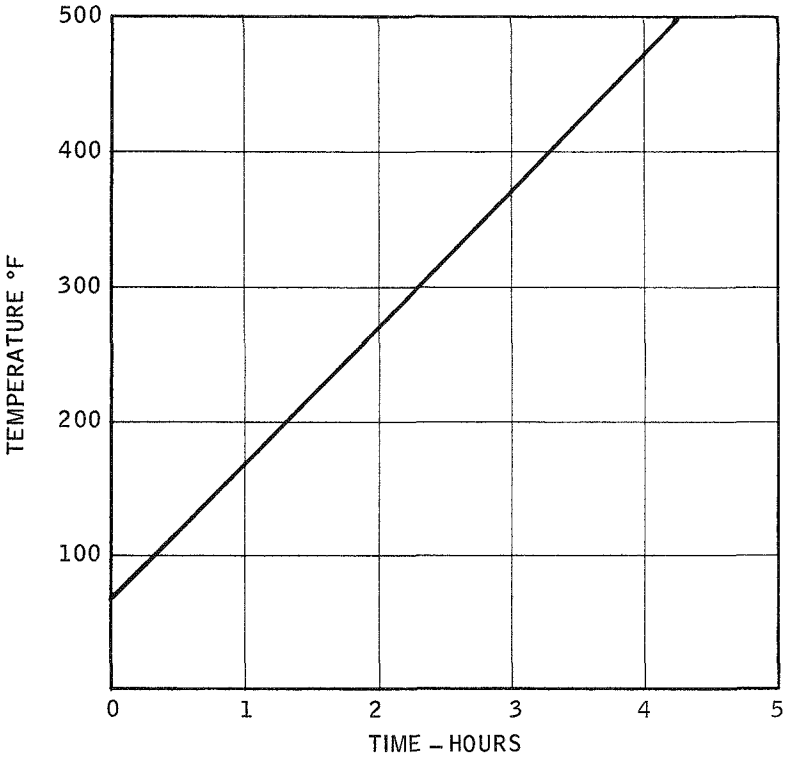

Figure 2-55. Average Shield Temperature After Fuel Insertion (200 watts Thermal)

3.0 TASK IIA – 20-WATT SYSTEM

Due to the impact of the Dynamic Load Criteria Study and Program Plan hold, no effort was expended on this task during this report period.

4.0 EFFORT PLANNED NEXT QUARTER

The following items are planned for the next quarter.

- Fabrication of NRDL test speciments (i.e., electrically heated fuel capsules, laboratory corrosion specimens and galvanic and marine fouling system components) will be started.
- Results of ultrasonic testing of first weld development closures on fuel capsules will be evaluated.
- Radiation effectiveness of the biological shield will be determined from radiation measurements taken on a 200 watt SrO source.
- Test plans for compatibility testing will be finalized.
- Compatibility test fixture design will be completed.
- Compatibility testing will start.
- The fuel capsule weld method (TIG or electron beam) will be selected.
- Test plans for fuel release (ocean environment) studies will be completed.
- The first four development generators will be fabricated and performance tested.
- Design of the in-line-concept generator will be completed.
- Results of the cold end heat transfer testing will be analyzed.
- The system heat balance will be initiated.

- Power conditioner development will be initiated.
- SNAP-21 residual Phase I system will be assembled.
- The pressure vessel material will be selected and ordered.
- The electrical receptacle and strain relief plug vendor will be selected.
- Segmented retaining ring design will be complete.
- Design of tension tie-rod connectors will be complete.
- Tension tie-rod development will be complete.
- Assembly of insulation system development unit 1 will be initiated.
- Insulation system shipping container design will be complete.
- Insulation system compatibility testing will be initiated.
- Task IIA effort will be initiated.

APPENDIX A
SHIELD WEIGHT REDUCTION ANALYSIS

CYLINDRICAL FUEL CAPSULE GEOMETRY

Shield with rounded ends - the radius being equal to the thickness.

FUEL - SrO

1. Capsule OD and ID:

   a) For power = 230 watts BOL

$$\text{Volume of pellet} = \frac{230 \text{ watt}}{\left(1.5 \frac{\text{watt}}{CM^3}\right)\left(16.38 \frac{CM^3}{in^3}\right)}$$

$$V = 9.37 \text{ in}^3 = \pi D^3/4$$

$$L = D = \left[\frac{(9.37)4}{\pi}\right]^{1/3} = 11.93^{1/3} = 2.285 \text{ inches with a clearance of } 0.032 \text{ inches, } D = 2.317 \text{ inches}$$

Calculation of Cylinder Wall Thickness:

The critical collapse pressure of the capsule was assumed to be equal to the maximum hoop stress because of the thick wall and low length-to-diameter ratio. Therefore:

$$\text{Collapsing Stress} = \sigma_c = \frac{2r_2^2 P_2}{r_2^2 - r_1^2}$$

where P_2 is external pressure and r_1 and r_2 the major and minor radii.

If the maximum allowable hoop stress is taken as the yield strength of Hastelloy-C, then:

$$\sigma_c = 80,000 \text{ psi} = \frac{2(10,000)r_2^2}{r_2^2 - (1.159)^2}$$

Hastelloy-C has corrosion rate of 10^{-4} in/yr in sea water; hence, after 300 years, 0.030 inch will have corroded. The OD of the capsule is, therefore, 2(1.338 + 0.030) - 2.736 inches. Conservatively, OD set at 2.754 inches.

Thus, wall thickness $= \frac{2.754 - 2.317}{2} = 0.2185$ inch

b) Power = 210 watts BOL

$$V = 210/(1.5)(16.30) = 8.55 \text{ in}^3$$

$$L = D = \left[\frac{(8.55)\,4}{\pi}\right]^{1/3} = 10.9^{1/3} = 2.22 \text{ inches}$$

with 0.032 inches clearance, D - 2.252 inches

Cylinder Wall Thickness:

$$\sigma_c = 80,000 = \frac{2(10,000)\,r_2^2}{r_2^2 - (1.126)^2}$$

$$r_2 = 1.30$$

Add 0.030 for corrosion

$$2(1.30 + 0.030) = 2.66$$

Conservatively, OD = 2.678

Thus, wall thickness $= \frac{2.678 - 2.252}{2} = 0.213$ inch

c) Power = 190 watts

$$V = 190/(1.5)(16.38) = 7.75 \text{ in}^3$$

$$L = D = \left[\frac{(7.75)\,4}{\pi}\right]^{1/3} = 9.875^{1/3} = 2.145 \text{ inches with}$$

0.032 inches clearance, D = 2.177 inches

Cylinder Wall Thickness:

$$\sigma_c = 80,000 = \frac{2\,(10,000)\,r_2^2}{r_2^2 - (1.089)^2}$$

$$r_2 = 1.258$$

Add 0.030 in. for corrosion

$$2\,(1.258 + 0.03) = 2.576$$

Conservatively, OD = 2.594

$$\text{Thus, Wall Thickness} = \frac{2.594 - 2.177}{2} = 0.2085 \text{ inch}$$

2. Capsule Length:

a) Power = 230 watts BOL

Length = OD Capsule + 1(0.030) spacer

L = 2.754 + 0.030 = 2.784 inches

b) Power = 210 watts BOL

L = 2.678 + 0.030

L = 2.708 inches

c) Power = 190 watts BOL

L = 2.594 + 0.030

L = 2.624 inches

3. Liner Dimensions:

a) Power = 230 watts BOL

ID = OD Capsule + Clearance = 2.754 + 0.030 = 2.784

ID = 2.784 inches

OD = ID + Thickness = 2.784 + 2(0.065) = 2.914

OD = 2.914 inches

b) Power = 210 watts BOL

ID = 2.678 + 0.030 = 2.708

ID = 2.708 inches

OD = 2.708 + 0.130 = 2.838

OD = 2.838 inches

c) Power = 190 watts BOL

ID = 2.594 + 0.030 = 2.624

ID = 2.624 inches

OD = 2.624 + 0.130 = 2.754

OD = 2.754 inches

4. Dimensions of Shield:

a) Power = 230 watts BOL

ID = OD Liner + Clearance

ID = 2.914 + 0.070 = 2.984

ID = 2.984 inches

Length of Cavity = Length Capsule

L = 2.784 inches

Thickness = r = 2.75 inches

b) Power = 210 watts BOL

ID = 2.838 + 0.070 = 2.908

ID = 2.908 inches

L = 2.708 inches

r = 2.75 inches

c) Power = 190 watts BOL

ID = 2.754 + 0.070 = 2.806

ID = 2.824 inches

L = 2.624 inches

r = 2.75 inches

5. Weight of Shield Plus Plug with SrO Only (i.e., Shield Thickness = 2.75 inches):

a) Power = 230 watts BOL

$$V = 2\pi_r [R^2 + 1.5708\ Rr + \frac{2}{3}r^2]l + \pi L(2Rr + r^2]$$

V = volume of shield

R = cavity radius = ID/2

L = length of cavity

r = shield thickness

wt = V_ζ $\quad \zeta = 0.629$ lbs/in^3

$$V = 2\pi (2.75) [1.492^2 + 1.5708 (1.492) (2.75) + \frac{2}{3} (2.75)^2]$$

$$+ \pi 2.784 [2(1.492) (2.75) + 2.75^2]$$

$$= 17.30 [2.23 + 6.45 + 5.05] + 8.75 [8.21 + 7.58]$$

$$V = 237.5 + 138.0 = 375.5 \text{ in}^3$$

$$wt = V_\zeta = (375.5) (0.629) = 236.2$$

Wt @ 230 watts BOL = 236.2 lbs.

b) Power = 210 watts BOL

$$V = 17.30 [1.454^2 + 1.5708 (1.454) 2.75 + 5.05]$$

$$+ \pi 2.708 [2(1.454) (2.75) + 7.58]$$

$$= 17.30 [2.12 + 6.28 + 5.05] + 8.51 [8.00 + 7.58]$$

$$V = 232.5 + 132.5 = 365.0 \text{ in}^3$$

$$wt = V_\zeta = (365.0) (0.629) = 229.5$$

Wt @ 210 watts BOL = 229.5 lbs.

c) Power = 190 watts BOL

$$V = 17.30\,[1.412^2 + 1.5708\,(1.412)\,(2.75) + 5.05]$$

$$+ \pi 2.624\,[2(1.412)\,(2.75) + 7.58]$$

$$= 17.30\,[1.99 + 6.08 + 5.05] + 8.25\,[7.76 + 7.58]$$

$$V = 227.0 + 126.6 = 353.6\ \text{in}^3$$

$$\text{wt} = V\zeta = (353.6)\,(0.629) = 222.3$$

Wt @ 190 watts BOL = 222.3 lbs.

6. Weight of Shield Plus Plug considering SrO as fuel form and a higher allowable radiation level (Thickness = 2.45 inches):

a) Power = 230 watts BOL

$$V = 2\pi\,(2.45)\,[2.23 + 1.5708\,(1.492)\,(2.45)$$

$$+ \frac{2}{3}\,2.45^2] + 8.75\,[2(1.492)\,2.45 + 2.45^2]$$

$$= 15.39\,[2.23 + 5.74 + 4.0] + 8.75\,[7.32 + 6.0]$$

$$V = 184.0 + 116.5 = 300.5$$

$$\text{wt} = V\zeta = (300.5)\,(0.620) = 188.9$$

Wt @ 230 watts BOL = 188.9 lbs.

b) Power = 210 watts BOL

$$V = 15.39\,[2.12 + 1.5708\,(1.454)\,(2.45) + 4.0]$$

$$+ 8.51\,[2(1.454)\,(2.45) + 6.0]$$

$$= 15.39\,(11.72) + 8.51\,(13.12)$$

$V = 180.4 + 111.7 = 292.1$

$wt = V\zeta = (292.1)(0.629) = 183.7$

Wt @ 210 watts BOL = 183.7 lbs.

c) Power = 190 watts BOL

$V = 15.39\,[1.99 + 5.35 + 4.0] + 8.25\,[6.92 + 6.0] = 174.5 + 106.6$

$V = 281.1 \text{ in}^3$

$wt = V\zeta = (281.1)(0.629) = 176.9$

Wt @ 190 watts BOL = 176.9 lbs.

7. Change in Center of Gravity when considering SrO fuel form and higher allowable radiation level:

a) Power = 230 watts BOL

Overall Length of Shield = 2(2.45) + 2.784

OL = 2 (thickness) + Length Cavity

OL = 7.684 inches

Original Length = 8.39 inches

Δ = amount C.G. shifts up

$$\Delta = \frac{\text{Orig. Length - OL}}{2}$$

$\Delta = (8.39 - 7.684)/2 = 0.353$

Δ = 0.353 inch

b) Power = 190 watts BOL

OL = 4.90 + 2.624 = 7.524

Δ = (8.39 - 7.524)/2 = 0.433

Δ = 0.433 inch

SPHERICAL FUEL CAPSULE GEOMETRY

FUEL - SrO

Allowable radiation level at surface - 200 mr/hr.

A. Capsule OD and ID:

1. Power = 230 watts BOL

$$V = 9.37 \text{ in}^3 = \frac{4}{3}\pi r^3 \quad r = \frac{D}{2}$$

$$V = \frac{4}{3}\pi \left(\frac{D}{8}\right)^3 = \frac{1}{6}\pi D^3$$

$$D = \left(\frac{6V}{\pi}\right)^{1/3} = \left(\frac{6 \times 9.37}{3.14}\right)^{1/3} = 2.618 \text{ inches}$$

with a clearance of 0.032 inches, D = 2.650 inches in ID

Calculation of sphere wall thickness and OD:

$$\text{Collapsing Stress} = \sigma_c = \frac{3\, r_2^3\, P_2}{2\,(r_2^3 - r_1^3)}$$

r_2 = outside radius

r_1 = inside radius

P_2 = external pressure = 10,000 psi

$$\sigma_c = 80,000 = \frac{3r_2^3\ (10,000)}{2\,(r_2^3 - 1.325^3)}$$

$$r_2^3 = 2.870$$

$$r_2 = 1.422$$

Hastelloy-C has a corrosion rate of 10^{-4} in/yr in sea water; hence, after 300 hours, 0.030 inch will have corroded. The OD of the capsule is, therefore, 2(1.422 + 0.030) = 2.904 inches.

Conservatively, OD set at 2.922 inches.

$$\text{Thus, wall thickness} = \frac{2.922 - 2.650}{2}$$

$$t = 0.136$$

2. Power = 210 watts BOL

$$V = 8.55 \text{ in}^3 = \frac{1}{6}\pi D^3$$

$$D = \left(\frac{6V}{\pi}\right)^{1/3} = \left(\frac{6 \times 8.55}{3.14}\right)^{1/3} = 2.535 \text{ inches}$$

with 0.032 inches clearance, ID = 2.567 inches

Calculation of sphere wall thickness:

$$\sigma_c = 80,000 = \frac{3r_2^3 \ (10,000)}{2\ (r_2^3 - 1.283^3)}$$

$$r_2 = 1.375 \text{ inches}$$

Add 0.030 inch for corrosion

$$2(1.375 + 0.030) = 2.810 \text{ inches}$$

$$\text{conservatively, OD} = 2.828 \text{ inches}$$

$$\text{Thus, wall thickness} = \frac{2.828 - 2.567}{2}$$

$$t = 0.131 \text{ inch}$$

3. Power = 190 watts BOL

$V = 7.75 \text{ in}^3$

$$D = \left(\frac{6 \times 7.75}{3.14} \right)^{1/3} = 2.460 \text{ inches}$$

with 0.032 inch clearance, ID = 2.492 inches

Calculation of sphere wall thickness:

$$\sigma_c = 80,000 = \frac{3r_2^3 \ (10,000)}{2 \ (r_2^3 - 1.246^3)}$$

$$r_2 = 1.337 \text{ inches}$$

Add 0.030 inches for corrosion,

$$2(1.337 + 0.030) = 2.734 \text{ inches}$$

Conservatively, OD = 2.752 inches

$$\text{Thus, wall thickness} = \frac{2.752 - 2.460}{2}$$

$$t = 0.130 \text{ inch}$$

NOTE: The weld corrodes faster than the capsule - about 0.090 inch in 300 years - thus, there appears to be a safety factor of about 1.5 for capsule thickness.

B. Liner Dimensions

1. Power = 230 watts BOL

ID = OD Capsule + Clearance = 2.922 + 0.030

ID = 2.952 inches

OD = ID + Thickness = 2.952 + 2(0.065) = 3.082

OD = 3.082 inches

2. Power = 210 watts BOL

ID = 2.828 + 0.030 = 2.858

ID = 2.858 inches

OD = 2.858 + 0.130 = 2.988

OD = 2.988 inches

3. Power = 190 watts BOL

ID = 2.752 + 0.030

ID = 2.782 inches

OD = 2.782 + 0.130

OD = 2.912 inches

C. Dimensions of Shield

1. Power = 230 watts BOL

ID = OD Liner + Clearance = 3.082 + 0.070 = 3.152

ID = 3.152 inches

OD = ID + 2 (thickness) = 3.152 + 2(2.75)

OD = 8.652 inches

2. Power = 210 watts BOL

ID = 2.988 + 0.070

ID = 3.058 inches

OD = 3.058 + 5.50

OD = 8.558 inches

3. Power = 190 watts BOL

D. Weight of Shield Plus Plug

1. Power = 230 watts BOL

Volume of shield = V

$$V = \frac{3.14}{6} (8.652^3 - 3.152^3) = 0.523 (616.5)$$

$$V = 322.0 \text{ in}^3$$

$$Wt = V\zeta \qquad \zeta(\text{Uranium}) = 0.629 \text{ lb/in}^3$$

$$Wt = (322)(0.629)$$

Wt @ 230 watts BOL = 202.7 lbs.

2. Power = 210 watts BOL

$$V = 0.523 (8.558^3 - 3.058^3)$$

$$V = 0.523 (6.01.5) = 314.5$$

$$V = 314.5 \text{ in}^3$$

$Wt = V_\delta = (314.5)(0.629) = 198.0$ lbs.

Wt @ 210 watts BOL = 198.0 lbs.

3. Power = 190 watts BOL

$V = 0.523 (8.482^3 - 2.982^3)$

$V = 305.0 \text{ in}^3$

$Wt = V_\zeta = (305)(0.629) = 191.9$

Wt @ 190 watts BOL = 191.9 lbs.

TUNGSTEN AS A SHIELD MATERIAL

Cylindrical shield configuration with rounded ends – the radius being equal to the thickness.

FUEL - SrO

Allowable radiation level at surface - 200 mr/hr.

In order to have 200 mr/hr at surface using tungsten shield, it is necessary to have shield thickness = 3.13 inches.

Density of tungsten = 18.5 gm/cm^3 = 0.669 lb/in^3

A. Weight of Shield Plus Plug

1. Power = 230 watts BOL

V = Volume of shield + plug

$$V = 2\pi r \left[R^2 + 1.5708\, Rr + \frac{2}{3} r^2\right] + \pi L \left[2Rr + \frac{2}{3} r^2\right]$$

R = Cavity radius $= \frac{ID}{2}$, (inches)

L = Length of cavity, (inches)

r = Shield thickness = 3.13 inches

$$V = 2\pi(3.13)\left[2.23 + 1.5708\,(1.492)\,(3.13) + \frac{2}{3}(3.13)^2\right]$$

$$+ \pi(2.784)\left[2(1.492)\,(3.13) + 3.13^2\right]$$

$$= 19.67\,[2.23 + 7.34 + 6.54] + 8.75\,[9.34 + 9.80]$$

$$V = 317.0 + 167.5 = 484.5\ in^3$$

$$Wt = V_{\zeta} = (484.5)\,(0.669) = 324.0$$

Wt @ 230 watts BOL = 324.0 lbs.

2. Power = 210 watts BOL

$V = 19.67\,[2.12 + 1.5708\,(1.454)\,3.13 + 6.54]$

$+ 8.51\,[2(1.454)\,3.13 + 9.80]$

$V = 311.0 + 160.7 = 471.7\ in^3$

$Wt = V_\zeta = (471.7)\,(0.669) = 315.0$

Wt @ 210 watts BOL = 315.0 lbs.

3. Power = 190 watts BOL

$V = 19.67\,[1.99 + 1.5708\,(1.412)\,(3.13) + 6.54]$

$+ 8.25\,[2(1.412)\,(3.13) + 9.80]$

$V = 304.0 + 153.8 = 457.8\ in^3$

$Wt = V_\zeta = (457.8)\,(0.669) = 306.0$

Wt @ 190 watts BOL = 306.0 lbs.

B. Change in Center of Gravity Due to Change in Material

1. Power = 230 watts BOL

Overall length of shield = OL

OL = 2(thickness) + length of cavity

$OL = 2(3.13) + 2.784 = 6.26 + 2.784$

OL = 9.044 inches

Original Length = 8.39 inches

Δ = amount C.G. shifts down

= (OL = Orig. Length)/2

Δ = (9.044 - 8.39)/2 = 0.654/2

$\boxed{\Delta = 0.327 \text{ inch}}$

2. Power = 210 watts BOL

OL = 6.26 + 2.708 = 8.968

Δ = (8.968 - 8.39)/2 = 0.578/2

$\boxed{\Delta = 0.289 \text{ inch}}$

3. Power = 190 watts BOL

OL = 6.26 + 2.624 = 8.884

Δ = (8.884 - 8.39)/2 = 0.494/2

$\boxed{\Delta = 0.247 \text{ inch}}$

NOTE: Reason tungsten shield thickness is greater than for uranium, even though tungsten has a greater density, is because the linear absorption coefficients are much less for tungsten.

Effect of Selected Parameters on Shield Weight

Shield Material Capsule Geometry Fuel Form Surface Radiation	Uranium Cylindrical $SrTiO_3$ 200 mr/hr	Tungsten Cylindrical SrO 200 mr/hr	Uranium Cylindrical SrO 200 mr/hr	Uranium Cylindrical $SrTiO_3$ 500 mr/hr	Uranium Spherical SrO 200 mr/hr	Uranium Cylindrical SrO 500 mr/hr
230 Watts BOL	261.7	324.0	236.2	~214	202.7	188.9
210 Watts BOL	254.5	315.0	229.5	~209	198.0	183.7
190 Watts BOL	247.0	306.0	222.3	~202	191.9	176.9

APPENDIX B

SAMPLE PRESSURE VESSEL CALCULATIONS FOR BERYLCO 165

PROPERTIES: (REF: BERYLCO TECH BULLETIN #1010-A)

ρ = 0.298 lb/in^3

F_{TU} = 150,000 - 165,000 psi (annealed and H.T.)

F_{PL} at 0.002% 60,000 - 75,000 psi

Elastic limit 0.002% permanent set, 65,000 - 80,000 psi

F_{TY}

0.01% offset	75,000 - 85,000 psi
0.20% offset	120,000 - 145,000 psi
0.50% strain	85,000 - 95,000 psi

E at 20° C = 19,000,000 psi

FORMULAS FOR WALL THICKNESS CALCULATIONS

1. Cylinder:

Design pressure "p" is related to wall thickness, outside diameter, mean diameter, modulus of elasticity, and modulus reduction factor by the following:

$$p = \left(\frac{E_T}{E}\right)\left[\frac{4E}{1-\mu^2}\left(\frac{t}{D_o}\right)\left(\frac{t}{D}\right)\right]^2$$

$$= \frac{4E_T}{1-\mu^2}\left(\frac{t}{D_o}\right)\left(\frac{t}{D}\right)^2$$

Also,

$$E_T = \frac{E}{1 + \frac{3N}{7}\left(\frac{f}{f_{0.70}}\right)^{n-1}}$$

By substitution:

$$p = \frac{4E}{(1-\mu^2)\left[1 + \frac{3N}{7}\left(\frac{f}{f_{0.70}}\right)^{n-1}\right]}\left(\frac{t}{D_o}\right)\left(\frac{t}{D}\right)^2$$

Value of f (existing stress level) is based on "thick" cylinder formula

$$f = \frac{3}{2}\,\frac{R_o^2 p}{tR}$$

Use $D = 2R$ and $D_o = 2R_o$ and by substitution and manipulation

$$p = \frac{E\,\frac{t}{R_o}\,\frac{t}{R}^2}{2(1-\mu^2)\left[1 + \frac{3n}{7}\,\frac{R^2{}_o p}{tRF_{0.70}}^{n-1}\right]}$$

By further algebraic manipulation we can write

$$n\left(\frac{R_o^2}{tR}\right)^{n-1} - \frac{t^3}{R_o R^2}\left(\frac{7E}{6(1-\mu^2)p}\right)\left(\frac{F_{0.70}}{p}\right)^{n-1} - \frac{7}{3}\left(\frac{F_{0.70}}{p}\right)^{n-1} = 0$$

2. Hemisphere

$$p = (E_S E_T)^{1/2} \ (3.36) \left(\frac{t}{D_o}\right)^2$$

$$E_S = \frac{E}{1 + \frac{3}{7}\left(\frac{f}{f_{0.70}}\right)^{n-1}}$$

$$E_T = \frac{E}{1 + \frac{3n}{7}\left(\frac{f}{f_{0.70}}\right)^{n-1}}$$

$$f = \frac{p R_o^2}{2 RT} \quad \text{(approximate)}$$

By substitution and manipulation

$$p = 0.84E \left[\frac{1}{1 + \frac{3}{7}(n+1)\left(\frac{pR_o^2}{2RtF_{0.70}}\right)^{n-1} + \frac{9n}{49}\left(\frac{pR_o^2}{2RtF_{0.70}}\right)^{2n-2}}\right]^{1/2} \left(\frac{t}{R_o}\right)$$

PRESSURE VESSEL WALL THICKNESS
BERYLCO 165 ALLOY

For the Cylinder:

$$n\left(\frac{R_o^2}{tR}\right)^{n-1} - \frac{t^3}{R_o R^2}\left(\frac{7E}{6(1-\mu^2)p}\right)\left(\frac{F_{0.70}}{p}\right)^{n-1} - \frac{7}{3}\left(\frac{F_{0.70}}{p}\right)^{n-1} = 0$$

Inside radius fixed at 6.25"

$$R = 6.25 + \frac{t}{2}$$

$$R_o = 6.25 + t$$

$$n = 6.38$$

$$E = 1.9 \times 10^7 \text{ psi}$$

$$p = 1.5 \times 10^4 \text{ psi}$$

$$\mu = 0.30$$

$$F_{0.70} = 1.27 \times 10^3$$

then

$$6.38\left[\frac{(6.25+t)^2}{t\left(6.25+\frac{t}{2}\right)}\right]^{5.38} - \frac{t^3}{(6.25+t)\left(6.25+\frac{t}{2}\right)^2}\left(\frac{7 \times 1.9 \times 10^7}{6 \times 0.91 \times 1.5 \times 10^4}\right)$$

$$\left(\frac{1.27 \times 10^5}{1.5 \times 10^4}\right)^{5.38} - \frac{7}{3}\left(\frac{1.27 \times 10^5}{1.5 \times 10^4}\right)^{5.38} = 0$$

$$6.38\left[\frac{(6.25+t)^2}{t\left(6.25+\frac{t}{2}\right)}\right]^{5.38} - 1.591 \times 10^8\left(\frac{t^3}{(6.25+t)\left(6.25+\frac{t}{2}\right)^2}\right)$$

$$- 2.286 \times 10^5 = 0$$

t = 0.911 OK for buckling stability.

Next check for material yield

$$F_y = 120,000 \text{ psi}$$

$$f = \frac{3}{2}\left(\frac{R_o^2 p}{2R}\right) = \frac{1.732}{2}\left(\frac{(6.25 + 0.911)^2\ 1.5 \times 10^4}{2\left(6.25 + \frac{0.911}{2}\right)}\right) = 49,670 \text{ psi}$$

OK since 49,670 < 120,000 psi

For the hemisphere:

$$p_c = 0.84E\left[\frac{1}{1 + \frac{3}{7}(n+1)\left(\frac{pR_o^2}{2RtF_{0.70}}\right)^{n-1} + \frac{9n}{49}\left(\frac{pR_o^2}{2RtF_{0.70}}\right)^{2n-2}}\right]^{1/2}\left(\frac{t}{R_o}\right)^2$$

with the same values of E, n, p and $F_{0.70}$ as used before plus

$$R_{hemi.} = R_{cyl} = 6.7055,\ R_o = 6.7055 + \frac{t}{2}$$

We now check for stress level

$$f = \frac{0.75p}{t}\left[\frac{(2R + t)^3}{12R^2 + t^2}\right] = \frac{0.75 \times 1.5 \times 10^4}{0.361}\left[\frac{(2 \times 6.705 + 0.361)^3}{12(6.705)^2 + (0.361)^2}\right]$$

= 150,200 psi which is too high ∴ t must be increased for purely elastic stress.

For t = 0.4, f = 137,300 psi

For t = 0.5, f = 112,300 psi

From a plot of these values, the thickness t = 0.465 corresponds to F = 120,000 psi.

APPENDIX C
HEAT LEAK CALCULATIONS
BLOCK MIN-K 1301 IN VACUUM

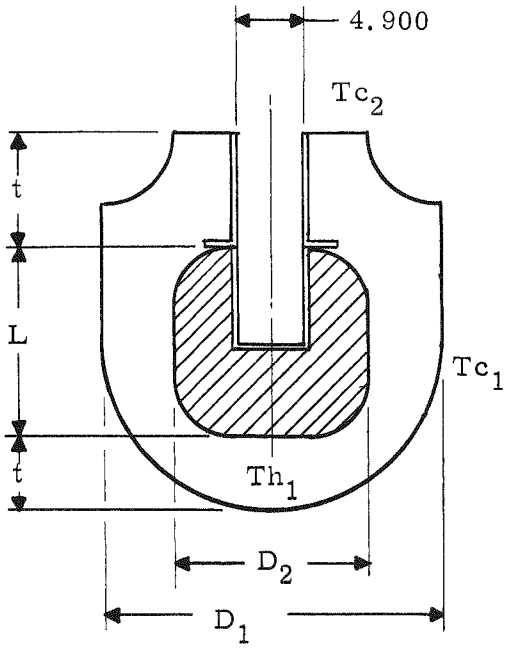

Outer Case Temperature $Tc_1 = 52°F$

Shield Temperature $Th_1 = 1350°F$

Shield Temperature $Th_2 = 1330°F$

Upper Head Temperature $Tc_2 = 150°F$

Shield Ave. Temperature $T_{ave} = 1340°F$

$$K_m = 0.0125 \frac{BTU}{FT\text{-}Hr\text{-}°F} \text{ (MIN-K-1301 vac.)}$$

Shield Length $L_1 = 8.5''$

Shield Diameter $D_2 = 8.5''$

Outer Case Diameter $D_1 = 16.5''$

Insulation Thickness $t = 4''$

The method of calculating the heat leak was one directional heat transfer by conduction.

Heat leak in radial direction

$$\text{(a)} \quad Q_r = \frac{2\pi K_m L_1 \Delta T}{\ln \frac{D_1}{D_2}} = \frac{2 \times 3.14 \times 0.0125 \times 8.4}{3.42 \ln \frac{16.5}{8.5} \times 12} \quad (1340\text{-}52)$$

$Q_r = 31.4$ Watts

(b) Heat leak through the bottom

$$Q_b = \frac{K_m A \Delta T}{} = \frac{0.0125 \times \pi (8.5)^2 (1350-52)}{3.42 \times 144 \times 4 \times \frac{4}{12}}$$

$Q_b = 5.51$ Watts

Heat leak through 0.011 inch thick neck tube 4" long. (ℓ)

$K_m = 13.2$ at 740° F for Hastelloy-X.

(c) $$Q_n = \frac{K_m A \Delta T}{\ell} = \frac{13.2 \times \pi Dt (1330-150)}{3.42 \times 144 \times \frac{4}{12}}$$

$Q_n = 15.9$ Watts

Heat leak through upper head 4" thick insulation

(d) $$Q_h = \frac{K_m A \Delta t}{} = \frac{0.0125 \times \pi (8.5^2 - 4.9^2) (1330-150)}{3.42 \times 4 \times 144 \times \frac{4}{12}}$$

$Q = 3.45$ Watts

Heat leak due to corner loss will be considered using a shape factor which has been empirically derived (Ref: Elements of Heat Transfer, Jacob and Hawkins)

$S = 0.54C$ shape factor
C is circumference or
edge length, ft.

(e) $$Q_c = SK_m \Delta T = \frac{0.54 \times \pi 16.5 \times 2\ (1340-52)\ 0.0125}{3.42 \times 12}$$

$$Q_c = 14.2 \text{ Watts}$$

Heat leak through 3 0.187 dia. Hastelloy-x tension rods 4 inches long (4):

(f) $$Q_t = \frac{K_m A \Delta T}{l} = \frac{13.2 \times \pi (0.187)^2\ (1350-52)\ 3}{4 \times 144 \times \frac{4}{12}}$$

$$Q_t = (3 \text{ rods}) = 8.7 \text{ Watts}$$

Total heat leak for the system

$$Q \text{ total} = Q_r + Q_b + Q_{nt} Q_n + Q_c + Q_t$$

$$Q \text{ total} = 31.4 + 5.51 + 15.9 + 3.45 + 14.2 + 9.0$$

$$Q \text{ total (system)} = 79.46 \text{ Watts}$$